

---

# Understanding metric-related pitfalls in image analysis validation

---

In the format provided by the authors and unedited

# Supplementary Notes – Understanding metric-related pitfalls in image analysis validation

## SUPPLEMENTARY METHODS

### Literature search

The literature search of metric pitfalls and limitations was conducted on the platform Google Scholar. The checkbox "include patents" was activated and the checkbox "include citations" was deactivated; other default settings were left unchanged. For each metric, a specific search string using the Boolean operators OR and AND was generated as follows:

- (Different notations of the metric name, including synonyms and acronyms, enclosed in quotation marks, respectively, and combined with OR)
- AND "metric"
- AND (different expressions pertaining to the concept of pitfalls, limitations and flaws, enclosed in quotation marks, respectively, and combined with OR)

For example, the following search string was used for the literature search of Dice Similarity Coefficient (DSC) pitfalls: ("DSC" OR "Dice Similarity Coefficient" OR "Sørensen-Dice coefficient" OR "F1 score" OR "DCE") AND "metric" AND ("pitfall" OR "limitation" OR "caveat" OR "drawback" OR "shortcoming" OR "weakness" OR "flaw" OR "disadvantage" OR "suffer").

A second literature search dedicated to the pitfalls collected during the Delphi process was conducted on the platforms Google Scholar and Google. This search served the purpose of determining how many of the proposed pitfalls could be found in either existing research literature or online resources such as blogs, assuming that the issue is already roughly known to the person conducting the search. We further determined whether or not a found pitfall was presented in a visual manner. We analyzed the first three results pages (corresponding to thirty results) from each search platform and excluded our own previous work on metric pitfalls from the analysis.

### Delphi process

The collection of pitfalls was achieved via a multi-stage Delphi process conducted among an international expert consortium comprised of more than 60 biomedical image analysis experts, as well as community feedback. A Delphi process is a structured group communication process that serves to pool opinions from an expert panel via a series of individual interrogations, usually in the form of questionnaires, interspersed with feedback from the respondents [8]. The technique is widely used for building consensus among experts in medicine, particularly in the development of best practices in areas where evidence may be limited, conflicting, or absent [49]. Expert selection was initially based on membership in major relevant societies such as the Biomedical Image Analysis ChallengeS (BIAS) initiative, the Medical Open Network for Artificial Intelligence (MONAI) Working Group for Evaluation, Reproducibility and Benchmarks, and the Medical Image Computing and Computer Assisted Interventions (MICCAI) Special Interest Group for Challenges (previously MICCAI board working group), as well as a track record of expertise in the areas of metrics, challenges and/or best practices. To reflect as broad a range of application areas and metric pitfalls as possible, the number of consortium members was increased throughout the process to a final

number of 62 members. The Delphi process comprised four surveys. Each survey was developed by the coordinating team of the process and sent out to the remaining members of the consortium. Upon completion, the coordinating team then analyzed the results and iteratively refined the list of pitfalls. The main stages of the compilation and consensus building process are detailed in the following:

- (1) *Compilation of pitfall sources*: The primary purpose of the first survey was obtaining agreement on sources of pitfalls.
- (2) *Collection of pitfalls*: The following survey specifically asked for concrete pitfalls in the presence of those problem characteristics.
- (3) *Community feedback*: The proposed list of pitfalls was further complemented by social media-based feedback from the general scientific community.
- (4) *Final agreement on pitfalls*: The subsequent survey served to obtain consensus agreement on which pitfalls to include. For each pitfall, it asked whether the pitfall should be included. In addition, the experts were given the opportunity to provide feedback on each pitfall and to suggest further pitfalls. The final collection of pitfalls was illustrated and all metric values were verified by two independent observers.
- (5) *Creation of taxonomy*: The collected pitfalls were analyzed and a taxonomy was created. In the final survey, approval of the consortium for the structure and phrasing of the taxonomy and the assignment of specific pitfalls to the taxonomy was obtained.

### **Expert consortium**

The expert consortium consisted of a total of 70 researchers (70% male, 30% female) from a total of 65 institutions. The majority of experts (50%) were professors, followed by postdoctoral researchers (39%). The median h-index of the consortium was 31.5 (mean: 36; minimum: 6; maximum: 113) and the median academic age was 18 years (mean: 19; minimum: 3; max: 42). Experts were from 19 countries and 5 continents. 60% of experts had a technical, 6% a clinical, 3% a biological, and 23% a mixed background. Of the 65 institutions, we could identify the number of employees for 89%. Of those, the majority of institutions had a size between 1,000 and 10,000 employees (57%), followed by even larger institutions between 10,000 and 100,000 employees (22%), and smaller institutions below 1,000 employees (20%). Only a small portion of institutions were above 100,000 employees (2%).

## SUPL. NOTE 1 METRIC FUNDAMENTALS

The present work focuses on biomedical image analysis problems that can be interpreted as classification tasks at the image, object, or pixel level. The vast majority of metrics for these problem categories are directly or indirectly based on epidemiological principles of True Positive (TP), False Negative (FN), False Positive (FP), True Negative (TN), i.e., the *cardinalities* of the so-called confusion matrix. The TP/FN/FP/TN are henceforth referred to as cardinalities. In the case of more than two classes  $C$ , we also refer to the entries of the  $C \times C$  confusion matrix as cardinalities. For simplicity and clarity in notation, we restrict ourselves to the binary case in most examples. Cardinalities can be computed at the image (segment), object, or pixel level. They are typically computed by comparing the prediction of the algorithm to a reference annotation. Modern neural network-based approaches commonly require a threshold to be set in order to convert the algorithm output comprising predicted class scores (also referred to as continuous class scores) to a confusion matrix. For the purpose of metric recommendation, the available metrics can be broadly classified as follows (see also [9]):

- **Counting metrics** operate directly on the confusion matrix and express the metric value as a function of the cardinalities. In the context of segmentation, they are typically referred to as **overlap-based** metrics [58]. We distinguish **multi-class counting metrics**, which are defined for an arbitrary number of classes and invariant under class order, from **per-class counting metrics**, which are computed by treating one class as foreground/positive class and all other classes as background. Popular examples for the former include Matthews Correlation Coefficient (MCC) or Accuracy, while examples for the latter are Sensitivity, Specificity and DSC.
- **Multi-threshold metrics** operate on a dynamic confusion matrix, reflecting the conflicting properties of interest, such as high Sensitivity and high Specificity. Popular examples include the Area under the Receiver Operating Characteristic Curve (AUROC) and Average Precision (AP).
- **Distance-based metrics** have been designed for semantic and instance segmentation tasks. They operate exclusively on the TPs and rely on the explicit definition of object boundaries. Popular examples are the Hausdorff Distance (HD) and the Normalized Surface Distance (NSD).

Depending on the context (e.g., image-level classification vs. semantic segmentation task) and the community (e.g., medical imaging community vs. computer vision community), identical metrics are referred to with different terminology. For example, Sensitivity, True Positive Rate (TPR) and Recall refer to the same concept. The same holds true for the DSC and the  $F_1$  Score. The most relevant metrics for the problem categories in the scope of this paper are introduced in the following.

Most metrics are recommended to be applied per class (except for the multi-class counting metrics), meaning that a potential multi-class problem is converted to multiple binary classification problems, such that each relevant class serves as the positive class once. This results in different confusion matrices depending on which class is used as the positive class.

### 1.1 Image-level Classification

**Image-level classification** refers to the process of assigning one or multiple labels, or *classes*, to an image. Modern algorithms usually output **predicted class scores** (or continuous class scores) between 0 and 1 for every image and class, indicating the probability of the image belonging

to a specific class. By introducing a threshold (e.g., 0.5), predictions are considered as positive (e.g., cancer = true) if they are above the threshold, or negative if they are below the threshold. Subsequently, predictions are assigned to the cardinalities (e.g., a cancer patient with prediction cancer = true is considered as TP) [15]. The most popular classification metrics are counting metrics, operating on a confusion matrix with fixed threshold on the class probabilities, and multi-threshold metrics, as detailed in the following.

**Counting metrics.** As stated previously, counting metrics rely on the confusion matrix. We distinguish between per-class and multi-class counting metrics. Popular multi-class counting metrics include:

**Accuracy** [60]: Fig. SN 3.38

**Balanced Accuracy (BA)** [60]: Fig. SN 3.39

**Expected Cost (EC)** (also referred to as Expected Prediction Error or Expected Loss) [7, 24, 32]: Fig. SN 3.42

**Matthews Correlation Coefficient (MCC)** (also referred to as Phi Coefficient) [46]: Fig. SN 3.46

**Weighted Cohen's Kappa (WCK)** (also referred to as Weighted Cohen's Kappa Coefficient, Weighted Kappa Statistic or Weighted Kappa Score) [13]: Fig. SN 3.54

Popular per-class counting metrics include:

**$F_\beta$  Score** [12, 63]: Fig. SN 3.43

**Net Benefit (NB)** [64]: Fig. SN 3.47

**Negative Predictive Value (NPV)** [60]: Fig. SN 3.48

**Positive Predictive Value (PPV)** (also referred to as Precision) [60]: Fig. SN 3.51

**Sensitivity** (also referred to as Recall, TPR or Hit Rate) [60]: Fig. SN 3.52

**Specificity** (also referred to as Selectivity or True Negative Rate (TNR)) [60]: Fig. SN 3.53

**Multi-threshold metrics.** The classical counting metrics presented above rely on fixed thresholds to be set on the predicted class probabilities (if available), resulting in them being based on the cardinalities of the confusion matrix. **Multi-threshold metrics** overcome this limitation by calculating metric scores based on multiple thresholds. Popular examples are:

**Area under the Receiver Operating Characteristic Curve (AUROC)** (also referred to as Area under the Curve (AUC), AUC - ROC (Area under the Curve - Receiver Operating Characteristics), C-Index, C-Statistics) [31]: Fig. SN 3.55

**Average Precision (AP)** [23, 42]: Fig. SN 3.56

**Calibration metrics.** While most research in biomedical image analysis focuses on the discrimination capabilities of classifiers, a complementary property of relevance is the *calibration* of predicted class scores (also known as *confidence scores*). Intuitively speaking, a system is well-calibrated if the predicted class scores (i.e., the output of the model) reflect the true probabilities of the outcome. In practice, this means that calibrated scores match the empirical success rate of associated predictions. For a binary classification task, calibration implies that of all the data samples assigned a predicted score of 0.8 for the positive class, empirically, 80% belong to this class. Popular examples are:

**Brier Score (BS)** [26]: Fig. SN 3.64

**Class-Wise Calibration Error (CWCE)** [40, 41]: Fig. SN 3.65

**Expected Calibration Error (ECE)** [47]: Fig. SN 3.66

**Expected Calibration Error Kernel Density Estimate (ECE<sup>KDE</sup>)** [52]: Fig. SN 3.67  
**Kernel Calibration Error (KCE)** [28, 68]: Fig. SN 3.68  
**Negative Log Likelihood (NLL)** [14]: Fig. SN 3.69  
**Root Brier Score (RBS)** [28]: Fig. SN 3.70

## 1.2 Semantic Segmentation

**Semantic segmentation** is commonly defined as the process of partitioning an image into multiple segments/regions. To this end, one or multiple labels are assigned to every pixel such that pixels with the same label share certain characteristics. Semantic segmentation can therefore also be regarded as pixel-level classification. As in image-classification problems, predicted class probabilities are typically calculated for each pixel, deciding on the class affiliation based on a threshold over the class scores [1]. In semantic segmentation problems, the pixel-level classification is typically followed by a post-processing step, in which connected components are defined as objects, and object boundaries are created accordingly. Semantic segmentation metrics can roughly be classified into: (1) counting metrics or overlap-based metrics, for measuring the overlap between the reference annotation and the prediction of the algorithm, (2) distance-based or boundary-based metrics, for measuring the distance between object boundaries, and (3) problem-specific metrics, measuring, for example, object volumes.

**Counting metrics.** The most frequently used segmentation metrics are **counting metrics**. In the context of segmentation they are also referred to as **overlap-based metrics**, as they essentially measure the overlap between a reference mask and the algorithm prediction. Popular examples of overlap-based metrics include:

**Dice Similarity Coefficient (DSC)** (also referred to as Sørensen–Dice Coefficient,  $F_1$  Score, Balanced F Score) [20]: Fig. SN 3.41  
**Intersection over Union (IoU)** (also referred to as Jaccard Index, Tanimoto Coefficient) [35]: Fig. SN 3.45  
**centerline Dice Similarity Coefficient (cIDice)** [57]: Fig. SN 3.40

**Distance-based metrics.** Overlap-based metrics are often complemented by **distance-based metrics** that operate exclusively on the TPs and compute one or several distances between the reference and the prediction. Besides few exceptions, distance-based metrics are often **boundary-based metrics** which focus on assessing the accuracy of object boundaries. Popular examples include:

**Average Symmetric Surface Distance (ASSD)** (also referred to as Weighted Bilateral Mean Contour Distance) [70]: Fig. SN 3.58  
**Boundary Intersection over Union (Boundary IoU)** [10]: Fig. SN 3.59  
**Hausdorff Distance (HD)** (also referred to as Maximum Symmetric Surface Distance, Hausdorff Metric, Pompeiu–Hausdorff Distance) [34]: Fig. SN 3.60  
**Hausdorff Distance 95th Percentile (HD95)** [34]: Fig. SN 3.63  
**Mean Average Surface Distance (MASD)** (also referred to as Mean Surface Distance) [6]: Fig. SN 3.61  
**Normalized Surface Distance (NSD)** (also referred to as Normalized Surface Dice, Surface Distance, Surface Dice, Surface DSC) [50]: Fig. SN 3.62

**Problem-specific segmentation metrics.** While overlap- and distance-based metrics are the standard metrics used by the general computer vision community, biomedical applications often have special domain-specific requirements. In medical imaging, for example, the actual volume of an object (e.g., a tumor) may be of particular interest. In this case, **volume metrics** such as the *Absolute* or *Relative Volume Error* and the *Symmetric Relative Volume Difference* can be computed [48].

### 1.3 Object Detection

**Object detection** refers to the detection of one or multiple objects (or: instances) of a particular class (e.g., lesion) in an image [42]. The following description assumes single-class problems, but translation to multi-class problems is straightforward, as validation for multiple classes on object level is performed individually per class. Notably, as multiple predictions and reference instances may be present in one image, the predictions need to include localization information, such that reference and predicted objects can be matched. Important design choices with respect to the validation of object detection methods include:

- (1) *How to represent an object?* Representation is typically composed of location information and a class affiliation. The former may for example take the form of a bounding box (i.e., a list of coordinates), a pixel mask, or the object's center point. Additionally, modern algorithms typically assign a confidence value to each object, representing the probability of a prediction corresponding to an actual object of the respective class. Note that a confusion matrix is later computed for a fixed threshold on the predicted class probabilities.<sup>1</sup>
- (2) *How to decide whether a reference instance was correctly detected?* This step is achieved by applying the *localization criterion*. A localization criterion may, for example, be based on comparing the object centers of the reference and prediction or computing their overlap.
- (3) *How to resolve assignment ambiguities?* The above step might lead to ambiguous matchings, such as two predictions being assigned to the same reference object. Several strategies exist for resolving such cases.

The following sections provide details on (1) applying the localization criterion, (2) applying the assignment strategy, and (3) computing the actual performance metrics.

**Localization criterion.** As one image may contain multiple objects or no object at all, the **localization criterion** or **hit criterion** measures the (spatial) similarity between a prediction (represented by a bounding box, pixel mask, center point or similar) and a reference object. It defines whether the prediction *hit/detected* (TP) or *missed* (FP) the reference. Any reference object not detected by the algorithm is defined as FN. Please note that TNs are not defined for object detection tasks. Popular localization criteria include:

**Box/Approx Intersection over Union (IoU)** [35]: Fig. SN 3.74

**Mask IoU > 0** [35, 66]: Fig. SN 3.75

**Center Distance** [30]: Fig. SN 3.72

**Point inside Mask/ Box/ Approx**<sup>2</sup>: Fig. SN 3.76

<sup>1</sup>Please note that we will use the term confidence scores analogously to predicted class probabilities in the context of object detection and instance segmentation.

<sup>2</sup><https://cada.grand-challenge.org/Assessment/>

**Assignment strategy.** The localization criterion alone is not sufficient to extract the final confusion matrix based on a fixed threshold for the predicted class probabilities (confidence scores), as ambiguities can occur. For example, two predictions may have been assigned to the same reference object in the localization step, or vice versa. These ambiguities need to be resolved in a further **assignment step**. This assignment and thus the resolving of potential assignment ambiguities can be done via different strategies:

**Greedy (by Score) Matching** [23]: Fig. SN 3.77

**Optimal (Hungarian) Matching** [38]: Fig. SN 3.79

**Matching via Overlap > 0.5** [21]: Fig. SN 3.80

**Greedy (by Localization Criterion) Matching** [44]: Fig. SN 3.78

**Metric computation.** Similar to image-level classification and semantic segmentation algorithms, object detection algorithms are commonly assessed with counting metrics, assuming a fixed confusion matrix. Popular examples include:

**$F_\beta$  Score** [12, 63]: Fig. SN 3.43

**False Positives per Image (FPPI)** [5, 62]: Fig. SN 3.44

**Positive Predictive Value (PPV)** (also referred to as Precision) [60]: Fig. SN 3.51

**Sensitivity** (also referred to as Recall, TPR or Hit Rate) [60]: Fig. SN 3.52

Similarly, multi-threshold metrics rely on a range of thresholds. Popular examples are:

**Average Precision (AP)** [23, 42]: Fig. SN 3.56

**Free-Response Receiver Operating Characteristic (FROC) Score** [62]: Fig. SN 3.57

## 1.4 Instance Segmentation

In contrast to semantic segmentation, **instance segmentation** problems distinguish different instances of the same class (e.g., different lesions). Similarly to object detection problems, the task is to detect individual instances of the same class, but detection performance is measured by pixel-level correspondences (as in semantic segmentation problems). Optionally, instances can be applied to one of multiple classes. Validation metrics in instance segmentation problems often combine common detection metrics with segmentation metrics applied per instance. For instance, segmentation problems, we consider different localization criteria, namely:

*Localization criteria:*

**Boundary Intersection over Union (Boundary IoU)** [10]: Fig. SN 3.71

**Mask IoU** [35]: Fig. SN 3.74

**Intersection over Reference (IoR)** [45]: Fig. SN 3.73

*Additional counting metric:* If detection and segmentation performance should be assessed simultaneously in a single score, the **Panoptic Quality (PQ)** metric can be utilized [36]: Fig. SN 3.49.

It should be noted that instance segmentation problems are often phrased as semantic segmentation problems with an additional post-processing step, such as connected component analysis [55].

## SUPL. NOTE 2 METRIC PITFALLS

This section presents common limitations of image processing metrics related to [P1] an inadequate choice of problem category (Suppl. Note 2.1), [P2] poor metric selection (Suppl. Note 2.2) and [P3] poor metric application (Suppl. Note 2.3) in an illustrated manner.

To preserve visual clarity, the most important of the presented metric values may be highlighted with color. Green metric values correspond to a "good" metric value (e.g. a high *Sensitivity* score), whereas red values correspond to a "bad" value (e.g. a low *Sensitivity*). Green check marks indicate desirable behavior of metrics, red crosses indicate undesirable behavior. Please note that a low metric value is not automatically a "bad" score. A metric value should always be put into perspective and compared to inter-rater variability. For simplicity, we still use the terms "good" and "bad/poor" throughout the section. Finally, our illustrations do not provide the concrete class probabilities of the presented classifiers.

### 2.1 Pitfalls related to an inadequate choice of the problem category

Performance metrics are typically expected to reflect a domain-specific (e.g., clinical) validation goal. Previous research, however, suggests that this is often not the case [56]. Before choosing validation metrics, the correct problem category needs to be defined. In the following, we present pitfalls related to metrics not being applied to the appropriate problem category. These can either be associated with a wrong choice of the problem category (here: Figs. 3 and SN 2.1; more examples are provided in [54]) or the lack of a matching problem category (Fig. SN 2.2).

Assessing object detection performance at image level yields misleading results

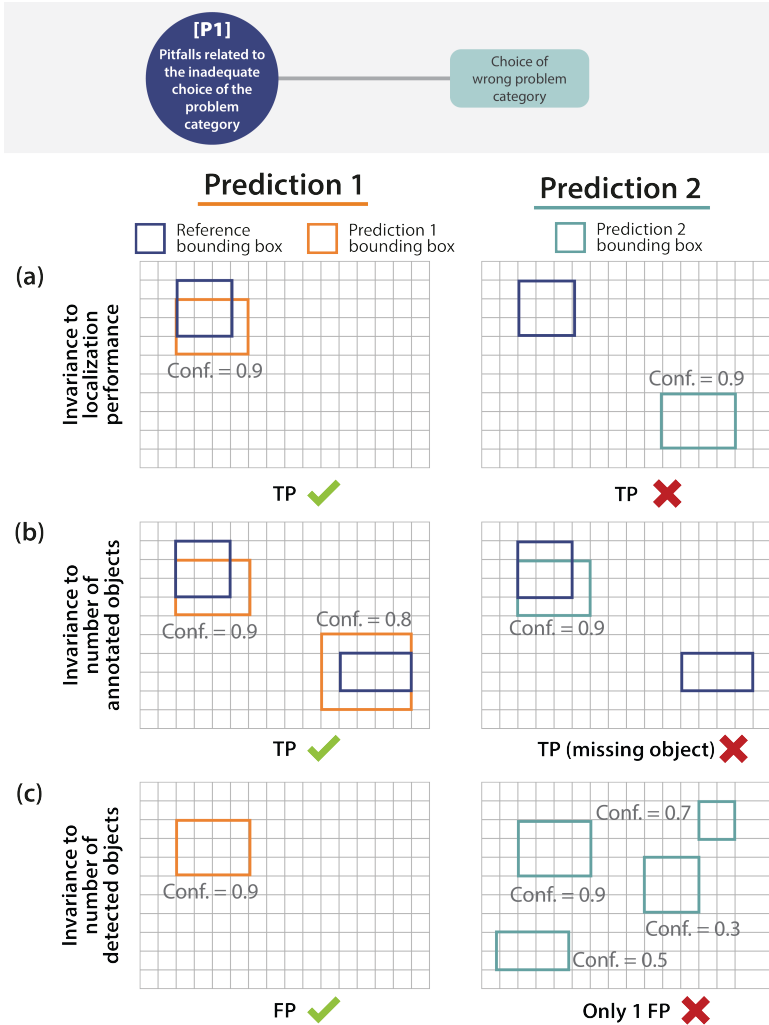


Fig. SN 2.1. Image-level classification metrics such as the Area under the Receiver Operating Characteristic Curve (AUROC) curve can be used to validate object detection models by first aggregating predictions to one image-level score (per class). This validation scheme discards the information on the object matching (localization, number of objects etc.). This leads to several problems: **(a)** The image-level Receiver Operating Characteristic (ROC) curve does not measure the localization performance. Both *Prediction 1* and *2* are considered as True Positive (TP) due to their score being very high, although *Prediction 2* does not hit the annotated object. **(b)** The image-level ROC is invariant to the number of annotated objects in an image. The curve does not discriminate between a model detecting all positives (*Prediction 1*) and a model detecting only one of the positives (*Prediction 2*), as long as the maximum score is the same. **(c)** The image-level ROC is invariant to the number of detections in an image. The curve does not discriminate between a model with many False Positives (FP) (*Prediction 2*), and a model with just one FP (*Prediction 1*), as long as the maximum score is the same. The class probabilities are represented by confidence scores (Conf.).

Common metrics may not reflect the domain interest

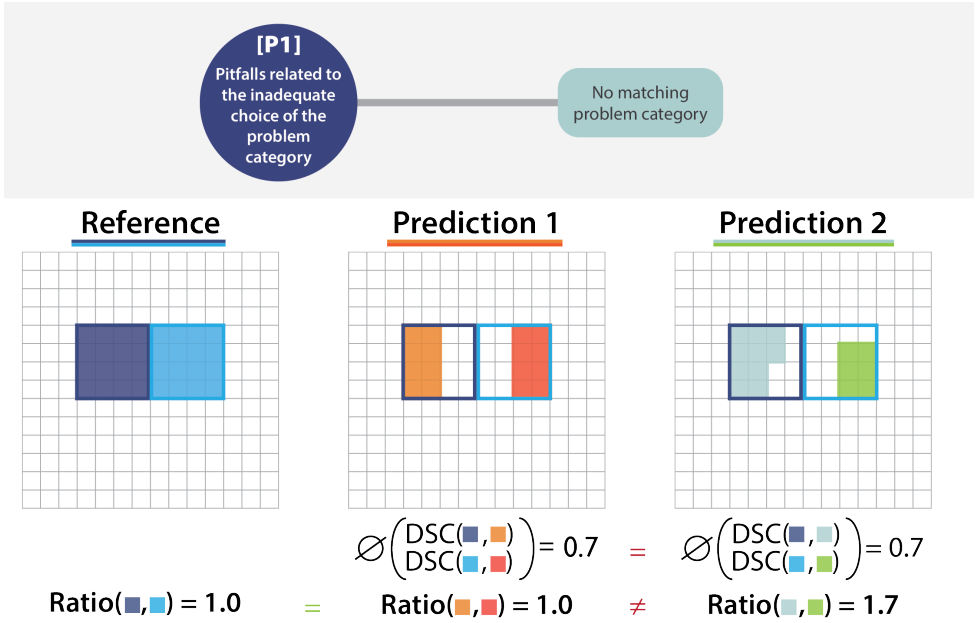


Fig. SN 2.2. In the absence of a matching problem category for the problem at hand, it may not be possible to find a common metric that ideally captures the domain interest. In this example, accuracy of the ratio between two volumes is the property of interest (e.g., the percentage of blood volume ejected in each cardiac cycle [4]). Using overlap-based segmentation metrics (here: Dice Similarity Coefficient (DSC)) to measure the volumetric ratio may be misleading. *Predictions 1* and *2* result in similar averaged DSC metric values although they result in a different ratio between structure volumes, which is the parameter of interest.  $\emptyset$  refers to the average DSC values.

## 2.2 Pitfalls related to poor metric selection

Validation metrics typically assess a specific property of interest. Thus, a metric designed for a particular purpose often cannot be used to appropriately validate another property. This is due to both the limitations as well as the mathematical properties of individual metrics, both of which are often neglected. In this section, we present pitfalls related to poor metric selection.

*2.2.1 Pitfalls related to disregard of the domain interest.* Several requirements for metric selection arise from the domain interest, which may clash with particular metric limitations. In the following, we present pitfalls related to disregard of the domain interest, stemming from the following sources:

- Importance of structure boundaries (Figs. 4a and SN 2.3)
- Importance of structure volume (Fig. SN 2.4)
- Importance of structure center(line) (Fig. SN 2.5)
- Importance of confidence awareness (Fig. SN 2.6)
- Importance of comparability across data sets (Figs. SN 2.7)
- Unequal severity of class confusions (Figs. 4b and SN 2.8)
- Importance of cost-benefit analysis (Fig. SN 2.9)

Volume-based metrics alone are inadequate for assessing performance

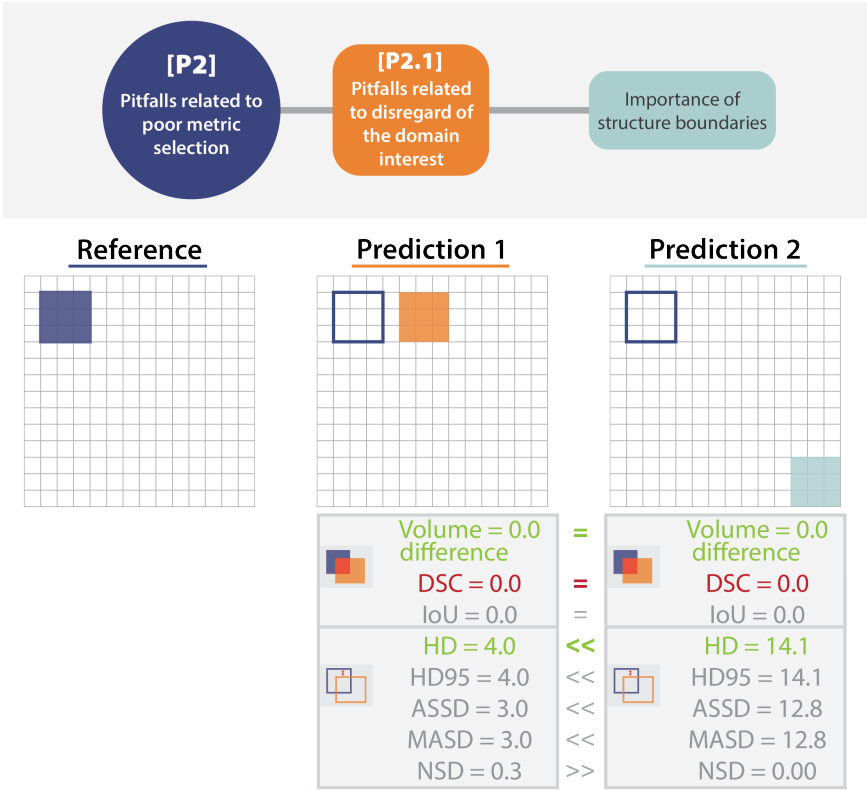
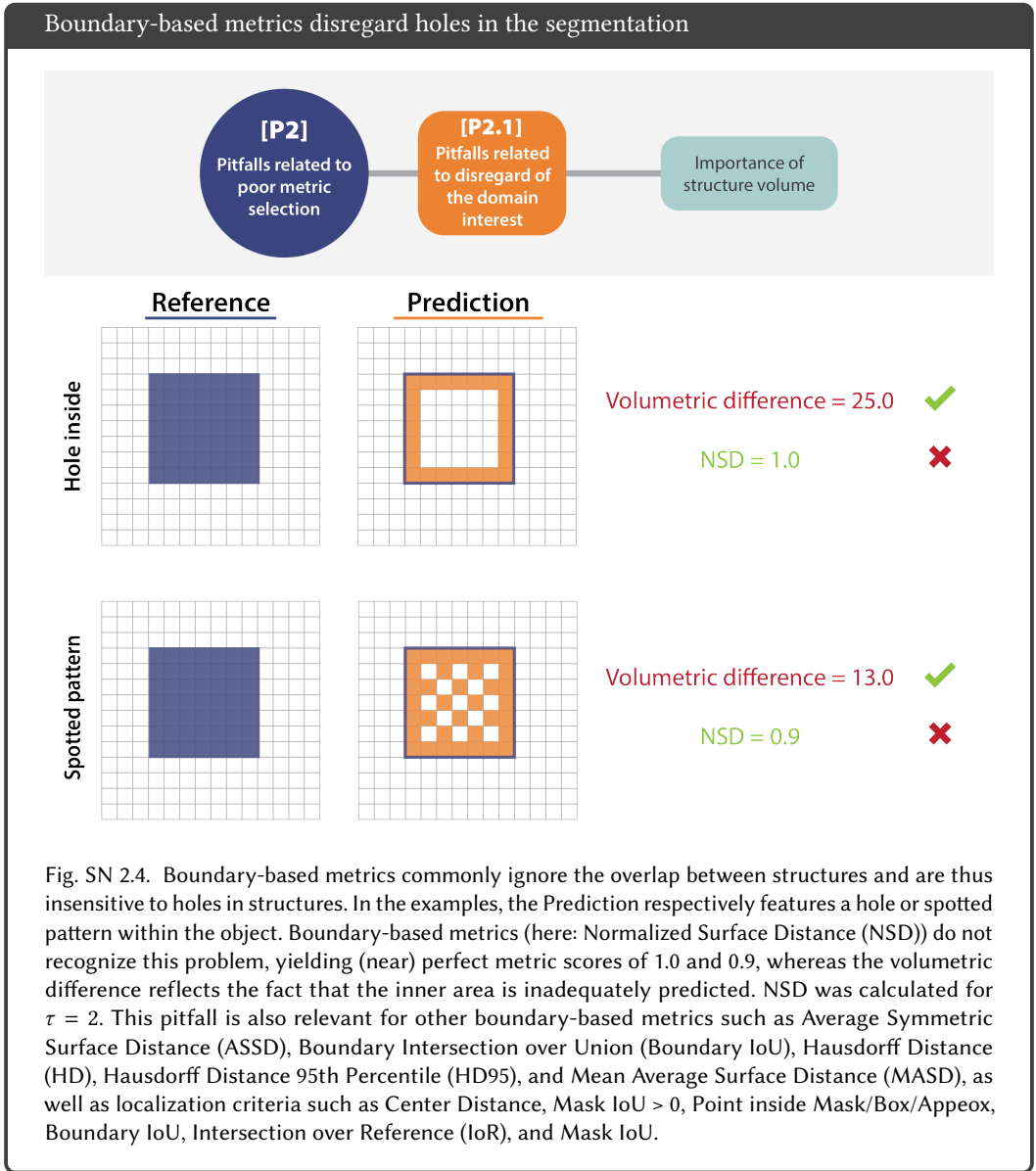


Fig. SN 2.3. Effect of only focusing on object volume. Both *Predictions 1* and *2* result in the correct volume difference of 0, but do not overlap the reference (Dice Similarity Coefficient (DSC) and Intersection over Union (IoU) of 0). Only the boundary-based measures (Hausdorff Distance (HD), Hausdorff Distance 95th Percentile (HD95), Average Symmetric Surface Distance (ASSD), Mean Average Surface Distance (MASD), and Normalized Surface Distance (NSD)) recognize the mislocalization. This pitfall is also relevant for localization criteria such as Box/Approx/Mask IoU, Center Distance, Mask IoU > 0, Point inside Mask/Box/Approx, and Intersection over Reference (IoR) .



## Overlap-based metrics are unaware of object centers

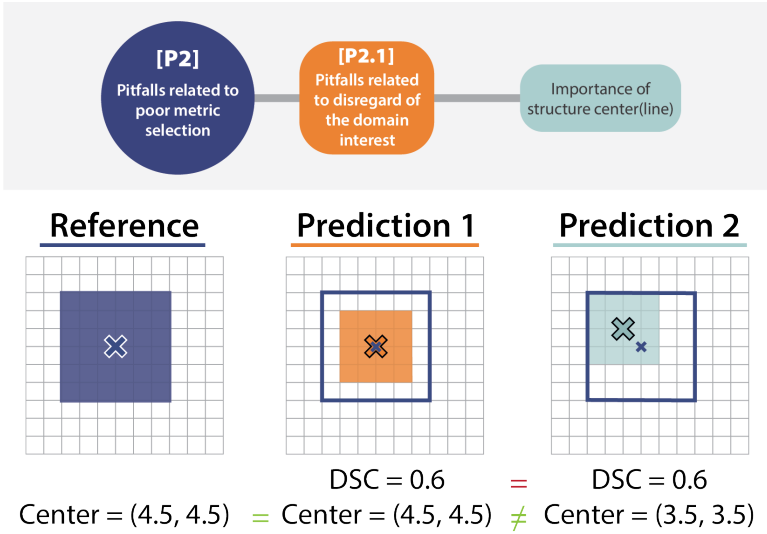


Fig. SN 2.5. The most common counting-based metrics are poor proxies for the center point alignment. Here, *Predictions 1* and *2* yield the same Dice Similarity Coefficient (DSC) value although *Prediction 1* approximates the location of the object much better. This pitfall is also relevant for other boundary- and overlap-based metrics such as Average Symmetric Surface Distance (ASSD), Boundary Intersection over Union (IoU), Hausdorff Distance (HD), Hausdorff Distance 95th Percentile (HD95), IoU, pixel-level  $F_\beta$  Score, and Mean Average Surface Distance (MASD), and localization criteria such as Box/Approx/Mask IoU, Mask IoU > 0, Point inside Mask/Box/Approx, Boundary IoU, and Intersection over Reference (IoR).

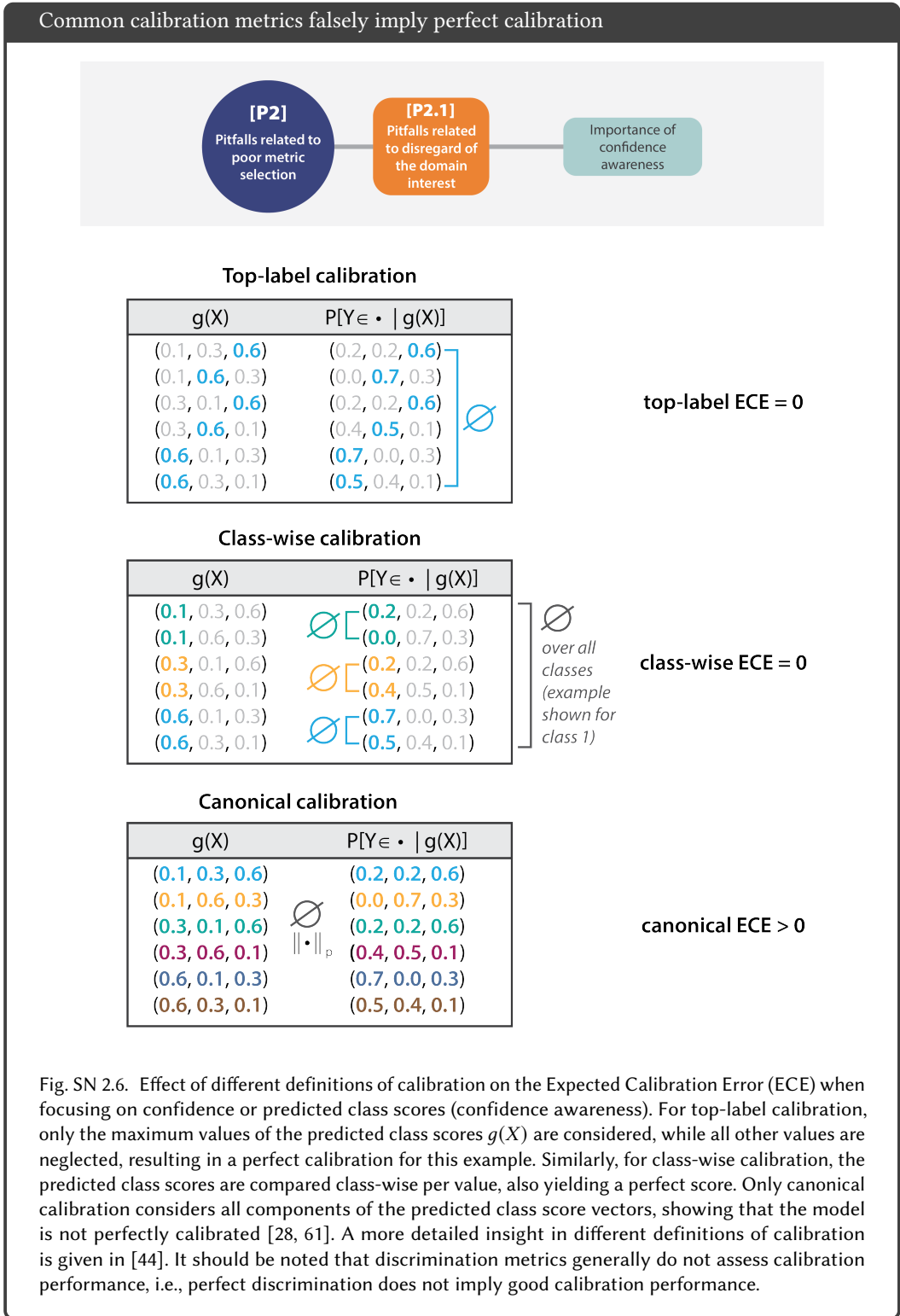
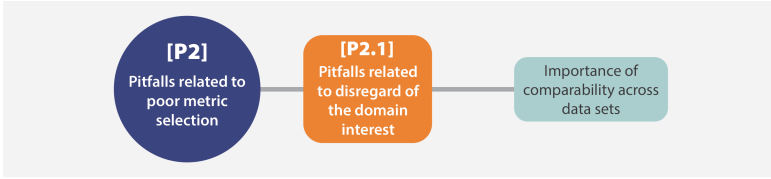


Fig. SN 2.6. Effect of different definitions of calibration on the Expected Calibration Error (ECE) when focusing on confidence or predicted class scores (confidence awareness). For top-label calibration, only the maximum values of the predicted class scores  $g(X)$  are considered, while all other values are neglected, resulting in a perfect calibration for this example. Similarly, for class-wise calibration, the predicted class scores are compared class-wise per value, also yielding a perfect score. Only canonical calibration considers all components of the predicted class score vectors, showing that the model is not perfectly calibrated [28, 61]. A more detailed insight in different definitions of calibration is given in [44]. It should be noted that discrimination metrics generally do not assess calibration performance, i.e., perfect discrimination does not imply good calibration performance.

Comparison of metric scores across data sets may be misleading



Inherent properties of a method:  $Sensitivity = 0.90$ ,  $Specificity = 0.80$

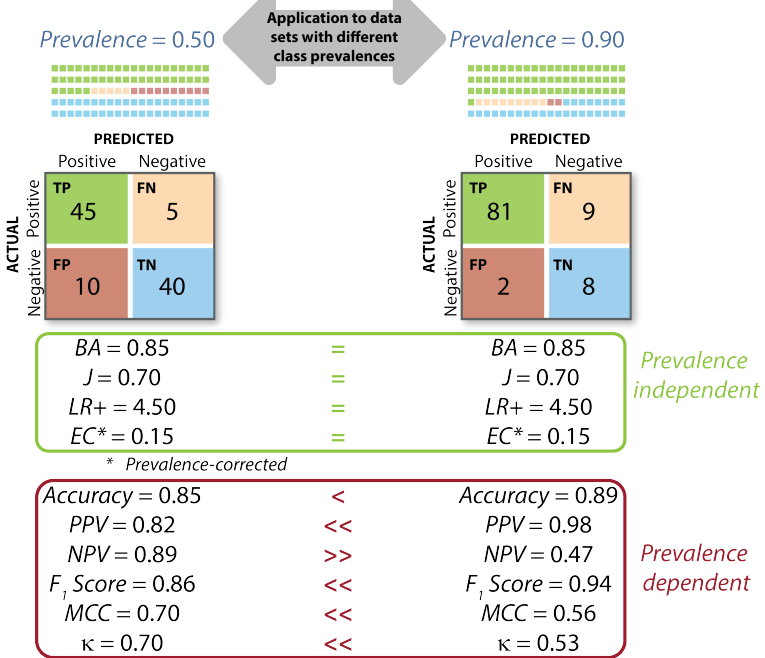
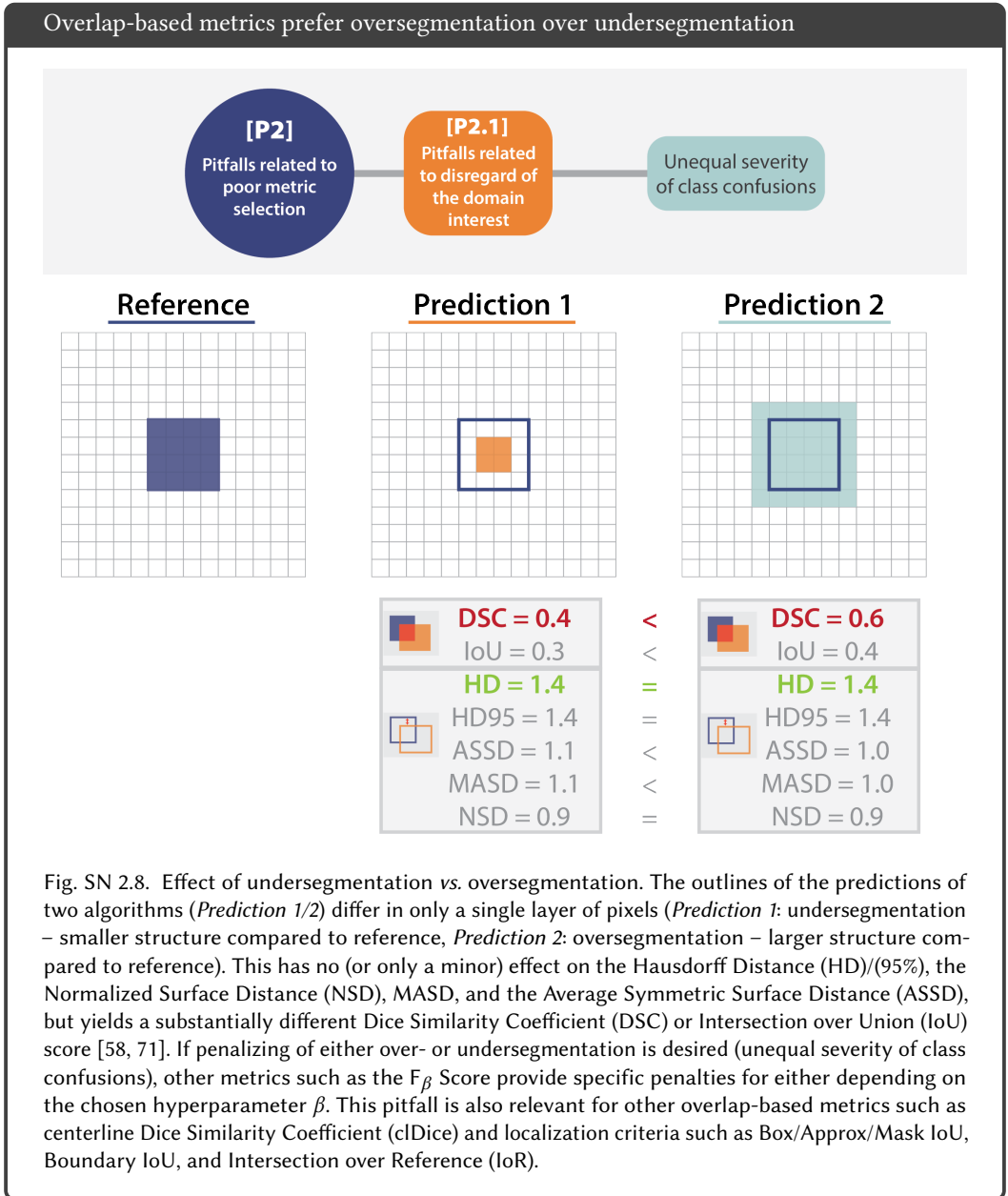
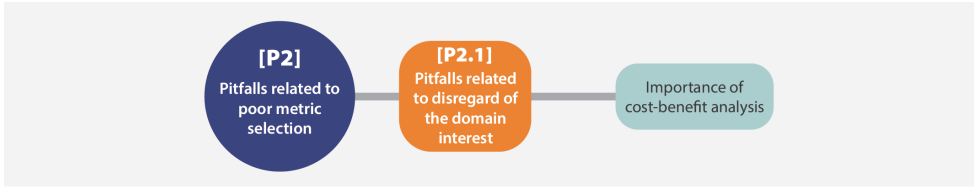


Fig. SN 2.7. Effect of prevalence dependency. An algorithm with specific inherent properties (here: Sensitivity of 0.9 and Specificity of 0.8) may perform completely differently on different data sets if the prevalences differ (here: 50% (left) and 90% (right)) and prevalence-dependent metrics are used for validation (here: Accuracy, Positive Predictive Value (PPV), Negative Predictive Value (NPV), F<sub>1</sub> Score, Matthews Correlation Coefficient (MCC), Cohen’s Kappa  $\kappa$ ). In contrast, prevalence-independent metrics (here: Balanced Accuracy (BA), Youden’s Index J, Positive Likelihood Ratio (LR+), and Expected Cost (EC)) can be used to compare validation results across different data sets. Used abbreviations: True Positive (TP), False Negative (FN), False Positive (FP) and True Negative (TN). This pitfall is also relevant for other counting metrics such as Net Benefit (NB).



Common metrics disregard cost-benefit analysis



**Cost-benefit analysis:**  
 ~9 unnecessary biopsies for one detected lesion are acceptable.

1) BIOPSY IN ALL PATIENTS:

		PREDICTED	
		Positive	Negative
ACTUAL	Positive	TP 30	FN 0
	Negative	FP 75	TN 0

Accuracy = 0.29

2) MARKER-BASED DECISION ON BIOPSY:

		PREDICTED	
		Positive	Negative
ACTUAL	Positive	TP 20	FN 15
	Negative	FP 60	TN 10

Accuracy = 0.29

=

75 unnecessary biopsies (FP)



60 unnecessary biopsies (FP)

NB metrics relate the benefit of TPs with the cost of FPs  
 (here: 1/9 based on benefit-cost analysis)

NB = 0.21

>

NB = 0.13

Same Accuracy, but better clinical utility

Same Accuracy, but poorer clinical utility

Fig. SN 2.9. Effect of neglecting a cost-benefit analysis. In a cost-benefit analysis, clinicians are able to define a risk-specific exchange rate that is used in the computation of the Net Benefit (NB) metric. Common metrics such as Accuracy do not consider this analysis and would favor the marker-based decision on biopsy, while NB indicates that biopsies of all patients actually yield a better clinical outcome [65]. This pitfall is also relevant for other counting metrics such as Balanced Accuracy (BA), Positive Likelihood Ratio (LR+), Matthews Correlation Coefficient (MCC), Negative Predictive Value (NPV), Positive Predictive Value (PPV), Sensitivity, and Specificity. For binary problems, the hyperparameter  $\beta$  of the  $F_\beta$  Score can be used as a dynamic penalty for class confusions.

*2.2.2 Pitfalls related to disregard of the properties of the target structure.* For problems that require capturing local properties (object detection, semantic or instance segmentation), the properties of the target structures to be localized and/or segmented may have severe implications for metric choice. Pitfalls can be further subdivided into *size-related* and *shape- and topology-related* pitfalls. In the following, we present pitfalls stemming from the following sources:

**Size-related pitfalls:**

- Small structure sizes (Extended Data Fig. 1a and Fig. SN 2.10)
- High variability of structure sizes (Fig. SN 2.11)

**Shape- and topology-related pitfalls**

- Complex structure shapes (Extended Data Fig. 1b and Fig. SN 2.12)
- Occurrence of overlapping or touching structures (Fig. SN 2.13)
- Occurrence of disconnected structures (Fig. SN 2.14)

Common localization criteria and overlap-based metrics are sensitive to structure sizes

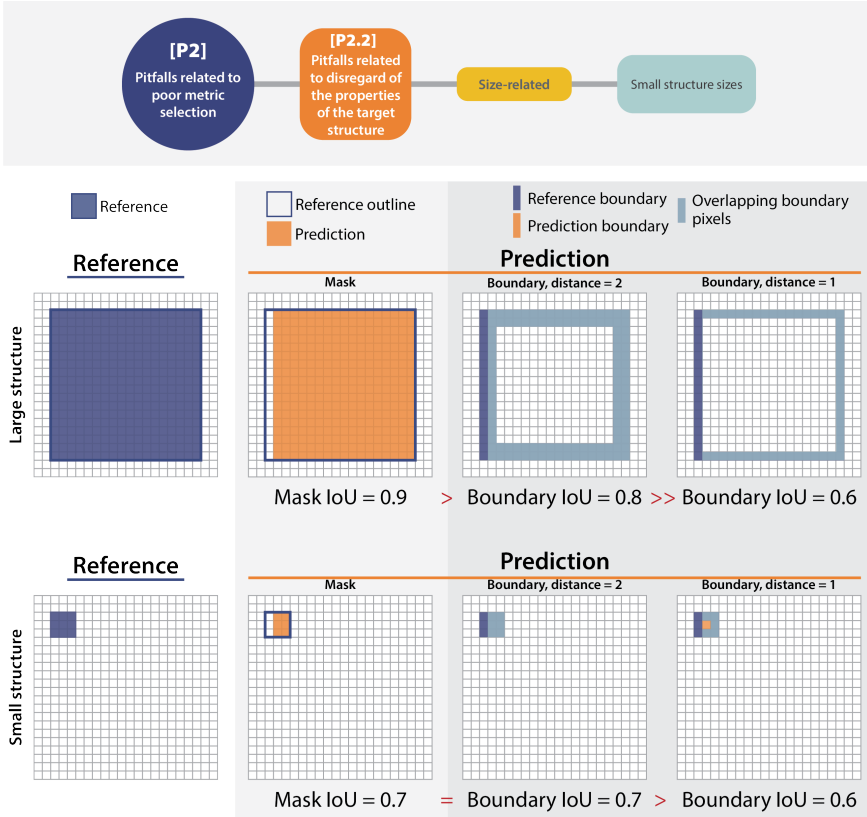
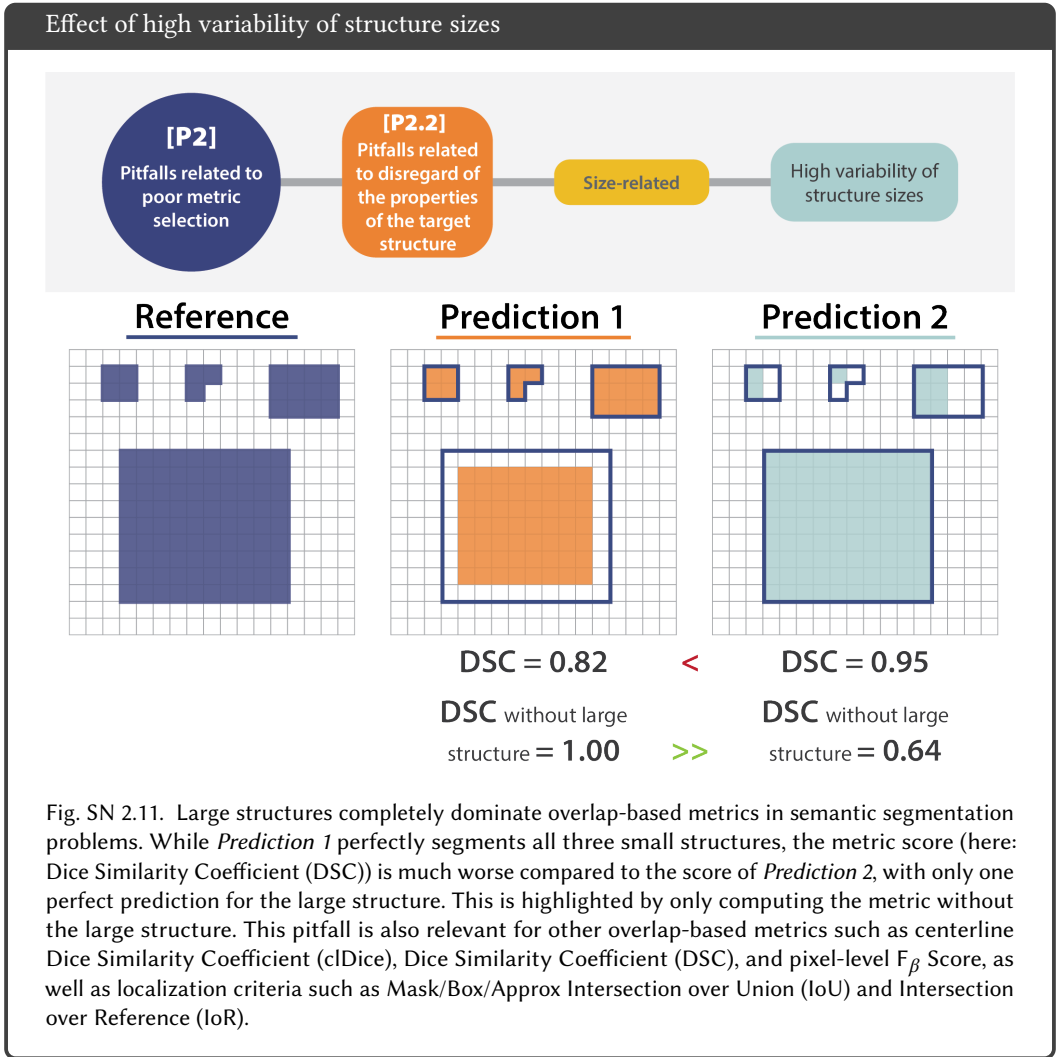


Fig. SN 2.10. Comparison of Mask and Boundary Intersection over Union (IoU) localization criteria in the case of particular importance of structure boundaries. Overlapping pixels from the reference and prediction are shown in light blue. The Mask IoU (second column) is less sensitive to boundary errors for large objects. The Boundary IoU (third and fourth column) especially considers contours, (1) yields smaller metric scores, thus penalizing errors in the boundaries, and (2) is more invariant to structure sizes, leading to very similar values for large and small structures (fourth column) [10]. This pitfall is also relevant for other overlap-based metrics such as centerline Dice Similarity Coefficient (cIDice), Dice Similarity Coefficient (DSC), and pixel-level  $F_{\beta}$  Score, as well as localization criteria such as Box/Approx IoU and Intersection over Reference (IoR).



## Common metrics are unaware of object shapes

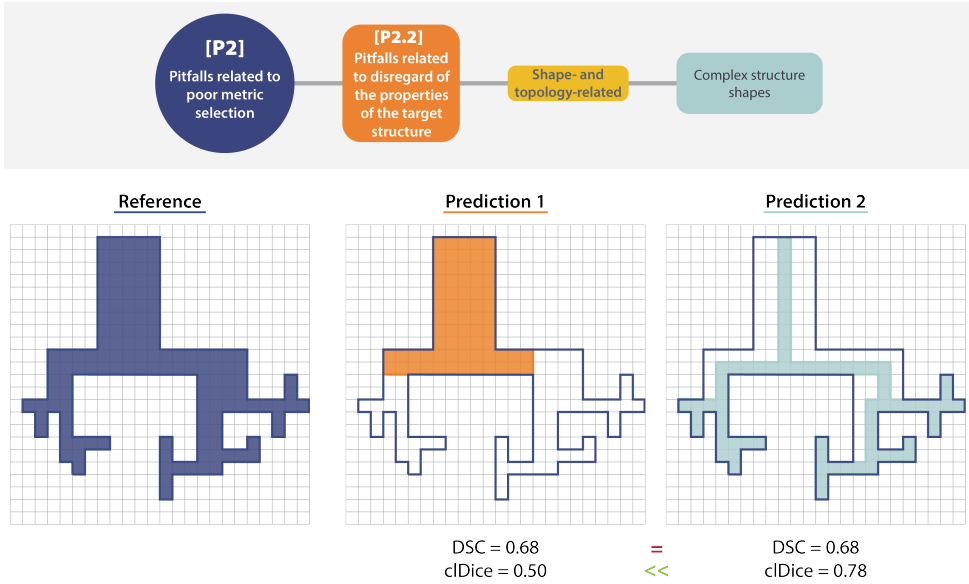
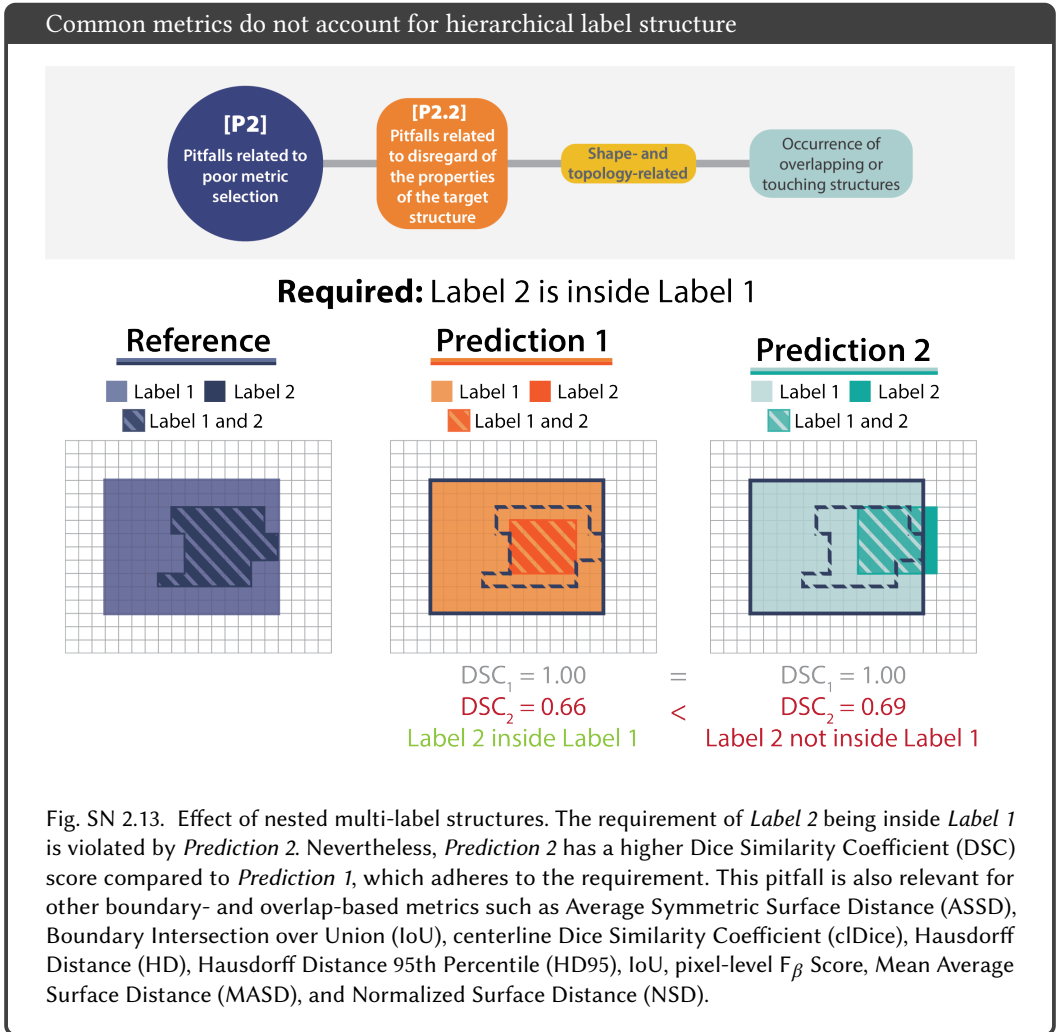


Fig. SN 2.12. Effect of complex shapes. Common overlap-based metrics such as the Dice Similarity Coefficient (DSC) are unaware of complex structure shapes and treat *Predictions 1* and *2* equally. The centerline Dice Similarity Coefficient (cDice) uncovers that *Prediction 1* misses the fine-granular branches of the reference and favors *Prediction 2*, which focuses on the object's center line and better captures its fine branches. This pitfall is also relevant for other overlap-based metrics such as Intersection over Union (IoU) and pixel-level  $F_{\beta}$  Score, and localization criteria such as Box/Approx/Mask IoU, Center Distance, Mask IoU > 0, Point inside Mask/Box/Approx, and Intersection over Reference (IoR).



Bounding boxes are inadequate for representing complex shapes and disconnected structures

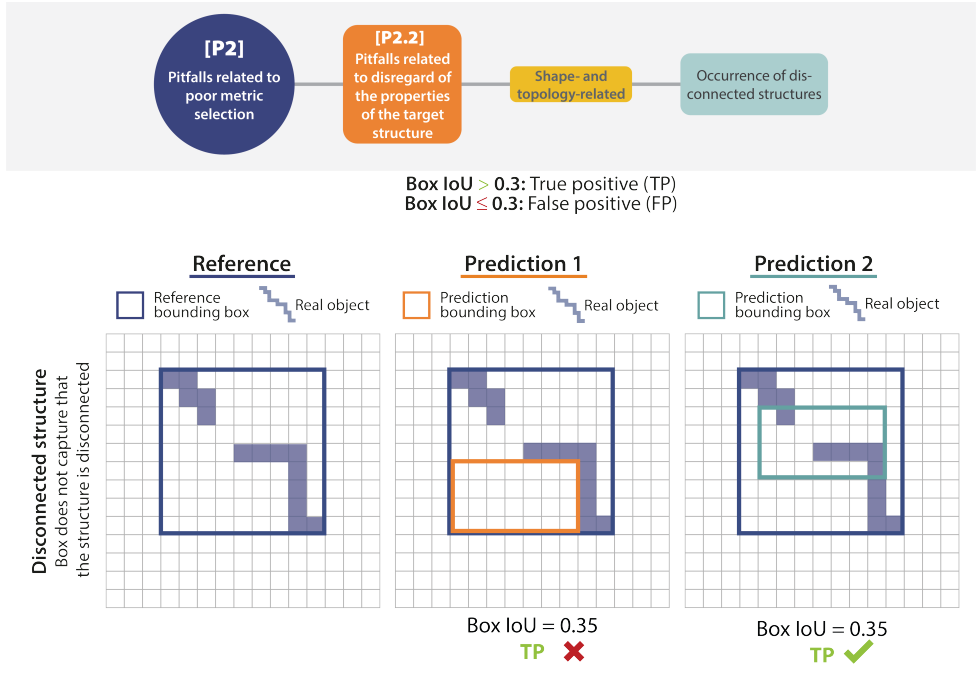


Fig. SN 2.14. Bounding boxes are not well-suited for representing disconnected shapes, in particular multi-component structures. *Predictions 1* and *2* both yield a True Positive (TP) detection, as the Box Intersection over Union (IoU) is larger than the threshold 0.3. However, *Prediction 1* does not hit the real object at all.

2.2.3 *Pitfalls related to disregard of the properties of the data set and algorithm output.* Properties of the data set such as class imbalances or high inter-rater variability may directly affect metric values. Pitfalls can be further subdivided into *class-related* and *reference-related* pitfalls. For reference-based metrics, the algorithm output will be compared against the reference annotation to compute a metric score. Thus, the content and format of the prediction is of high relevance for metric choice. In the following, we present pitfalls stemming from the following sources:

**[P2.3] Disregard of the properties of the data set**

- High class imbalance (Figs. 5a and SN 2.15)
- Small test set size (Figs. 5b and SN 2.16)
- Imperfect reference standard (Figs. 5c and SN 2.17)

**[P2.4] Disregard of the properties of the algorithm output**

- Possibility of empty prediction (Extended Data Fig. 2b and Fig. SN 2.18)
- Possibility of overlapping predictions (Extended Data Fig. 2a and Fig. SN 2.19)
- Lack of predicted class scores (Fig. SN 2.20)

Common metrics yield implausible results in the presence of class imbalance

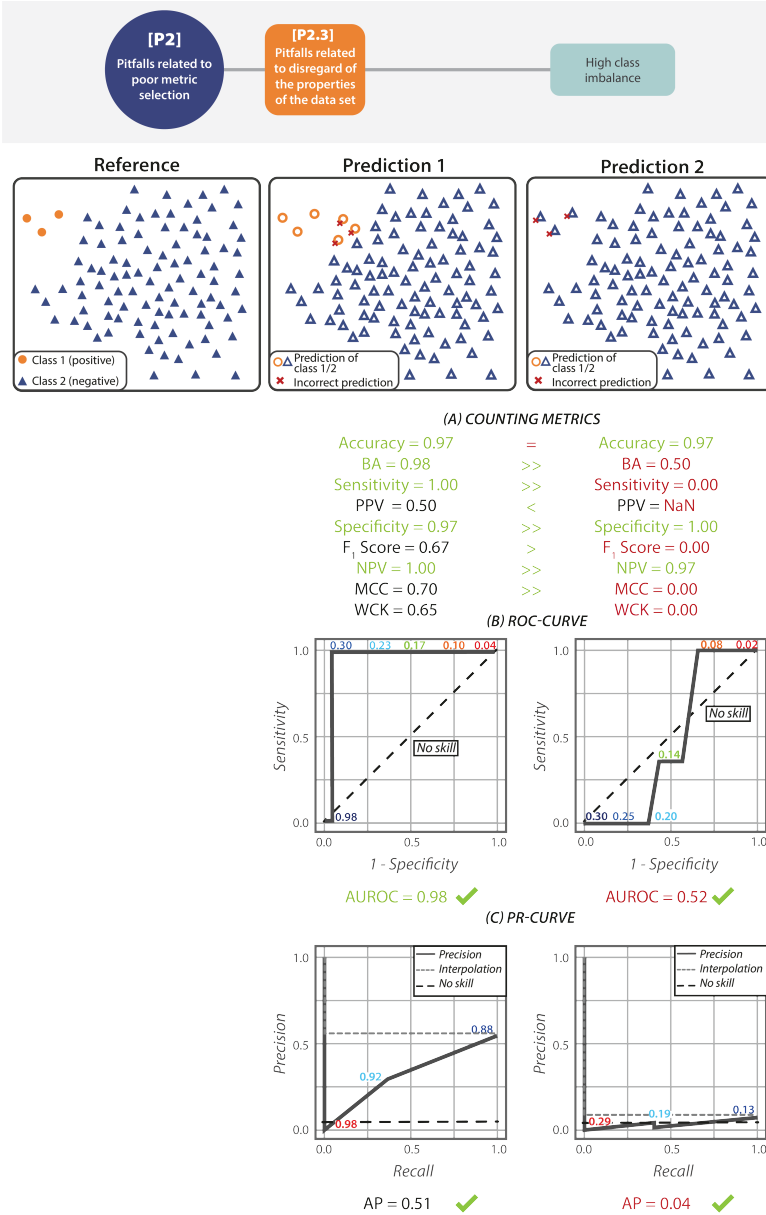


Fig. SN 2.15. Effect of class imbalance. Not every metric is designed to reflect class imbalance [11]. In the case of underrepresented classes, an unsuitable metric, such as Accuracy, yields a high value even if the classifier performs very poorly for one of the classes (here: *Prediction 2*). Multi-threshold metrics, such as the Area under the Receiver Operating Characteristic Curve (AUROC) and the Average Precision (AP), reveal the weakness, indicating that *Prediction 2* is not better than random guessing. For comparison, a no-skill classifier (random guessing) is shown as a black dashed line. For the Precision-Recall (PR) curves, the interpolation applied to compute the AP metric is shown as a dashed grey line. Thresholds used for curve generation are provided as small numbers above the curve. Further abbreviations: Positive Predictive Value (PPV), Negative Predictive Value (NPV), Matthews Correlation Coefficient (MCC), Weighted Cohen’s Kappa (WCK). This pitfall is also relevant for other counting metrics such as Net Benefit (NB).

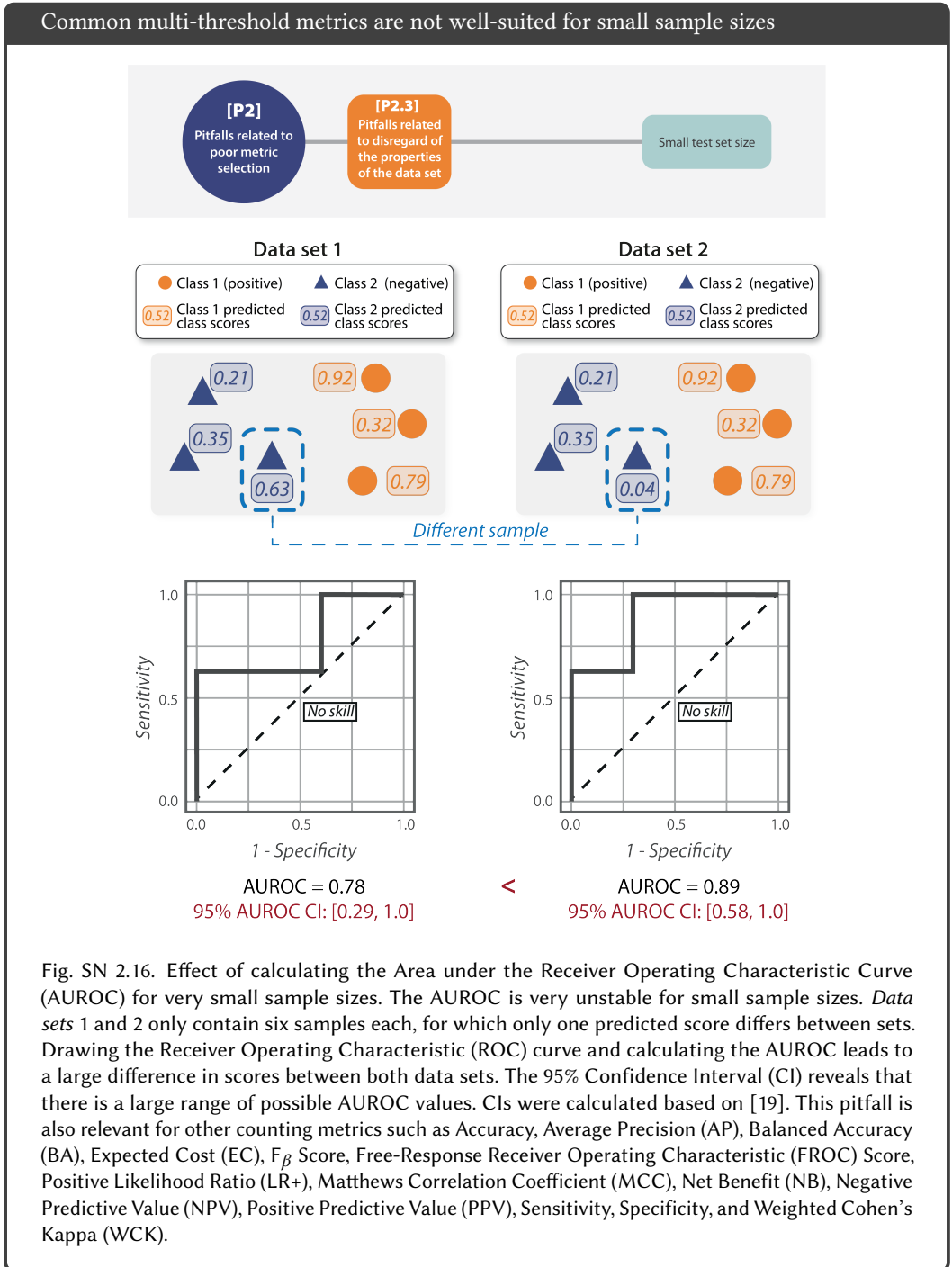


Fig. SN 2.16. Effect of calculating the Area under the Receiver Operating Characteristic Curve (AUROC) for very small sample sizes. The AUROC is very unstable for small sample sizes. *Data sets 1 and 2* only contain six samples each, for which only one predicted score differs between sets. Drawing the Receiver Operating Characteristic (ROC) curve and calculating the AUROC leads to a large difference in scores between both data sets. The 95% Confidence Interval (CI) reveals that there is a large range of possible AUROC values. CIs were calculated based on [19]. This pitfall is also relevant for other counting metrics such as Accuracy, Average Precision (AP), Balanced Accuracy (BA), Expected Cost (EC),  $F_\beta$  Score, Free-Response Receiver Operating Characteristic (FROC) Score, Positive Likelihood Ratio (LR+), Matthews Correlation Coefficient (MCC), Net Benefit (NB), Negative Predictive Value (NPV), Positive Predictive Value (PPV), Sensitivity, Specificity, and Weighted Cohen’s Kappa (WCK).

## Common metrics do not account for inter-rater variability

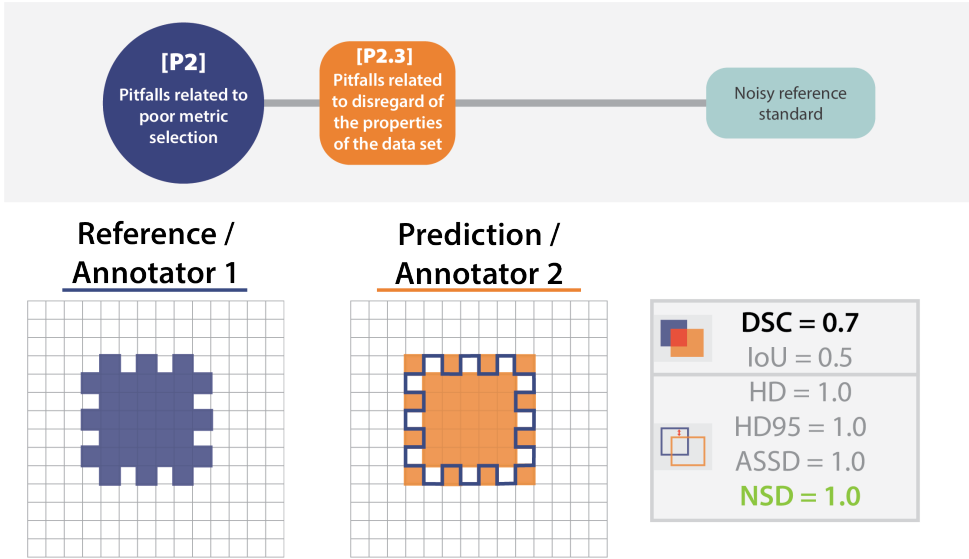
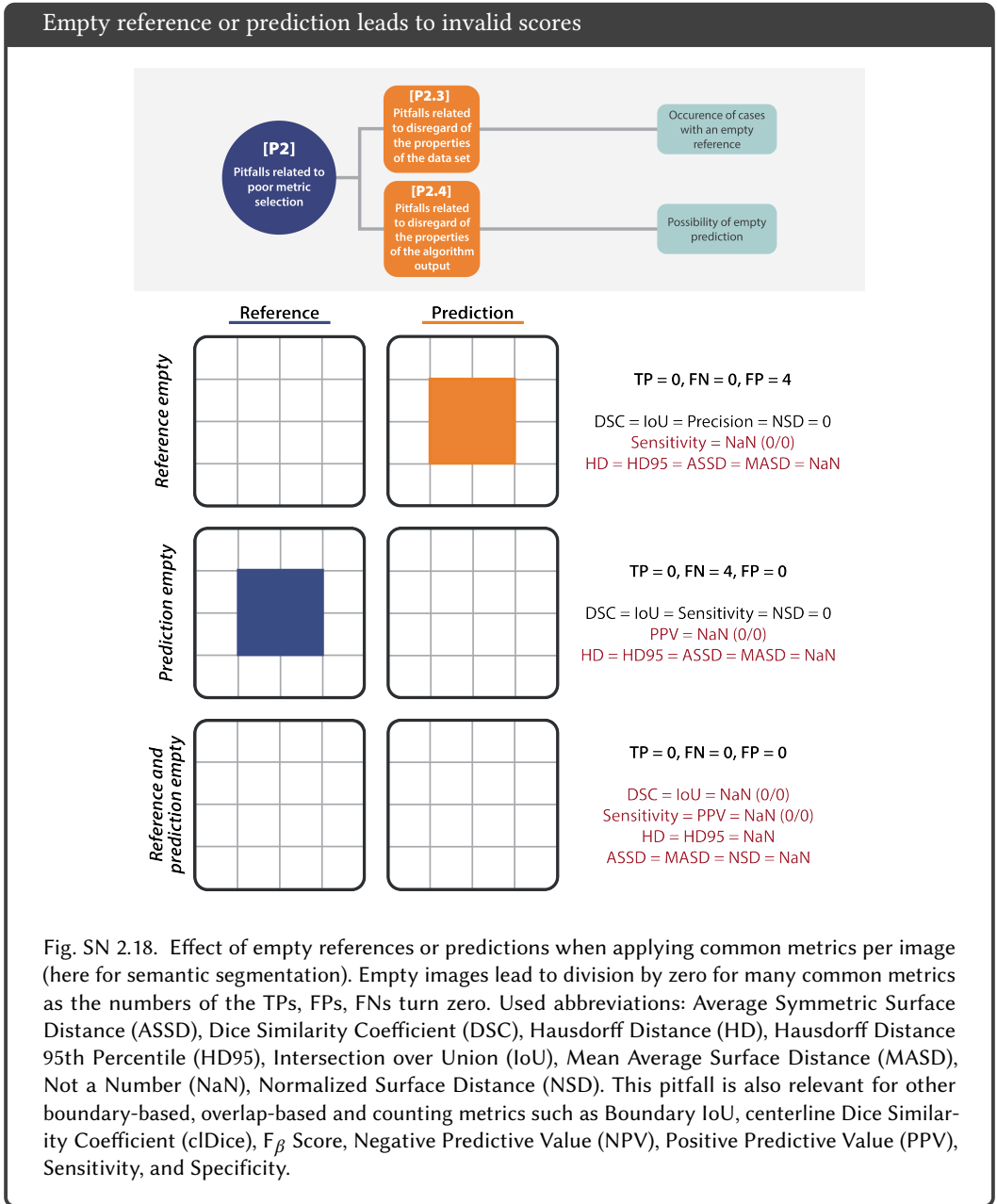


Fig. SN 2.17. Effect of inter-rater variability between two annotators. Assessing the performance of *Annotator 2* while using a reference annotation created by *Annotator 1* leads to a low Dice Similarity Coefficient (DSC) score because inter-rater variability is not taken into account by common overlap-based metrics. In contrast, the Normalized Surface Distance (NSD), applied with a threshold of  $\tau = 1$ , captures this variability. It should be noted, however, that this effect occurs primarily in small structures as overlap-based metrics tend to be robust to variations in the object boundaries in large structures. Further abbreviations: Intersection over Union (IoU), Hausdorff Distance (HD), Hausdorff Distance 95th Percentile (HD95), Average Symmetric Surface Distance (ASSD), Mean Average Surface Distance (MASD). This pitfall is also relevant for other boundary- and overlap-based metrics Boundary IoU, centerline Dice Similarity Coefficient (clDice), pixel-level  $F_\beta$  Score and Mean Average Surface Distance (MASD) and localization criteria such as Mask IoU  $> 0$ , Point inside Mask, Boundary IoU, IoR, and Mask IoU.



## Common segmentation metrics are not well-suited for overlapping structures

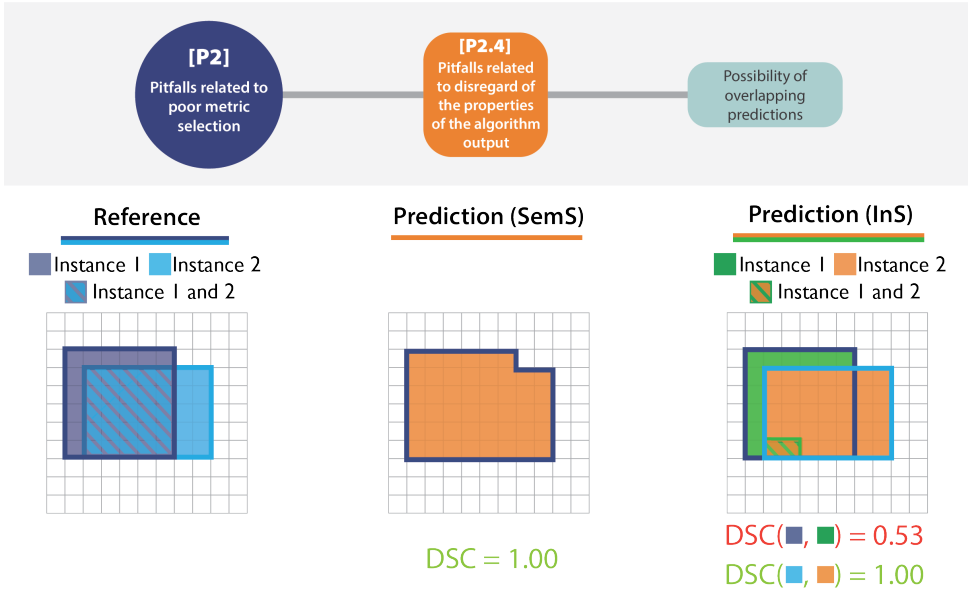


Fig. SN 2.19. Effect of overlapping predictions in segmentation problems. In semantic segmentation problem (SemS; right), overlapping predictions are merged into a single object, yielding a perfect metric score. Phrasing the problem as an instance segmentation problem reveals that the dark blue instance is not well-approximated at all. This issue is not revealed by common metrics if only semantic segmentation is performed (here: Dice Similarity Coefficient (DSC)). This pitfall is also relevant for other boundary- and overlap-based metrics such as Average Symmetric Surface Distance (ASSD), Boundary Intersection over Union (IoU), centerline Dice Similarity Coefficient (cIDice), pixel-level  $F_\beta$  Score, Hausdorff Distance (HD), Hausdorff Distance 95th Percentile (HD95), IoU, Mean Average Surface Distance (MASD), and Normalized Surface Distance (NSD).

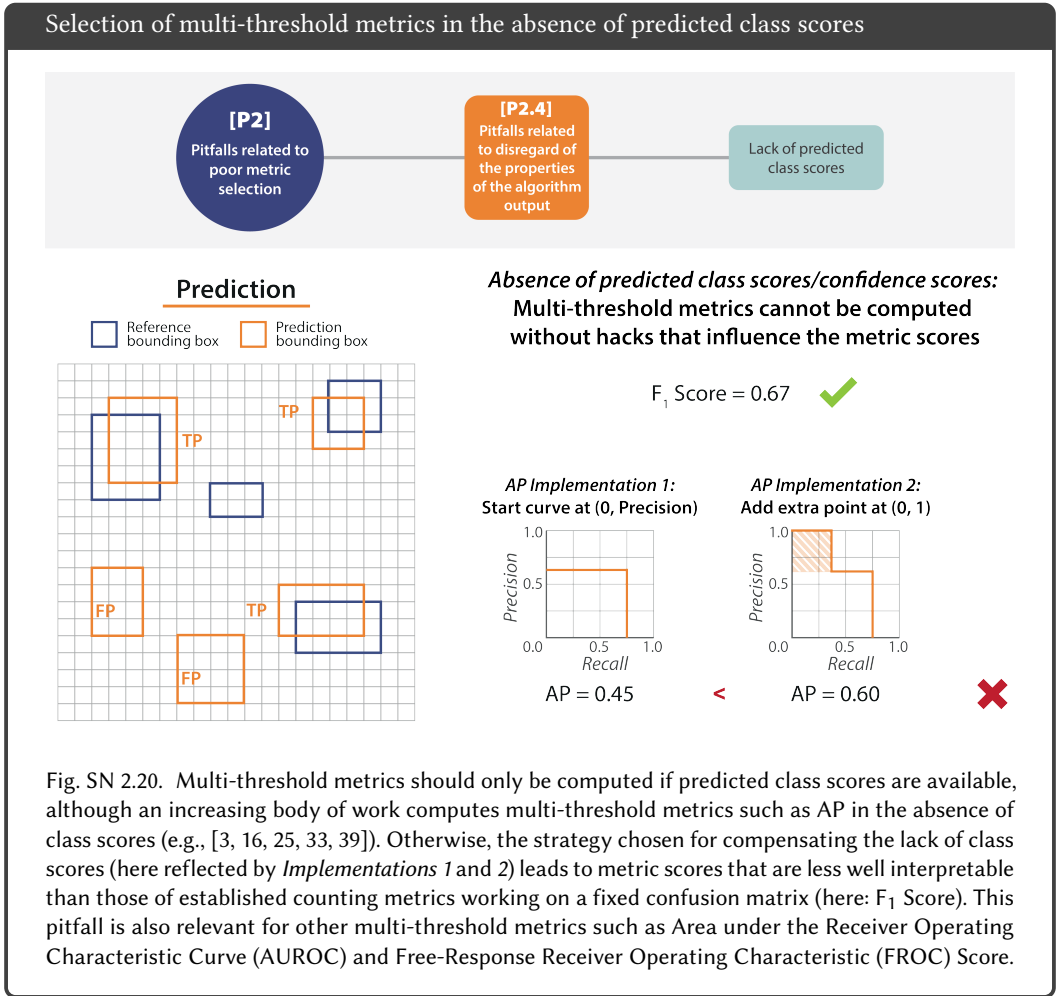


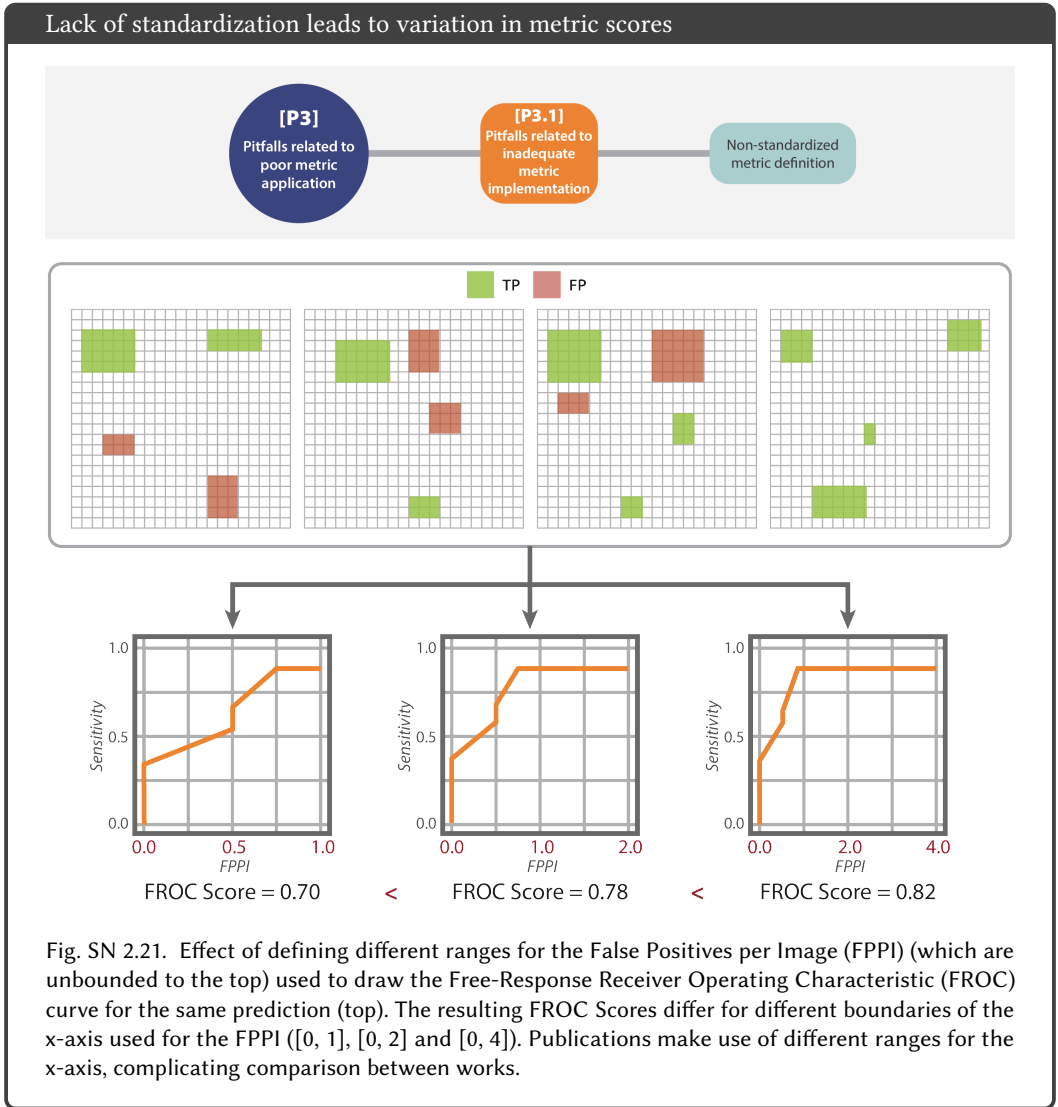
Fig. SN 2.20. Multi-threshold metrics should only be computed if predicted class scores are available, although an increasing body of work computes multi-threshold metrics such as AP in the absence of class scores (e.g., [3, 16, 25, 33, 39]). Otherwise, the strategy chosen for compensating the lack of class scores (here reflected by *Implementations 1* and *2*) leads to metric scores that are less well interpretable than those of established counting metrics working on a fixed confusion matrix (here:  $F_1$  Score). This pitfall is also relevant for other multi-threshold metrics such as Area under the Receiver Operating Characteristic Curve (AUROC) and Free-Response Receiver Operating Characteristic (FROC) Score.

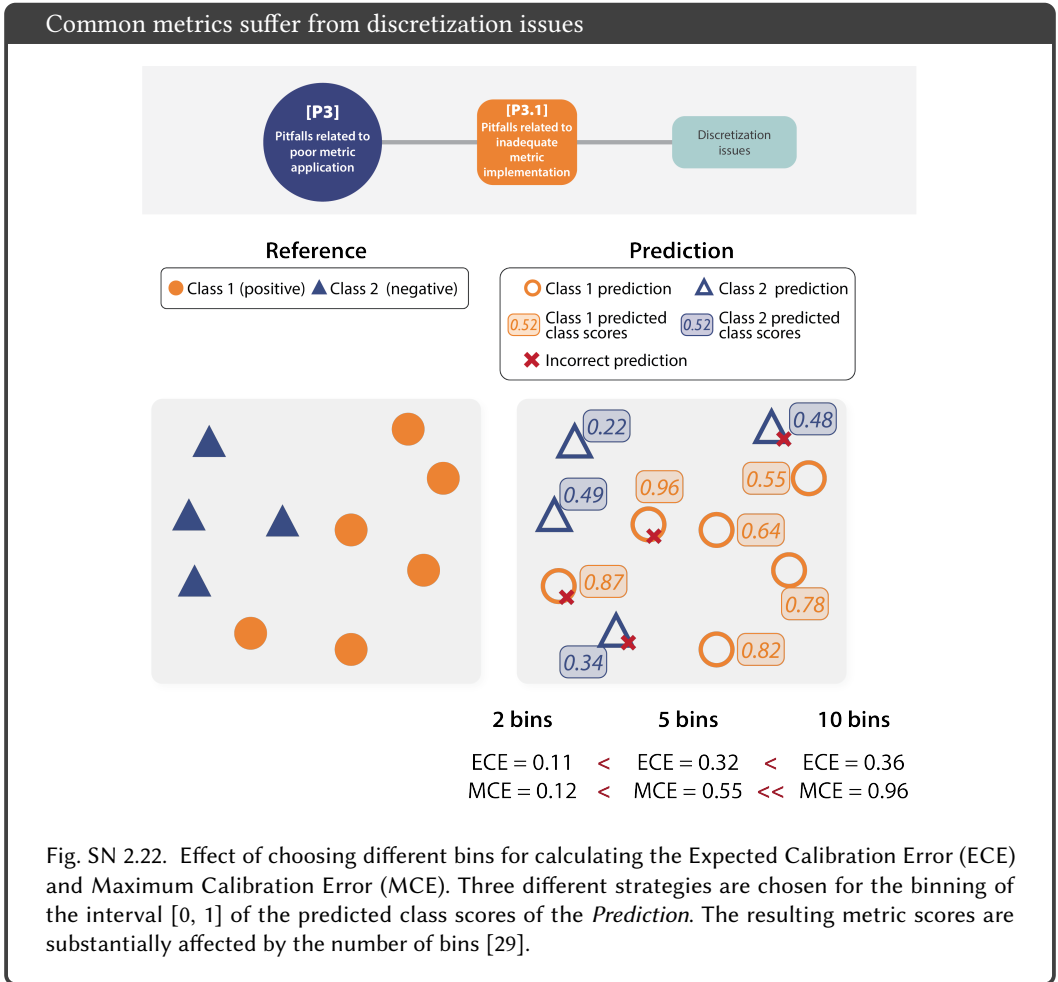
## 2.3 Pitfalls related to poor metric application

A data set typically contains several hundreds or thousands of images. When analyzing, aggregating and combining metric values, a number of factors need to be taken into account.

*2.3.1 Pitfalls related to inadequate metric implementation.* The implementation of metrics is, unfortunately, not standardized. While some metrics are straightforward to implement, others require more advanced techniques and offer a variety of implementation possibilities. Sources of metric implementation pitfalls include:

- Non-standardized definitions (Figs. 6a and SN 2.21)
- Discretization issues (Fig. SN 2.22)
- Sensitivity to hyperparameters (Fig. SN 2.23)
- Metric-specific issues (Fig. SN 2.24)





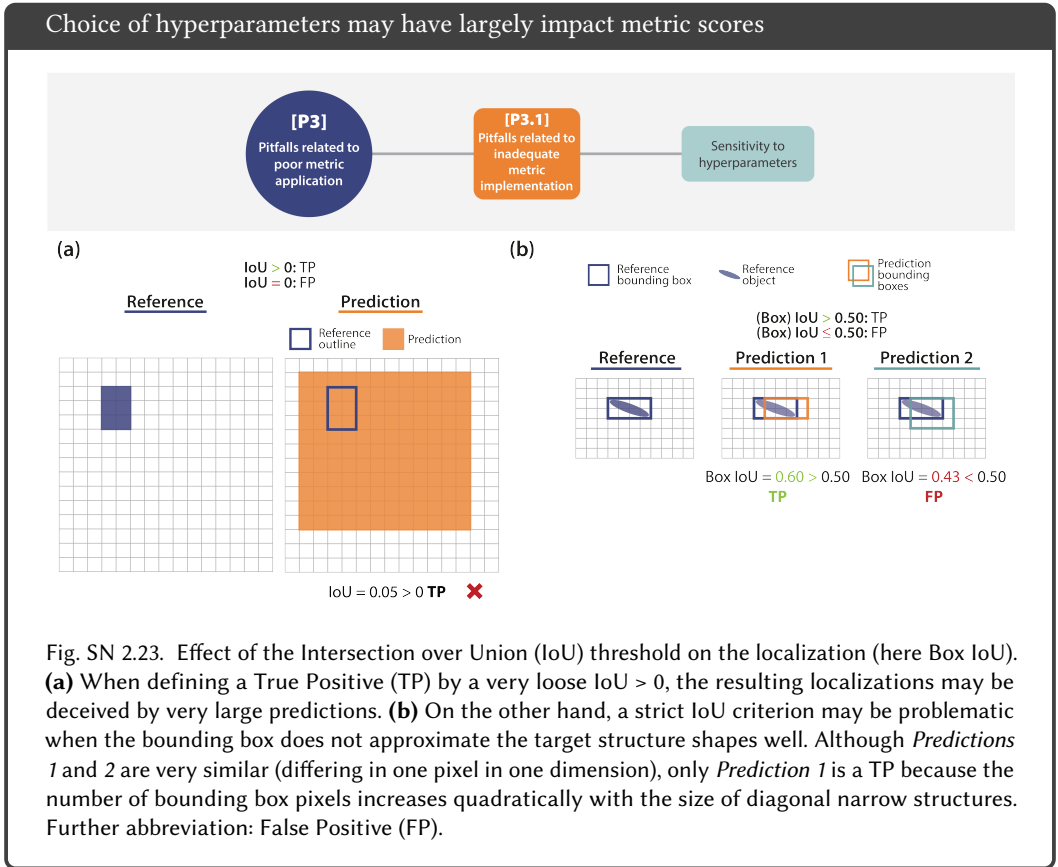


Fig. SN 2.23. Effect of the Intersection over Union (IoU) threshold on the localization (here Box IoU). **(a)** When defining a True Positive (TP) by a very loose  $IoU > 0$ , the resulting localizations may be deceived by very large predictions. **(b)** On the other hand, a strict IoU criterion may be problematic when the bounding box does not approximate the target structure shapes well. Although *Predictions 1* and *2* are very similar (differing in one pixel in one dimension), only *Prediction 1* is a TP because the number of bounding box pixels increases quadratically with the size of diagonal narrow structures. Further abbreviation: False Positive (FP).

Per-class tuning of the decision threshold yields misleading results

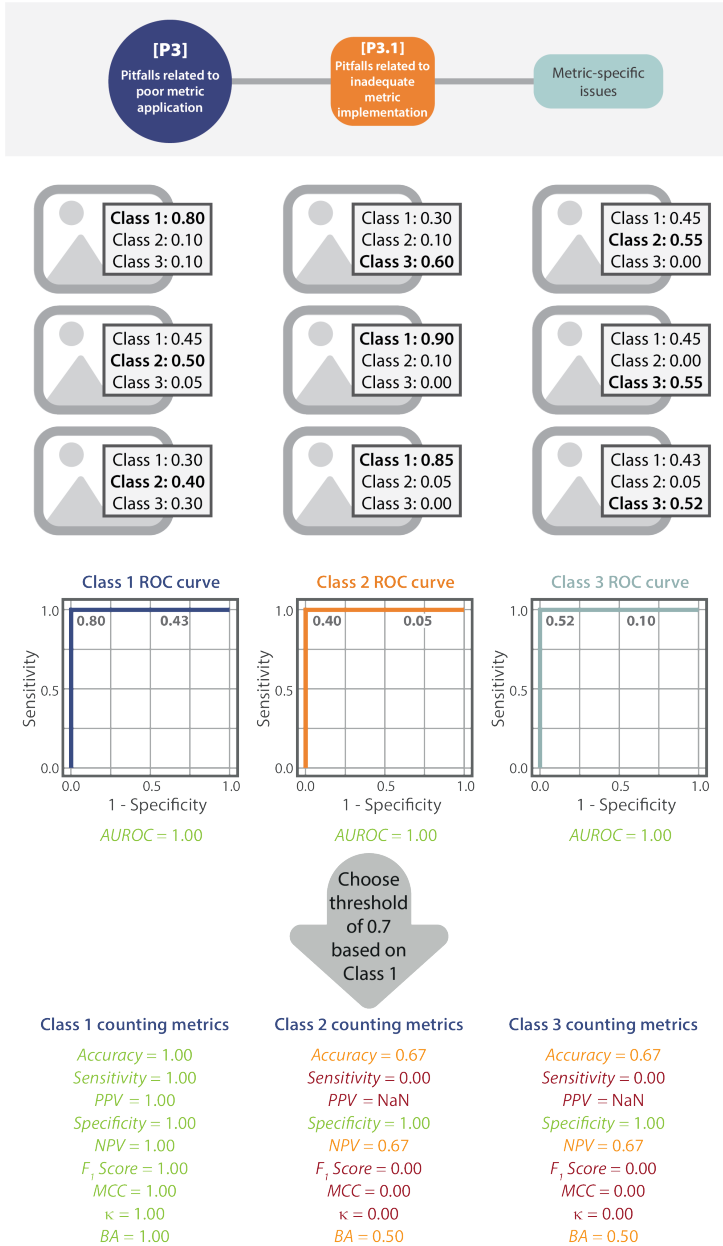


Fig. SN 2.24. Effect of the determination of a global threshold for all classes based on a single class. In a data set of three classes and nine images, the Area under the Receiver Operating Characteristic Curve (AUROC) score is 1.0 for every class. In practice, however, a global decision threshold needs to be set in multi-class problems, which typically renders substantially worse results. Here, the optimal threshold for *Class 1* yields poor results for *Classes 2* and *3* (see e.g., [17, 37]). Used abbreviations: Positive Predictive Value (PPV), Negative Predictive Value (NPV), Matthews Correlation Coefficient (MCC), Cohen’s Kappa  $\kappa$ , and Balanced Accuracy (BA).

2.3.2 *Pitfalls related to inadequate metric aggregation.* When aggregating metric values over multiple cases (data points), the method of metric aggregation should be clearly defined and reported including details for example on the aggregation operator (e.g., mean or median) and missing value handling. In addition, special care should be taken when aggregating across classes or different hierarchy levels. Pitfalls can be further subdivided into *class-related* and *data set-related* pitfalls. In the following, we present pitfalls stemming from the following sources:

#### **Class-related pitfalls**

- Hierarchical label structure (Fig. SN 2.25)
- Multi-class problem (Fig. SN 2.26)

#### **Data set-related pitfalls**

- Non-independence of test cases (Figs. 6b and SN 2.27)
- Risk of bias (Fig. SN 2.28)
- Possibility of invalid prediction (Fig. SN 2.29)

## Standard aggregation schemes disregard hierarchical class structures

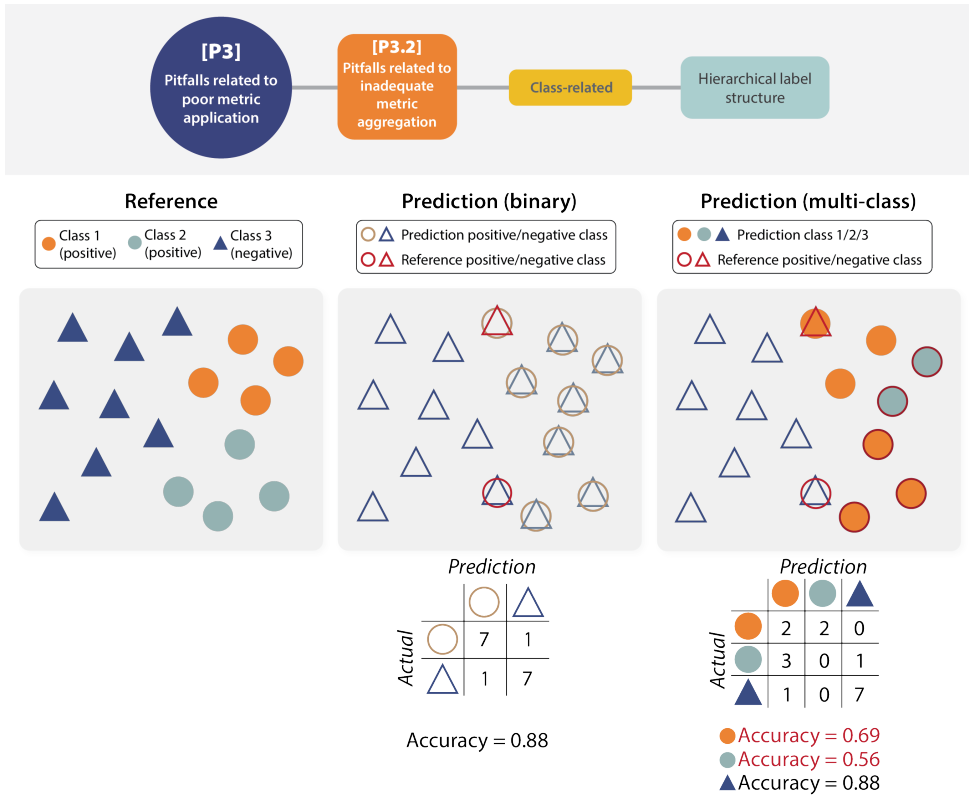
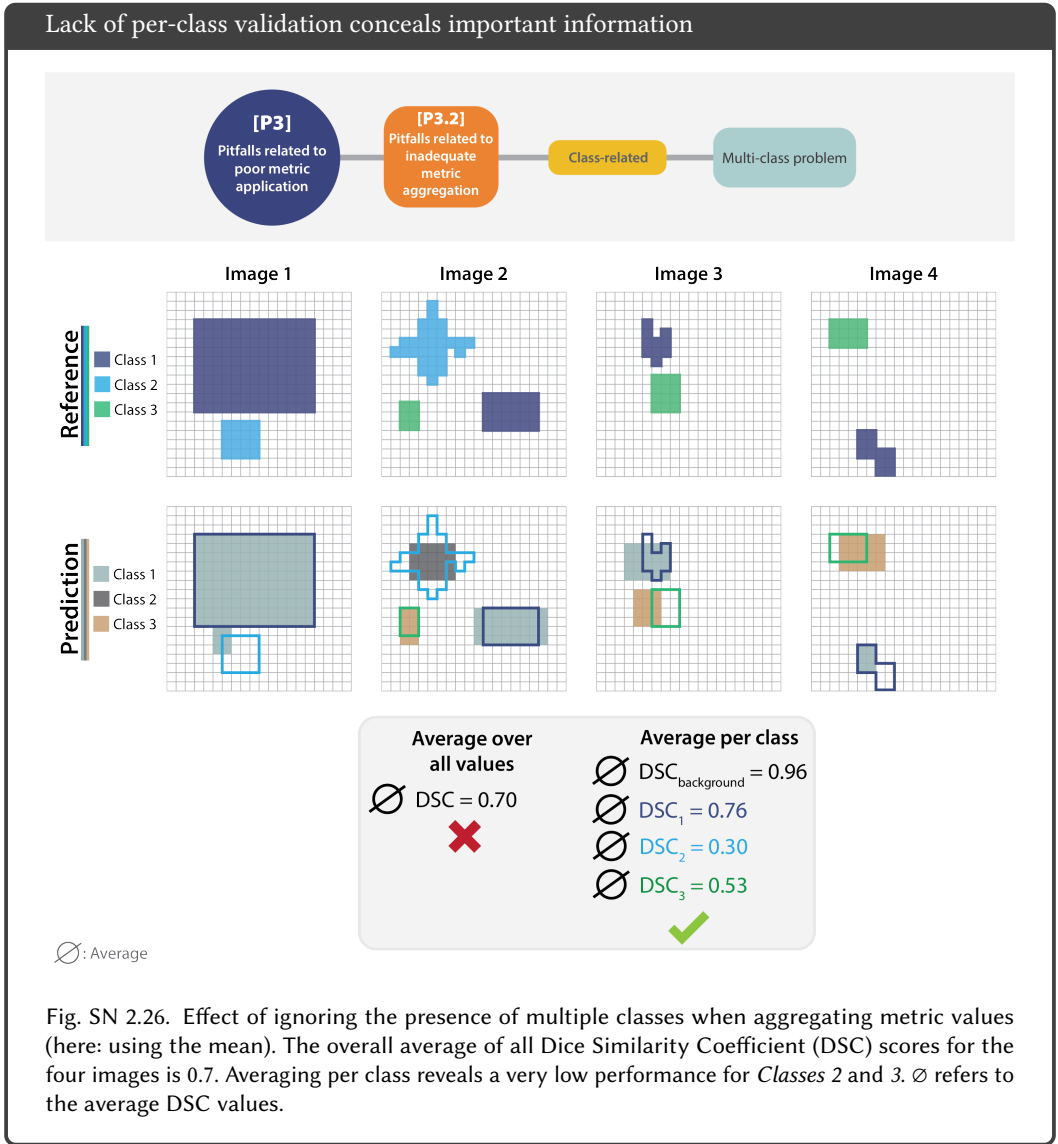


Fig. SN 2.25. Classes in categorical classification may be hierarchically structured, for example in the form of multiple positive classes and one negative class. The phrasing of the problem as binary vs. multi-class hugely affects the validation result. Binary classification (middle), differentiating triangles from circles, yields a good Accuracy, while per-class validation yields a poor score because the two circle classes cannot be distinguished well. Incorrect predictions are overlaid by a red shape of the correct reference class.



## Inter-class dependencies are concealed in standard aggregation schemes

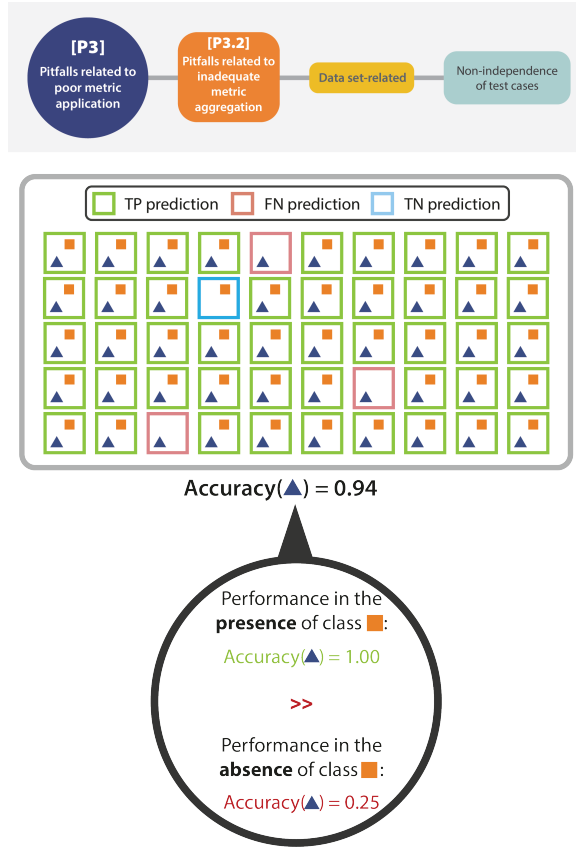


Fig. SN 2.27. Effect of interdependencies between classes. A prediction may show a near-perfect Accuracy score of 0.94 for the dark blue triangle as it frequently appears in conjunction with the orange square. By calculating the Accuracy in the *presence* and *absence* of the orange square class, it can be seen that the algorithm only works well in the presence of the orange square class.

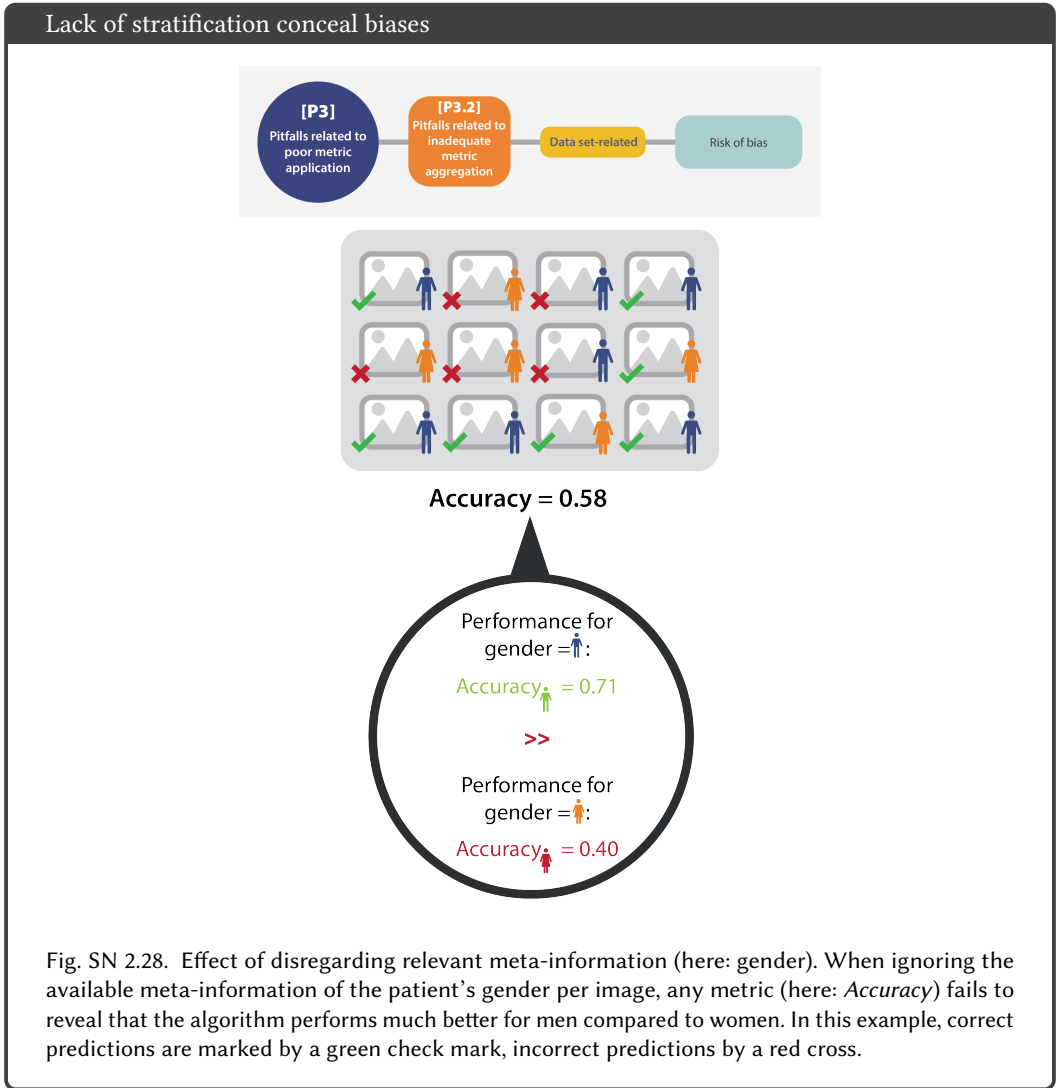


Fig. SN 2.28. Effect of disregarding relevant meta-information (here: gender). When ignoring the available meta-information of the patient's gender per image, any metric (here: Accuracy) fails to reveal that the algorithm performs much better for men compared to women. In this example, correct predictions are marked by a green check mark, incorrect predictions by a red cross.

## Lack of missing data handling strategy yields misleading results

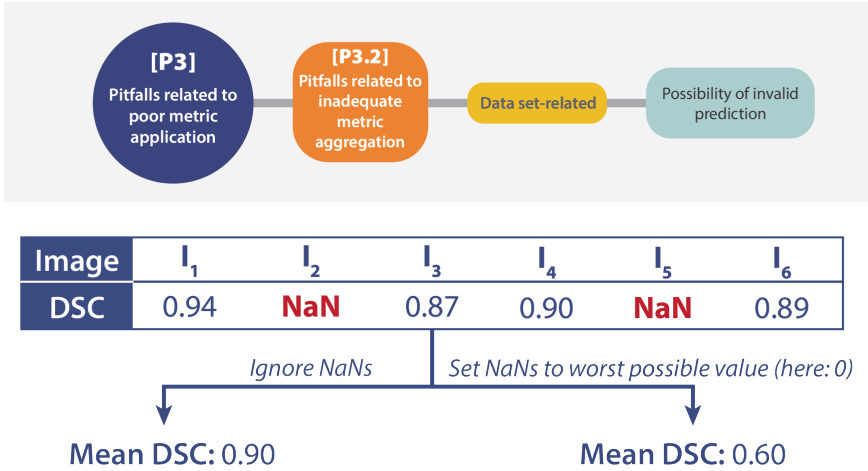
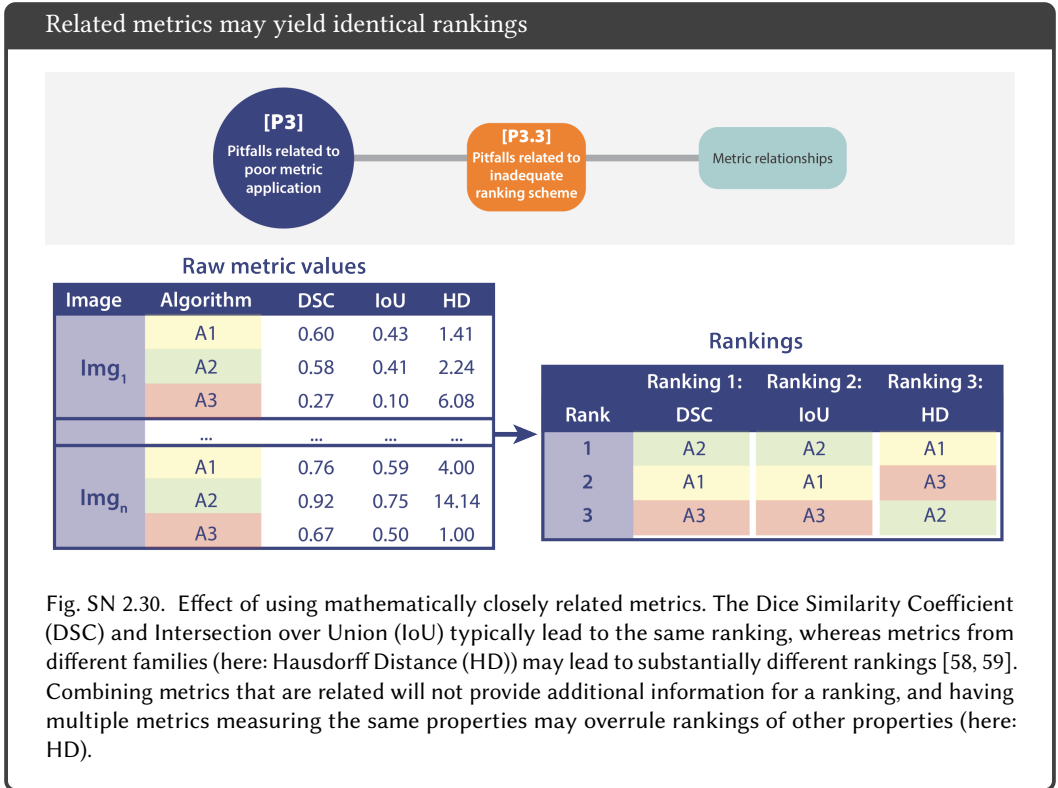


Fig. SN 2.29. Effect of invalid predictions (missing values) when aggregating metric values. In this example, ignoring missing values leads to a substantially higher Dice Similarity Coefficient (DSC) compared to setting missing values to the worst possible value (here: 0).

2.3.3 *Pitfalls related to inadequate ranking scheme.* Rankings are often created to compare algorithm performances. In this context, we present pitfalls stemming from the following sources:

- Metric relationships (Fig. SN 2.30)
- Ranking uncertainty (Fig. SN 2.31)



## Ranking tables do not reflect ranking uncertainty

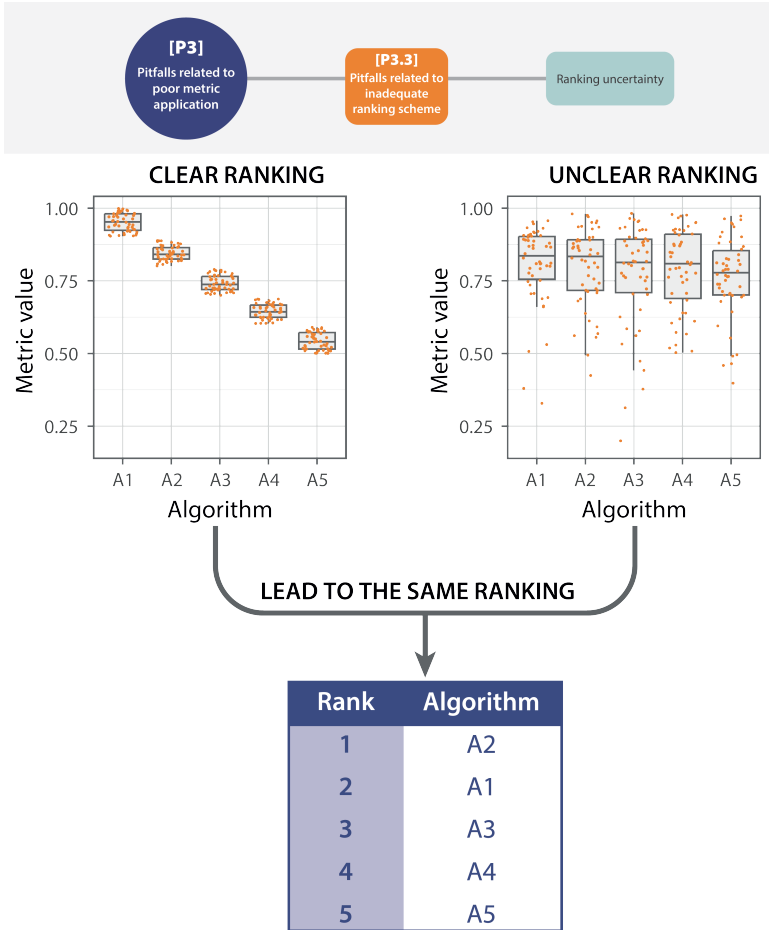
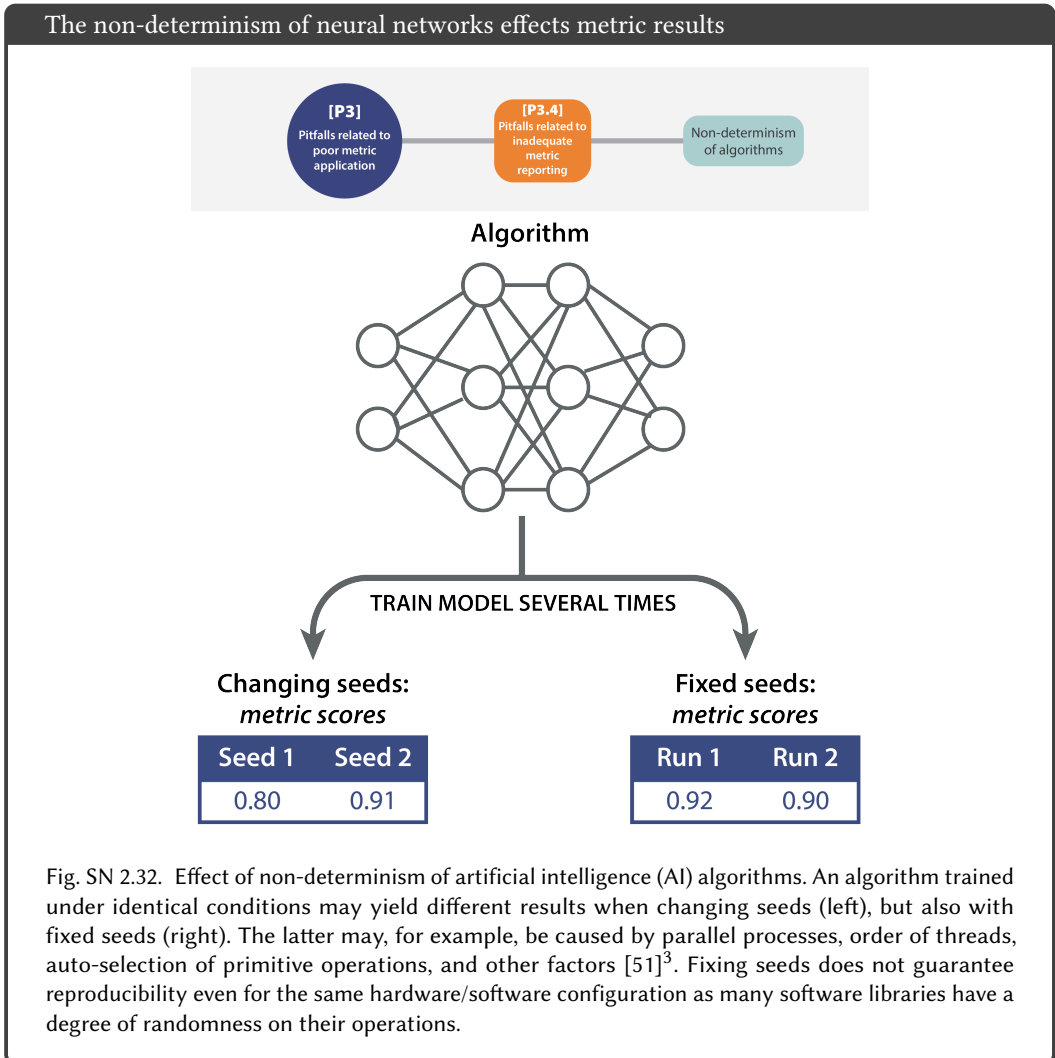


Fig. SN 2.31. Effect of ranking uncertainty. The results of two benchmarking experiments with five algorithms A1-A5 differ substantially, as shown by the boxplots of the metric values for every algorithm. While the left situation introduces a clear ranking visible from the boxplots, the right use case is not clear as performance is very similar across algorithms. However, both situations lead to the same ranking [43, 69]. Thus, solely providing ranking tables conceals information on ranking uncertainty.

2.3.4 *Pitfalls related to inadequate metric reporting.* A thorough reporting of metric values and aggregates is important both in terms of transparency and interpretability. However, several pitfalls are to be avoided in this regard. Sources of metric reporting pitfalls include:

- Non-determinism of algorithms (Fig. SN 2.32)
- Uninformative visualization (Figs. 6c and SN 2.33)



<sup>3</sup>See for example: <https://pytorch.org/docs/stable/notes/randomness.html>

## Common visualization schemes conceal relevant information

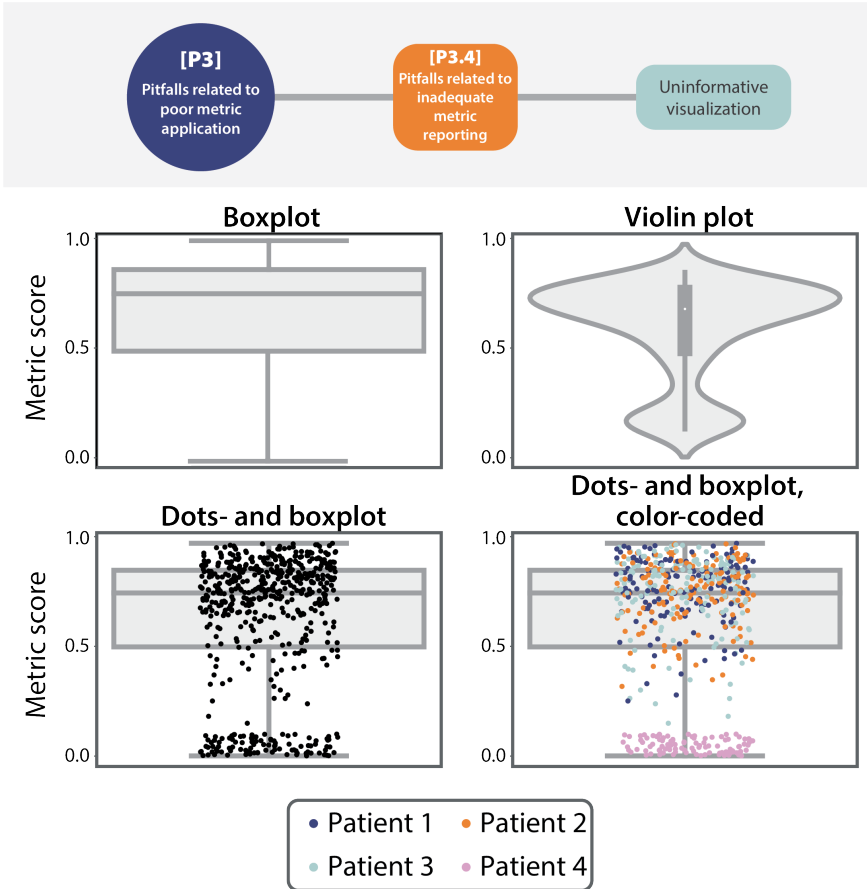


Fig. SN 2.33. Effect of different visualization types. A single boxplot (top left) does not provide sufficient information about the raw metric value distribution (here: Dice Similarity Coefficient (DSC)). Using a violin plot (top right) or adding the raw metric values as jittered dots on top (bottom left) adds important information. In the case of non-independent validation data, color/shape-coding helps reveal data clusters (bottom right).

2.3.5 *Pitfalls related to inadequate interpretation of metric values.* Interpreting metric scores and aggregates is an important step in algorithm performance analysis. However, several pitfalls can arise from interpretation. In the following, we present pitfalls related to:

- Low resolution (Fig. SN 2.34)
- Lack of upper/lower bounds (Fig. SN 2.35)
- Insufficient domain relevance of metric score differences (Fig. SN 2.36)

Image resolution affects metric scores

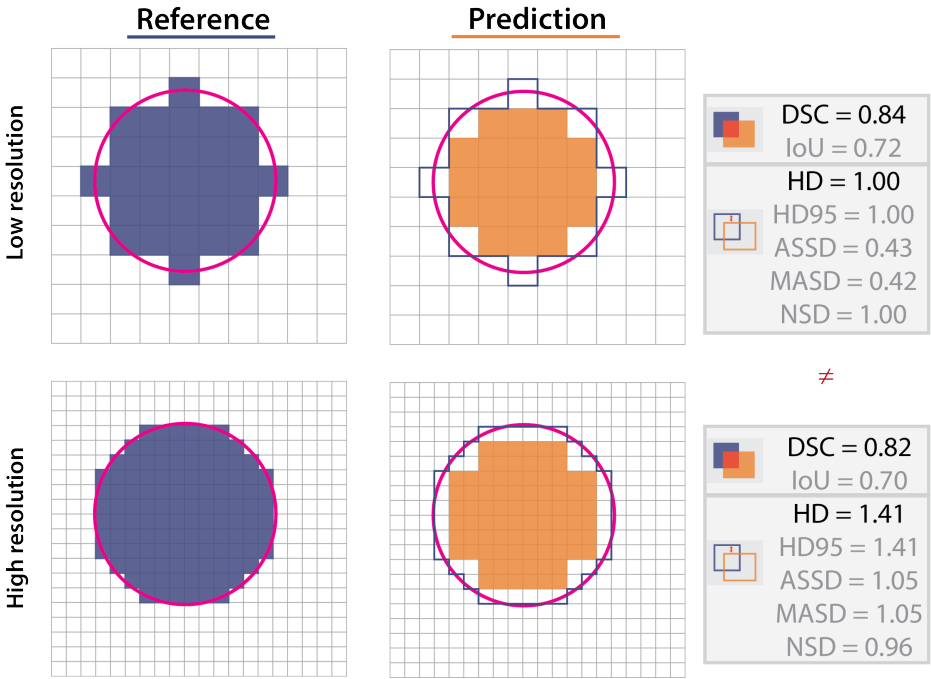
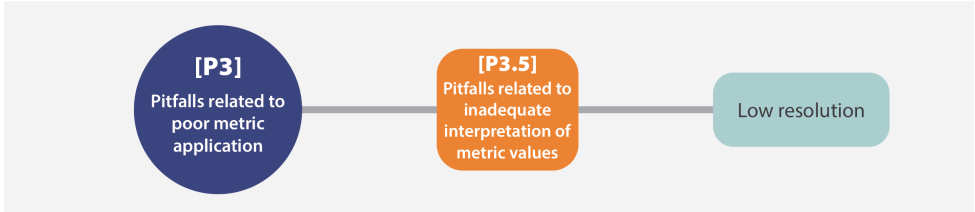


Fig. SN 2.34. Effect of different grid sizes. Differences in the grid size (resolution) of an image highly influence the image and the reference annotation (dark blue shape (reference) vs. pink outline (desired circle shape)), with a prediction of the exact same shape leading to different metric scores. Abbreviations: Dice Similarity Coefficient (DSC), Intersection over Union (IoU), Hausdorff Distance (HD), Hausdorff Distance 95th Percentile (HD95), Average Symmetric Surface Distance (ASSD), Mean Average Surface Distance (MASD), Normalized Surface Distance (NSD).

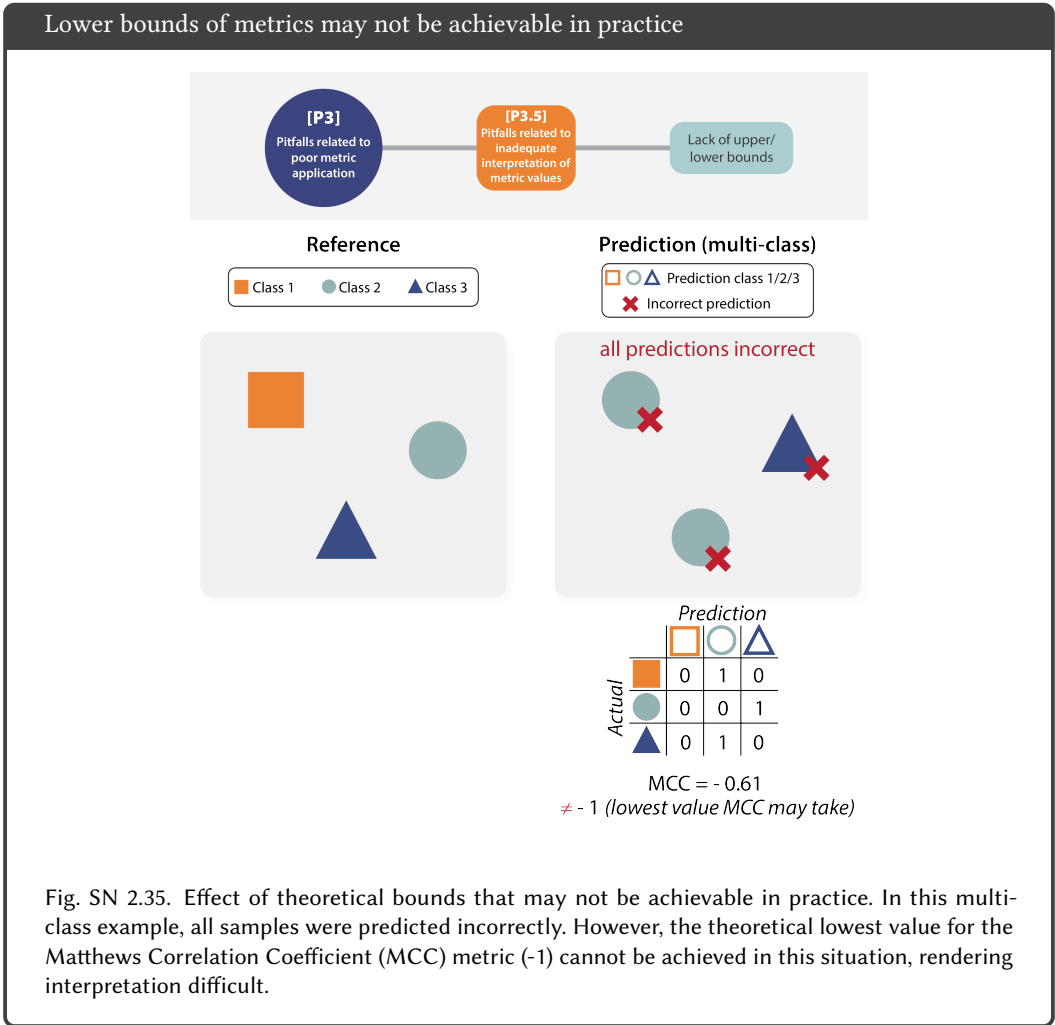
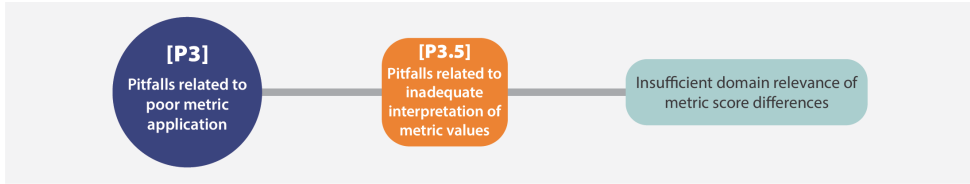


Fig. SN 2.35. Effect of theoretical bounds that may not be achievable in practice. In this multi-class example, all samples were predicted incorrectly. However, the theoretical lowest value for the Matthews Correlation Coefficient (MCC) metric (-1) cannot be achieved in this situation, rendering interpretation difficult.

Metric score differences leading to different rankings may be irrelevant



Rank	Algorithm	Aggregated metric score
1	A2	0.9543
2	A1	0.9542
3	A3	0.8703

} *Difference: 0.0001* ✘  
 } *Difference: 0.0839* ✔

Fig. SN 2.36. Effect of irrelevant metric score differences in rankings. The difference of the metric score aggregates of algorithms *A1* and *A2* is extremely low and not of biomedical relevance. However, the numerical difference would assign them different ranks.

**SUPL. NOTE 3 METRIC PROFILES**

This section presents profiles for the metrics deemed particularly relevant by the *Metrics Reloaded* consortium [44]. For each metric, the respective description, formula, and value range (upward arrow: higher values better than lower values; downward arrow: lower values are better than higher values) are provided, along with further important characteristics, such as the used cardinalities of a confusion matrix, or potential prevalence dependency. Finally, relevant pitfalls are highlighted. Many of the presented metrics rely on the confusion matrix, which is illustrated in Fig. SN 3.37.

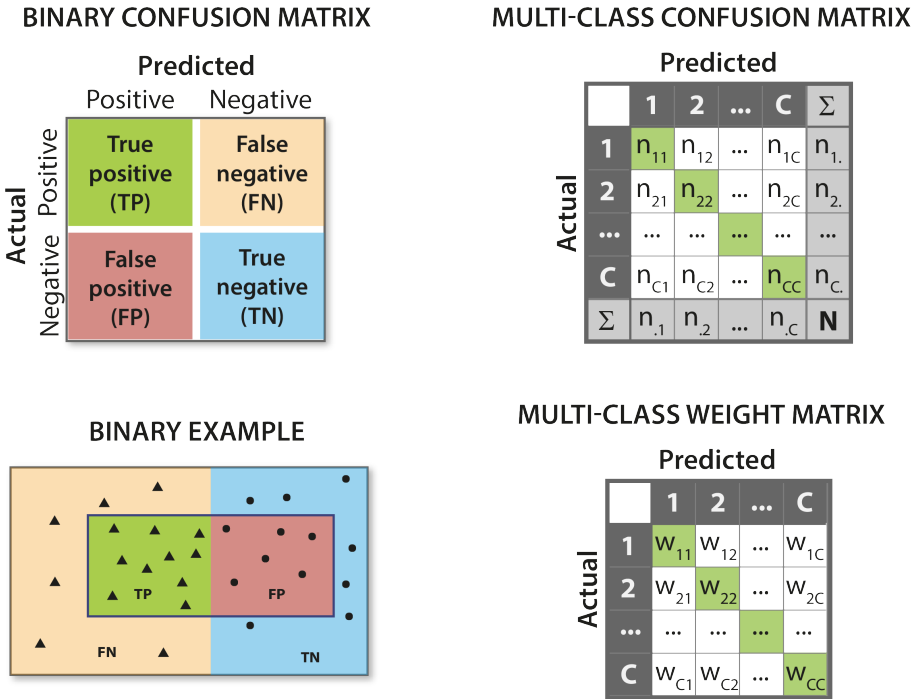


Fig. SN 3.37. Schematic example of the confusion matrix for two and for  $C$  classes. For the latter case, we also present a weight or cost matrix with weights  $w_{ij} > 0$  without loss of generality. For the binary confusion matrix, we show an example illustrating the cardinalities for a prediction of triangles and circles.

3.1 Discrimination metrics

3.1.1 Counting metrics.

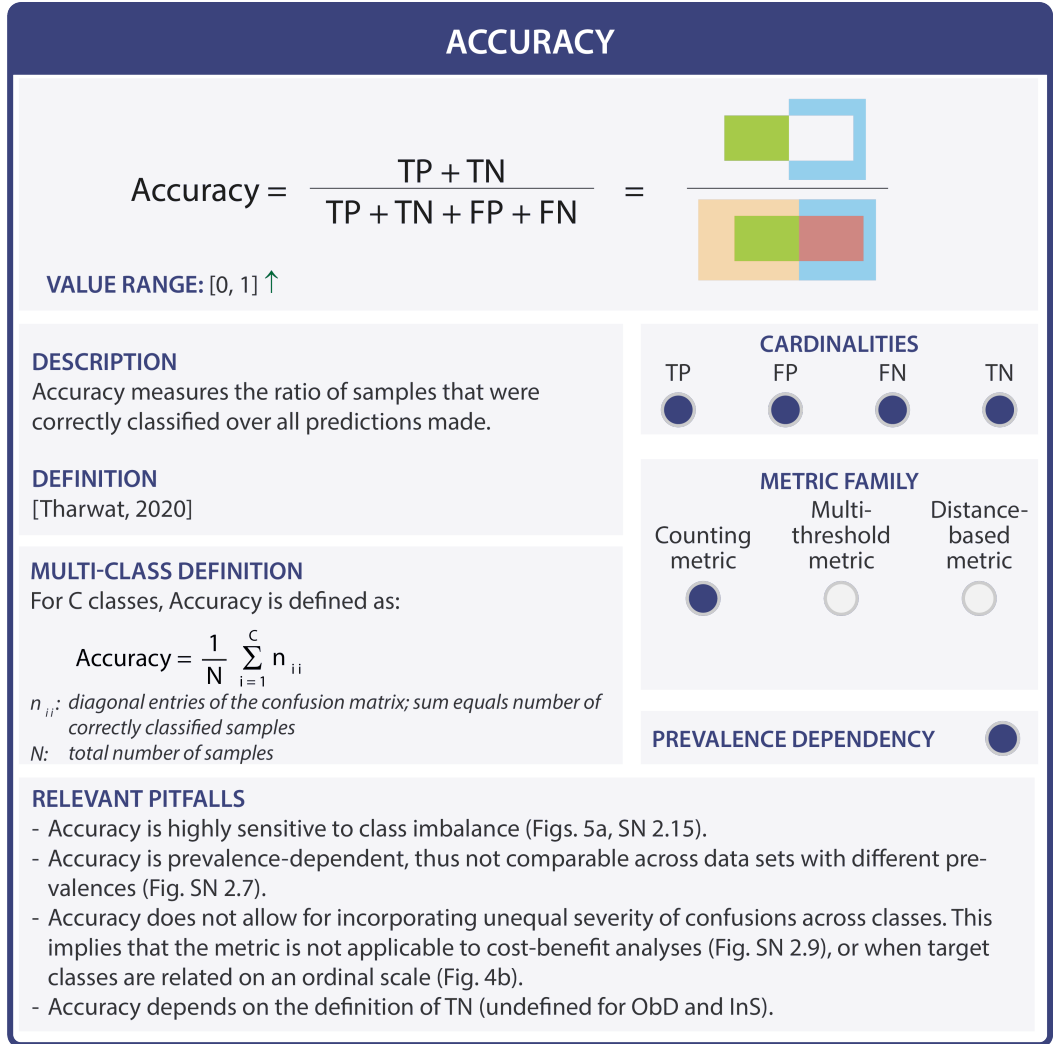


Fig. SN 3.38. Metric profile of Accuracy. The upward arrow in the value range indicates that higher values are better than lower values. Abbreviations: False Negative (FN), False Positive (FP), Instance Segmentation (InS), Object Detection (ObD), True Negative (TN), True Positive (TP). Reference: Tharwat, 2020: [60]. Mentioned figures: Figs. 4b, 5a, SN 2.7, SN 2.9, SN 2.15.

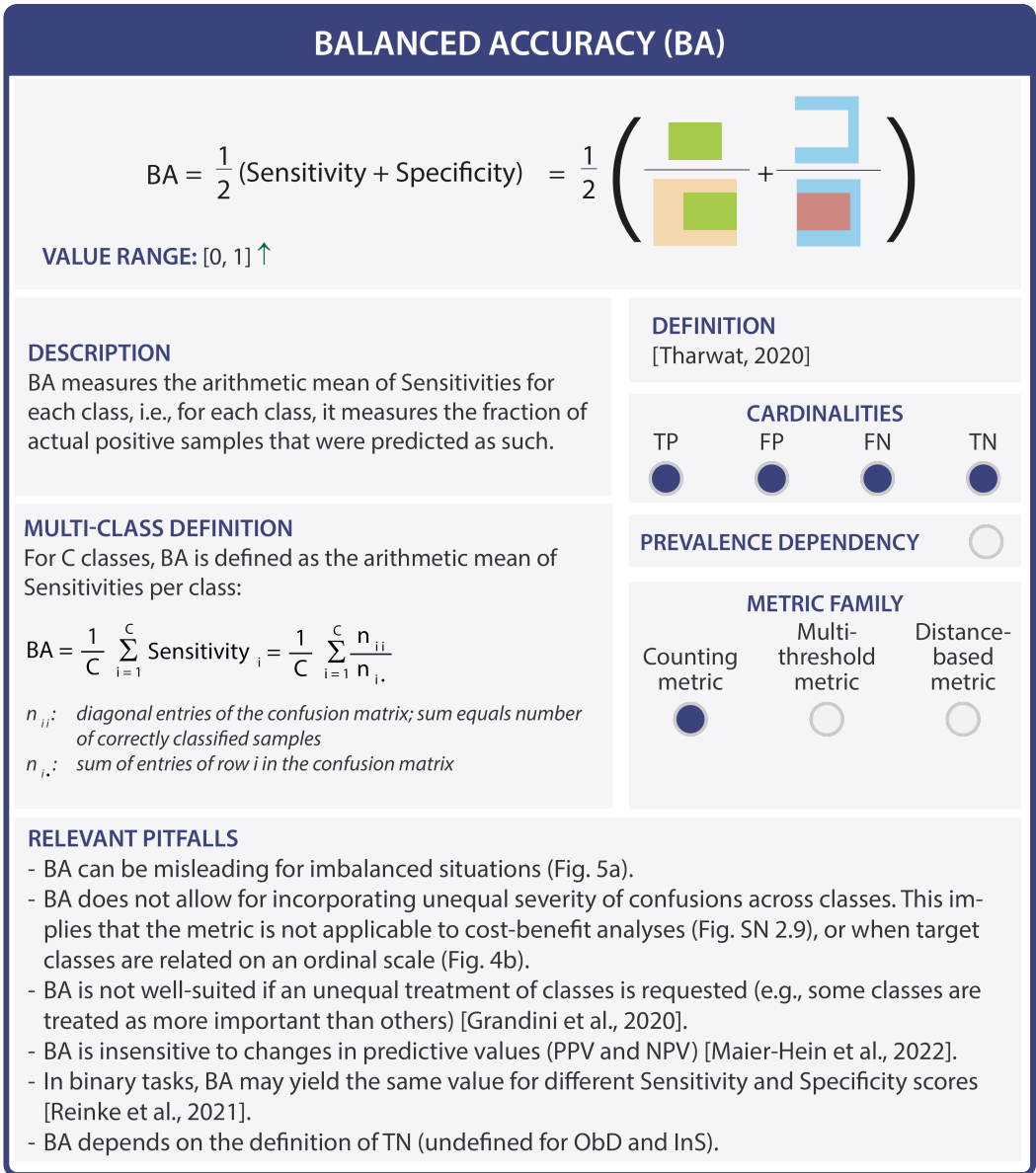


Fig. SN 3.39. Metric profile of Balanced Accuracy (BA). The upward arrow in the value range indicates that higher values are better than lower values. Abbreviations: False Negative (FN), False Positive (FP), Instance Segmentation (InS), Object Detection (ObD), Positive Predictive Value (PPV), True Negative (TN), True Positive (TP). References: Grandini et al., 2020: [27], Maier-Hein et al., 2022: [44], Reinke et al., 2021: [54], Tharwat, 2020: [60]. Mentioned figures: Figs. 4b, 5a, SN 2.9.

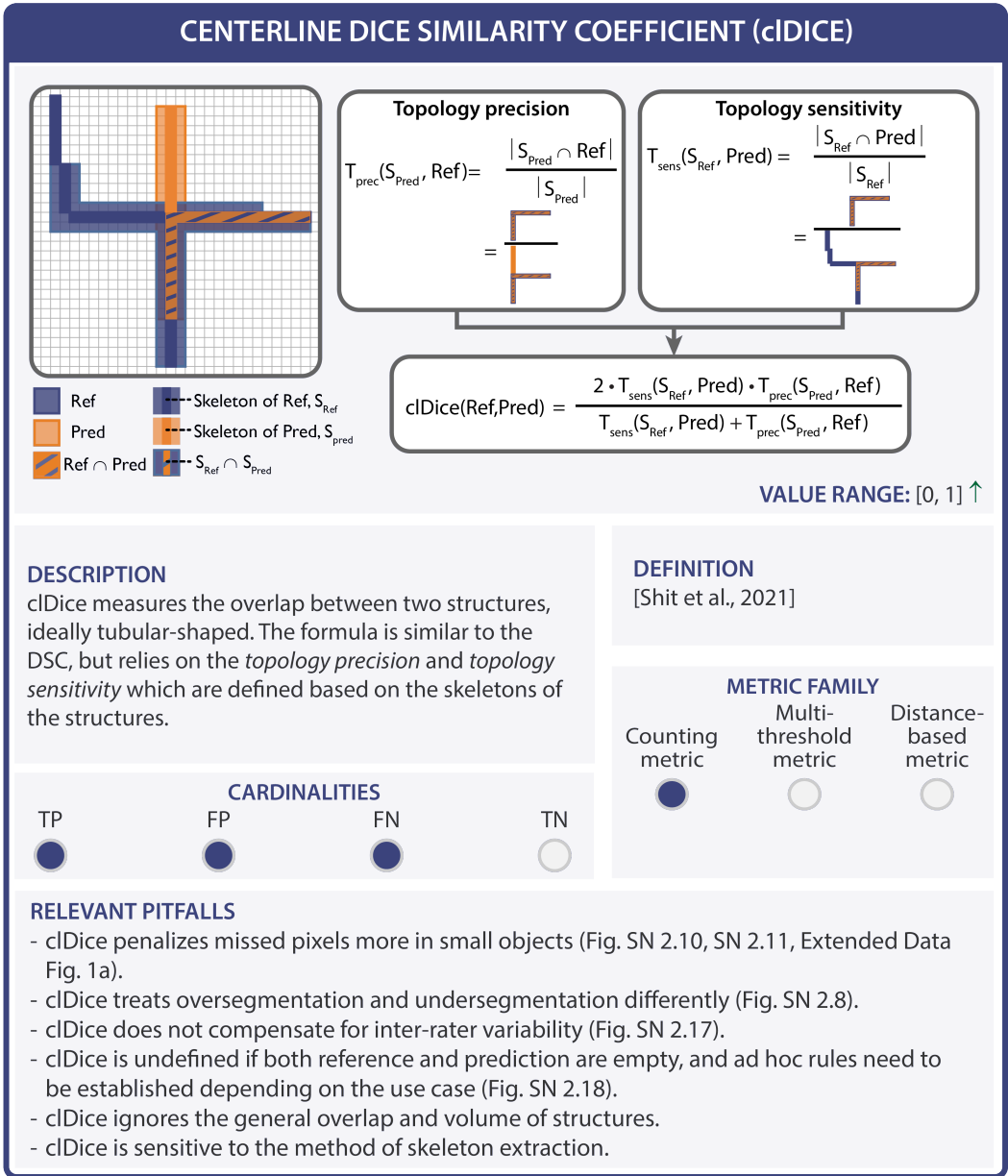


Fig. SN 3.40. Metric profile of centerline Dice Similarity Coefficient (cIDice). The upward arrow in the value range indicates that higher values are better than lower values. Abbreviations: False Negative (FN), False Positive (FP), True Negative (TN), True Positive (TP). Reference: Shit et al., 2021: [57]. Mentioned figures: Extended Data Fig. 1a, Figs. SN 2.8, SN 2.10, SN 2.11, SN 2.17, SN 2.18.

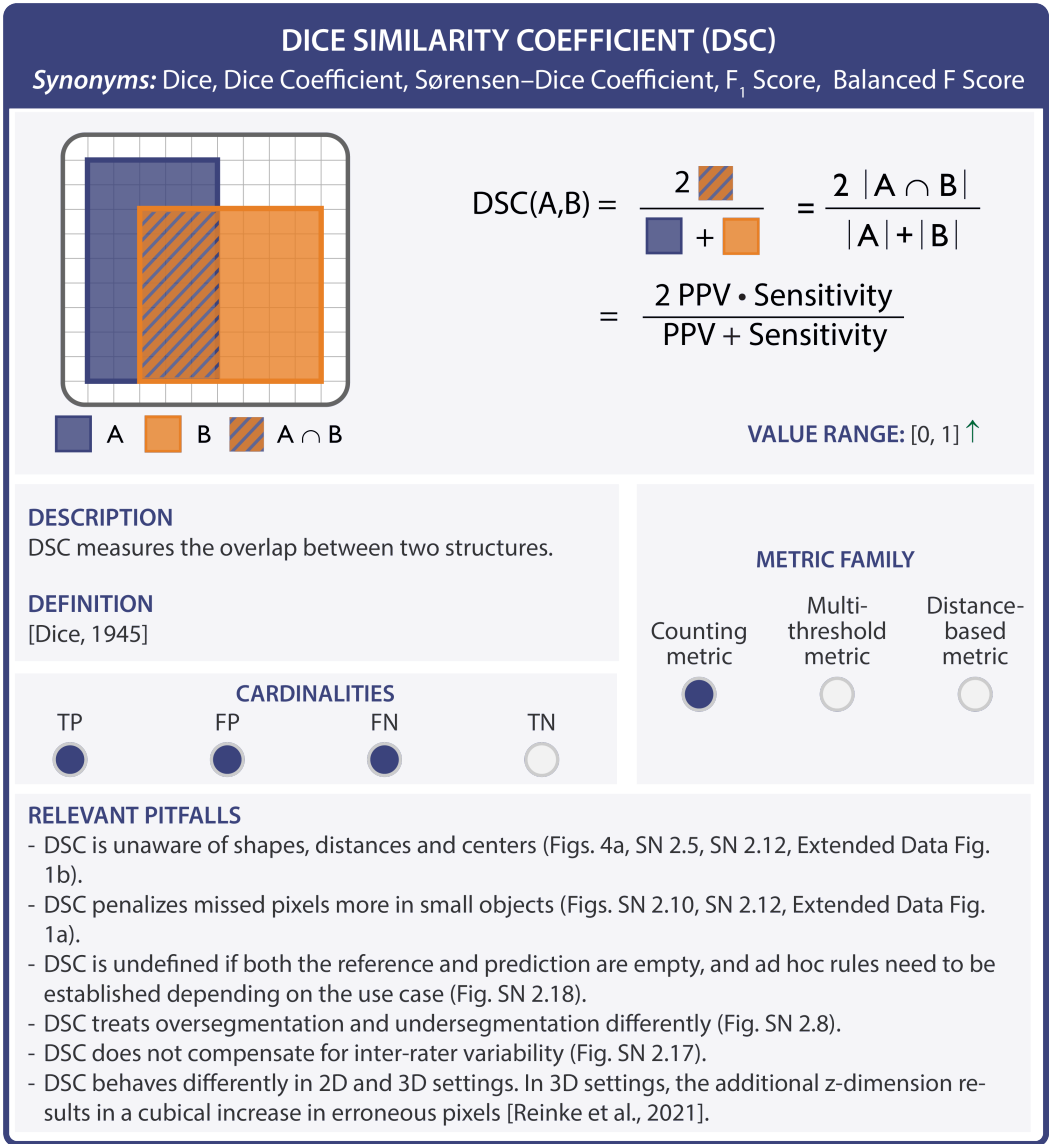


Fig. SN 3.41. Metric profile of Dice Similarity Coefficient (DSC). The upward arrow in the value range indicates that higher values are better than lower values. Abbreviations: False Negative (FN), False Positive (FP), Positive Predictive Value (PPV), True Negative (TN), True Positive (TP). References: Dice, 1945: [20], Reinke et al., 2021: [54]. Mentioned figures: Figs. 4a, SN 2.5, SN 2.8, SN 2.10, SN 2.11, SN 2.12, SN 2.17, SN 2.18, Extended Data Fig. 1a-b.

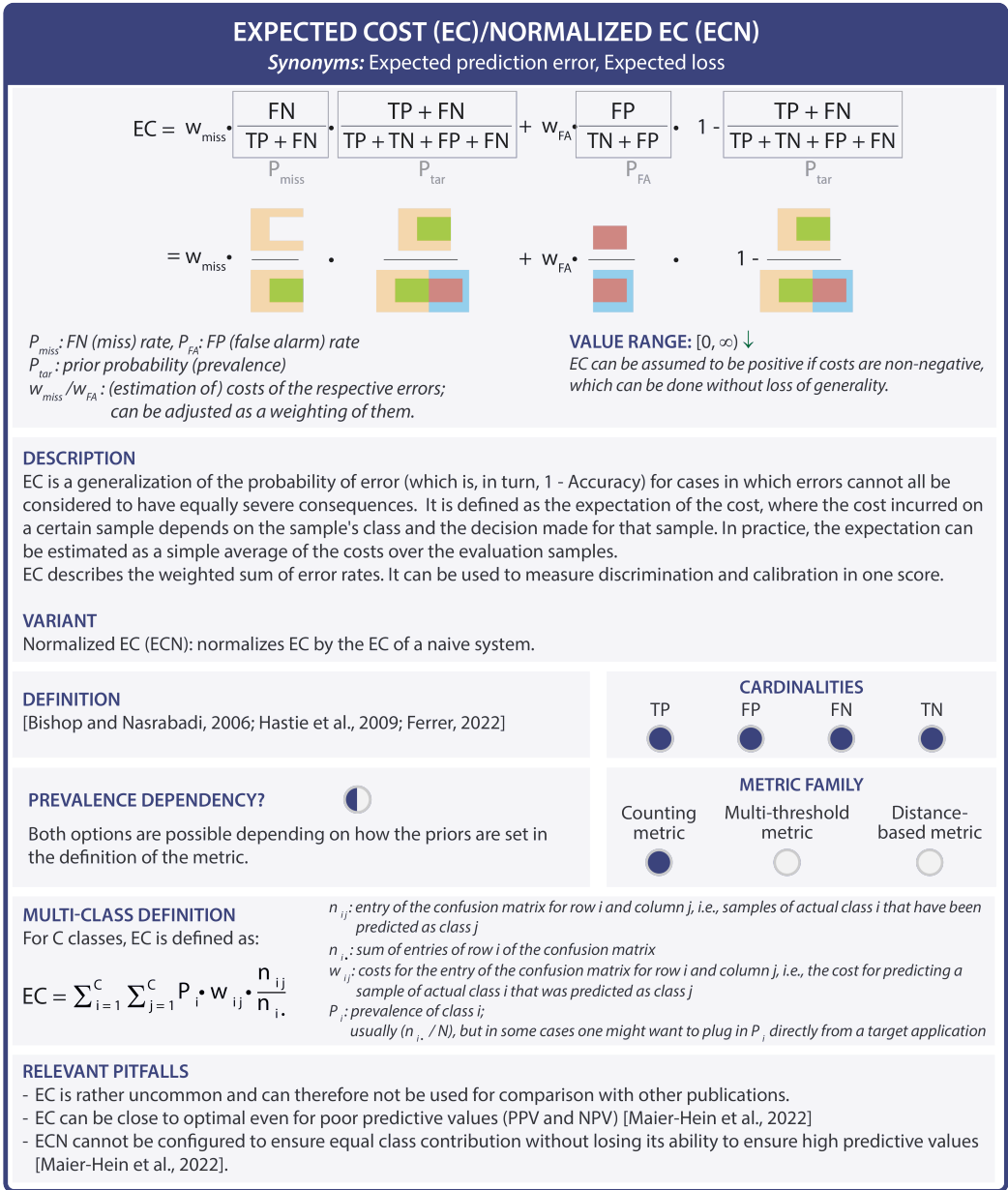


Fig. SN 3.42. Metric profile of Expected Cost (EC). The downward arrow in the value range indicates that lower values are better than higher values. Abbreviations: False Negative (FN), False Positive (FP), True Negative (TN), True Positive (TP). References: Bishop and Nasrabadi, 2006: [7], Ferrer 2022: [24], Hastie et al., 2009: [32], Maier-Hein et al., 2022: [44].

## F<sub>β</sub> SCORE

$$F_{\beta} \text{ Score} = \frac{(1+\beta^2) \cdot \text{Precision} \cdot \text{Sensitivity}}{\beta^2 \cdot \text{Precision} + \text{Sensitivity}}$$

$$= \frac{(1+\beta^2) \cdot \text{TP}}{(1+\beta^2) \cdot \text{TP} + \beta^2 \cdot \text{FN} + \text{FP}} = \frac{(1+\beta^2) \cdot \text{TP}}{(1+\beta^2) \cdot \text{TP} + \beta^2 \cdot \text{FN} + \text{FP}}$$

**VALUE RANGE:** [0, 1] ↑

**DESCRIPTION**

The F<sub>β</sub> Score weights PPV (FP) and Sensitivity (FN) with the parameter β.

The special case of β = 1 is the harmonic mean of PPV and Sensitivity and is a common metric in segmentation problems (here usually referred to as DSC). In segmentation problems, F<sub>β</sub> Score weights the penalization of oversegmentation (FP) and undersegmentation (FN) with the parameter β.

**DEFINITION**  
[Van Rijsbergen, 1979; Chinchor 1992]

**CARDINALITIES**

TP	FP	FN	TN
<input checked="" type="radio"/>	<input checked="" type="radio"/>	<input checked="" type="radio"/>	<input type="radio"/>

**PREVALENCE DEPENDENCY**

**METRIC FAMILY**

Counting metric	Multi-threshold metric	Distance-based metric
<input checked="" type="radio"/>	<input type="radio"/>	<input type="radio"/>

**RELEVANT PITFALLS**

**F<sub>β</sub> Score for classification/detection assessment:**

- F<sub>β</sub> Score is prevalence-dependent, thus not comparable across data sets with different prevalences (Figs. SN 2.7, SN 2.15).
- Compared to other per-class counting metrics (e.g., LR+) it lacks the interpretability with respect to a naive classifier
- F<sub>β</sub> Score depends on the definition of the positive class [Reinke et al., 2021].

**F<sub>β</sub> Score for segmentation assessment:**

- F<sub>β</sub> Score is unaware of the structure shape and center (Figs. 4a, SN 2.5, SN 2.12, Extended Data Fig. 1b).
- F<sub>β</sub> Score penalizes missed pixels more in small objects (Fig. SN 2.10, Extended Data Fig. 1a).
- F<sub>β</sub> Score does not compensate for inter-rater variability (Fig. 2.17).
- F<sub>β</sub> Score behaves differently in 2D and 3D settings. In 3D settings, the additional z-dimension results in a cubical increase in erroneous pixels [Reinke et al., 2021].

F<sub>β</sub> Score is undefined if both reference and prediction are empty, and ad hoc rules need to be established depending on the use case (Fig. SN 2.18, Extended Data Fig. 2b).

Fig. SN 3.43. Metric profile of F<sub>β</sub> Score.[12, 63]. The upward arrow in the value range indicates that higher values are better than lower values. Abbreviations: Dice Similarity Coefficient (DSC), False Negative (FN), False Positive (FP), Positive Predictive Value (PPV), True Negative (TN), True Positive (TP).References: Chinchor 1992: [12], Reinke et al., 2021: [54], Van Rijsbergen, 1979: [63]. Mentioned figures: Figs. 4a, SN 2.5, SN 2.7, SN 2.10, SN 2.12, SN 2.15, SN 2.17, SN 2.18, Extended Data Figs. 1a-b and 2b.

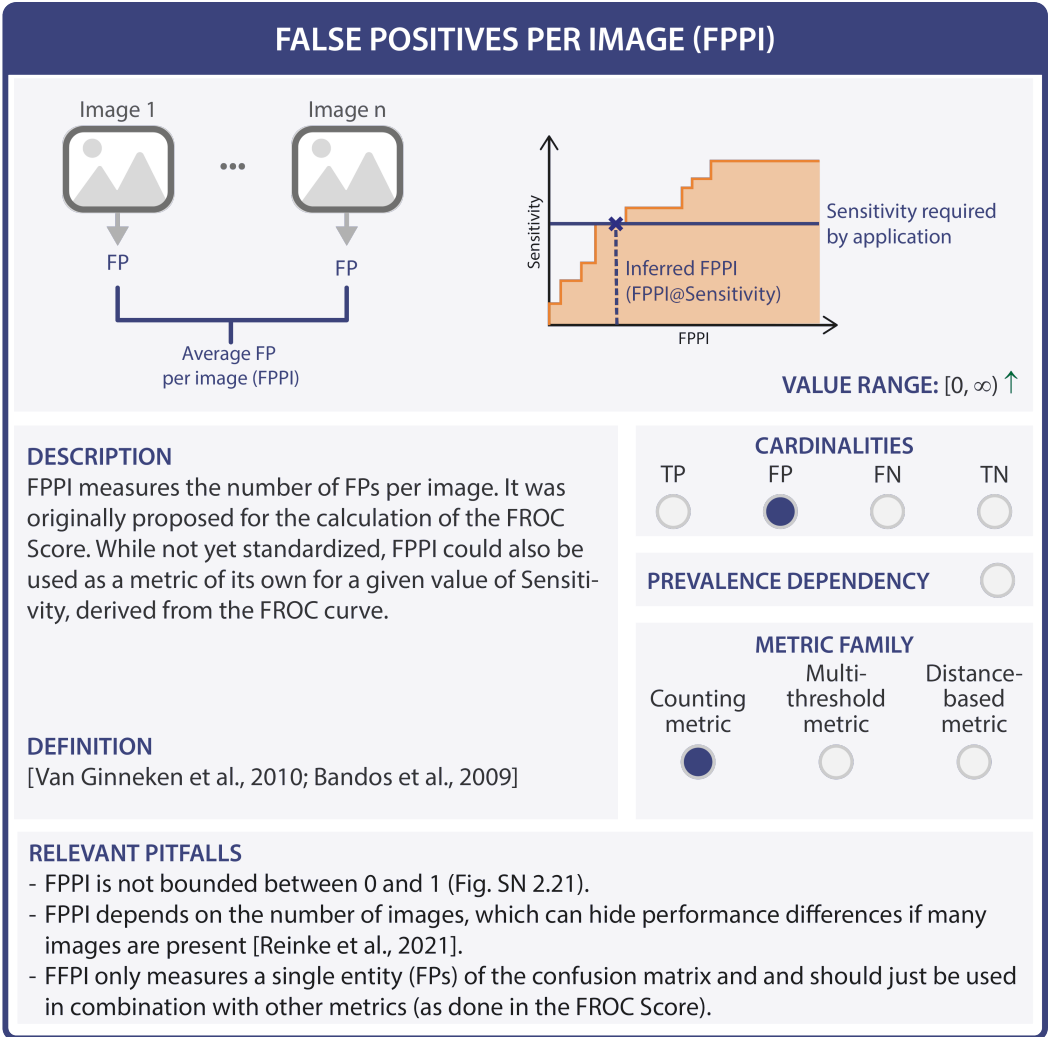


Fig. SN 3.44. Metric profile of False Positives per Image (FPPI). The upward arrow in the value range indicates that higher values are better than lower values. Abbreviations: False Negative (FN), False Positive (FP), Free-Response Receiver Operating Characteristic (FROC), True Negative (TN), True Positive (TP). References: Bandos et al., 2009: [5], Reinke et al., 2021: [54], Van Ginneken et al., 2010: [62]. Mentioned figure: Fig. SN 2.21.

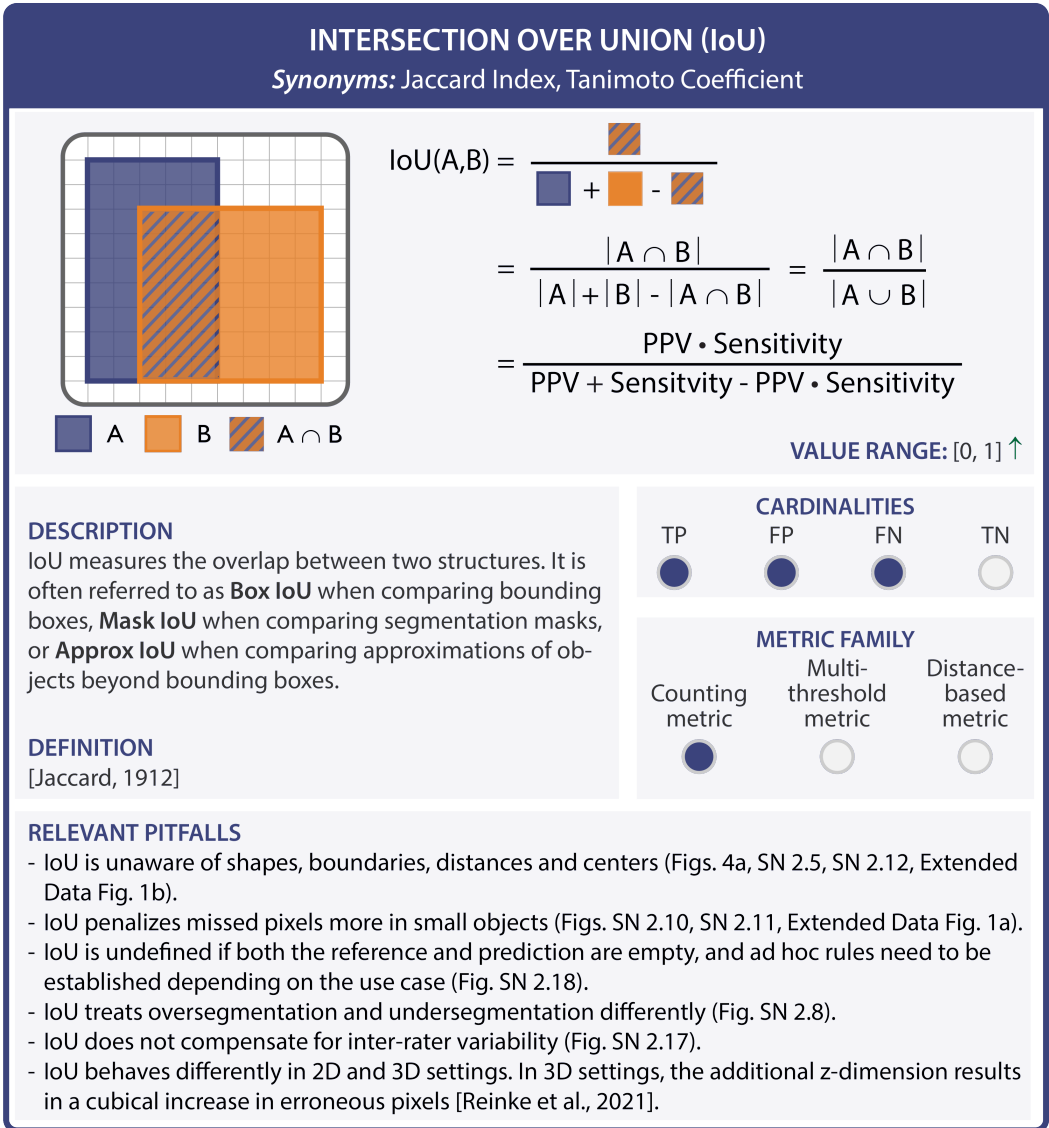


Fig. SN 3.45. Metric profile of Intersection over Union (IoU). The upward arrow in the value range indicates that higher values are better than lower values. Abbreviations: False Negative (FN), False Positive (FP), Positive Predictive Value (PPV), True Negative (TN), True Positive (TP). References: Jaccard, 1912: [35], Reinke et al., 2021: [54]. Mentioned figures: Figs. 4a, SN 2.5, SN 2.8, SN 2.10, SN 2.11, SN 2.12, SN 2.17, SN 2.18, Extended Data Fig. 1a-b.

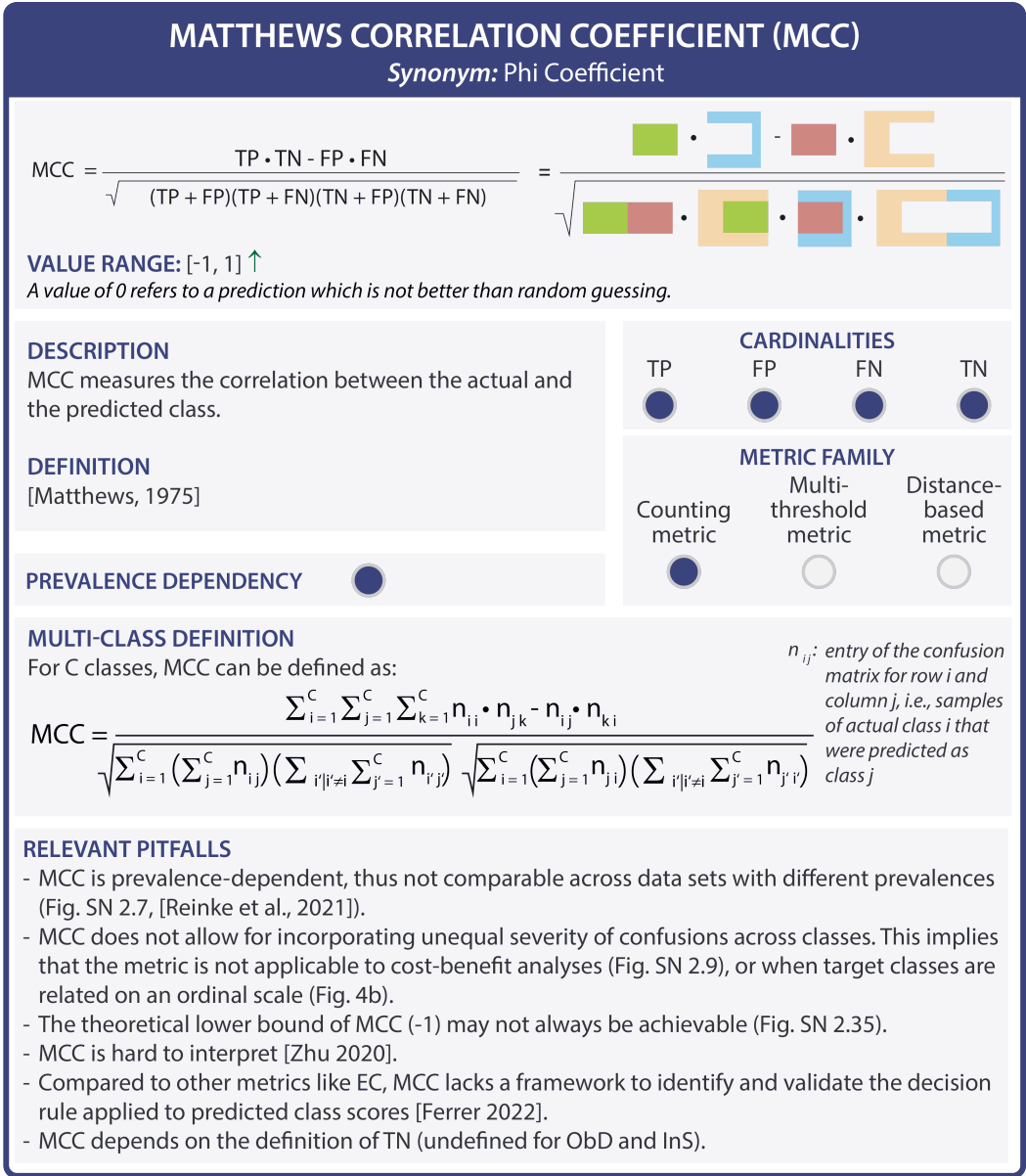


Fig. SN 3.46. Metric profile of Matthews Correlation Coefficient (MCC). The upward arrow in the value range indicates that higher values are better than lower values. Abbreviations: Expected Cost (EC), False Negative (FN), False Positive (FP), Instance Segmentation (InS), Object Detection (ObD), True Negative (TN), True Positive (TP). References: Ferrer, 2022: [24], Matthews, 1975: [46], Reinke et al., 2021: [54], Zhu, 2020: [72]. Mentioned figures: Figs. 4b, SN 2.7, SN 2.9, SN 2.35.

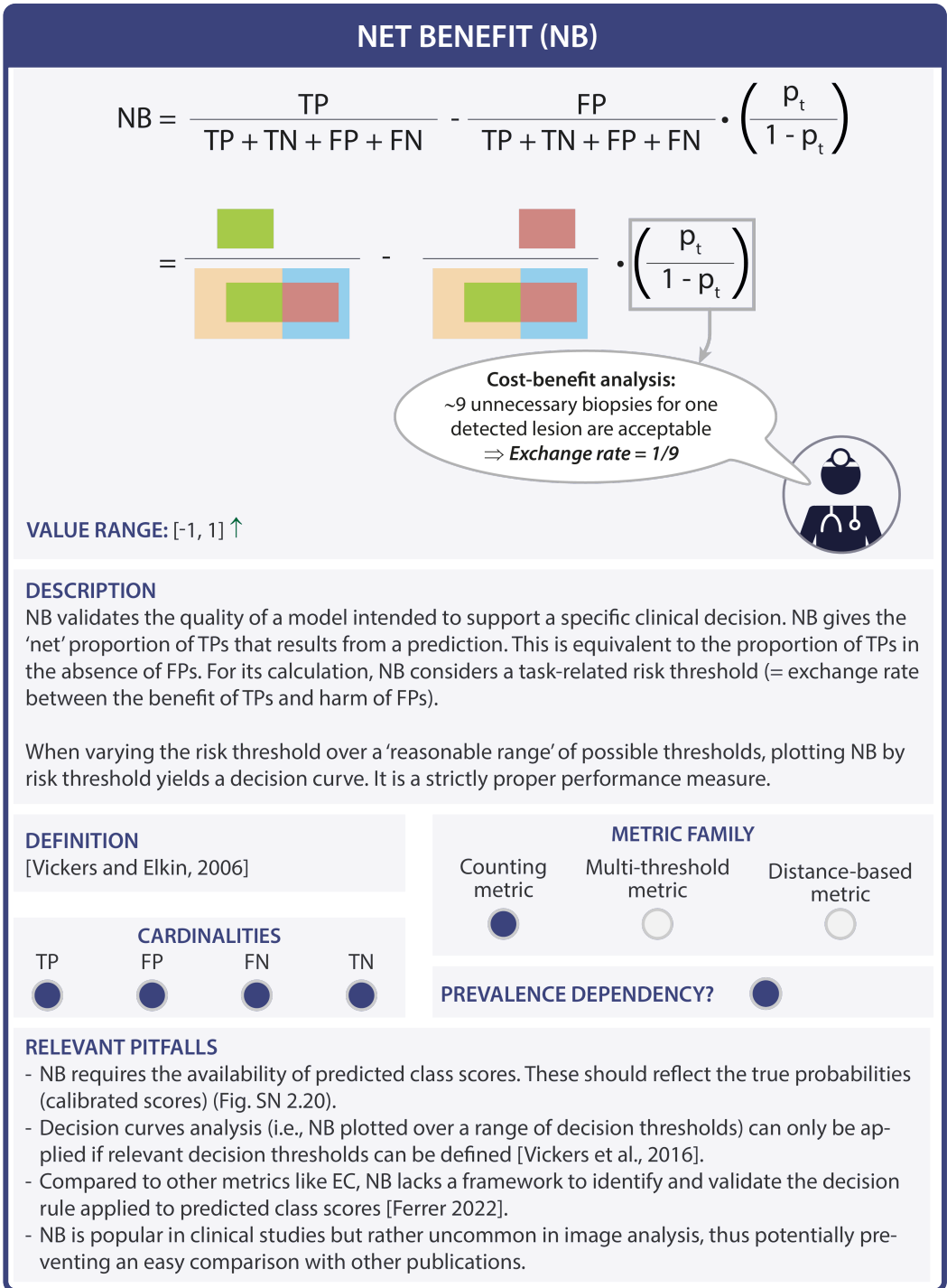


Fig. SN 3.47. Metric profile of Net Benefit (NB). The upward arrow in the value range indicates that higher values are better than lower values. Abbreviations: Expected Cost (EC), False Negative (FN), False Positive (FP), True Negative (TN), True Positive (TP). References: Ferrer, 2022: [24], Vickers and Elkin, 2006: [64], Vickers et al., 2016: [65]. Mentioned figure: Fig. SN 2.20.

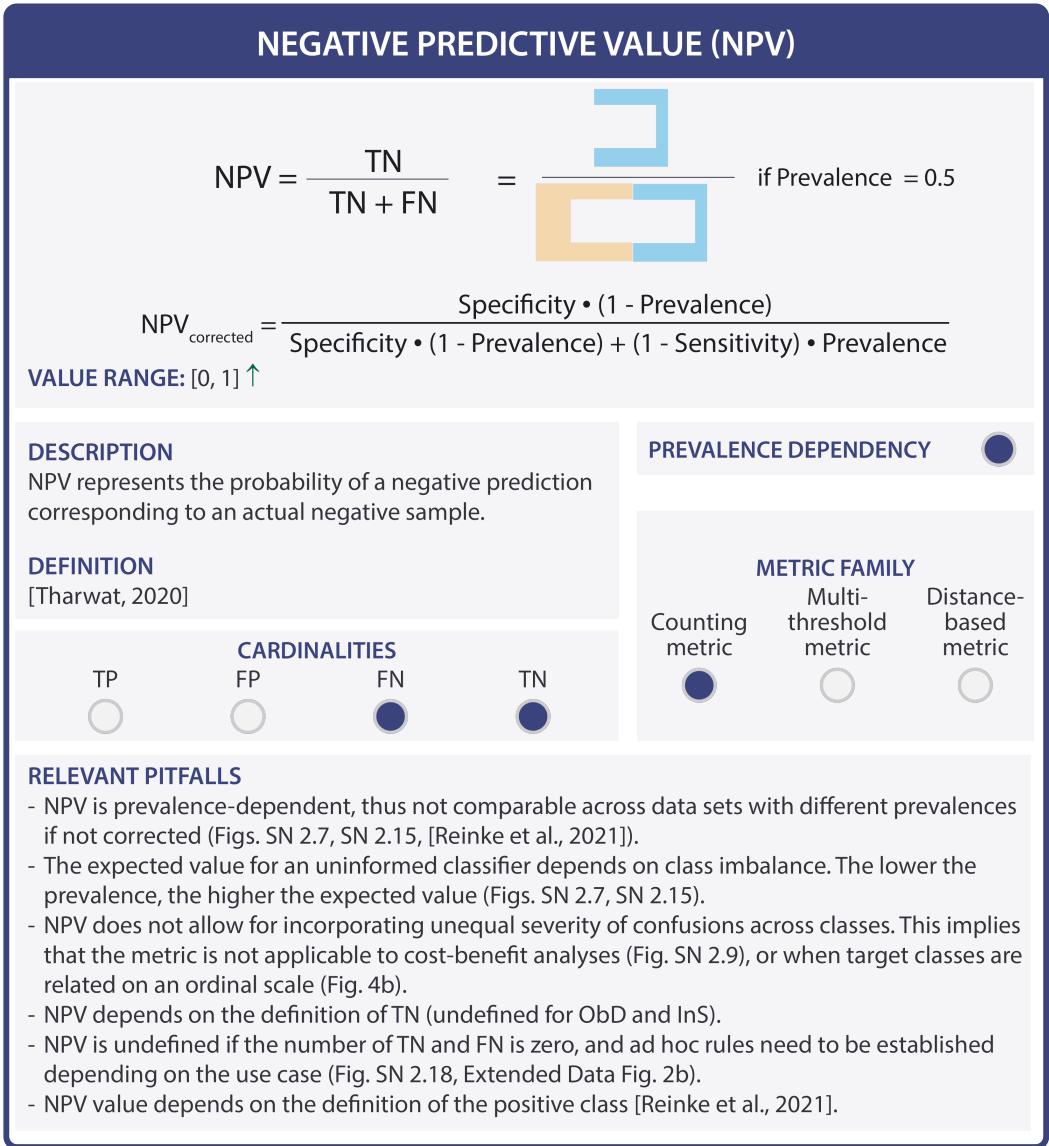


Fig. SN 3.48. Metric profile of Negative Predictive Value (NPV). The upward arrow in the value range indicates that higher values are better than lower values. Abbreviations: False Negative (FN), False Positive (FP), Instance Segmentation (InS), Object Detection (ObD), True Negative (TN), True Positive (TP). References: Reinke et al., 2021: [54], Tharwat, 2020: [60]. Mentioned figures: Figs. 4b, SN 2.7, SN 2.9, SN 2.15, SN 2.18, Extended Data Fig. 2b.

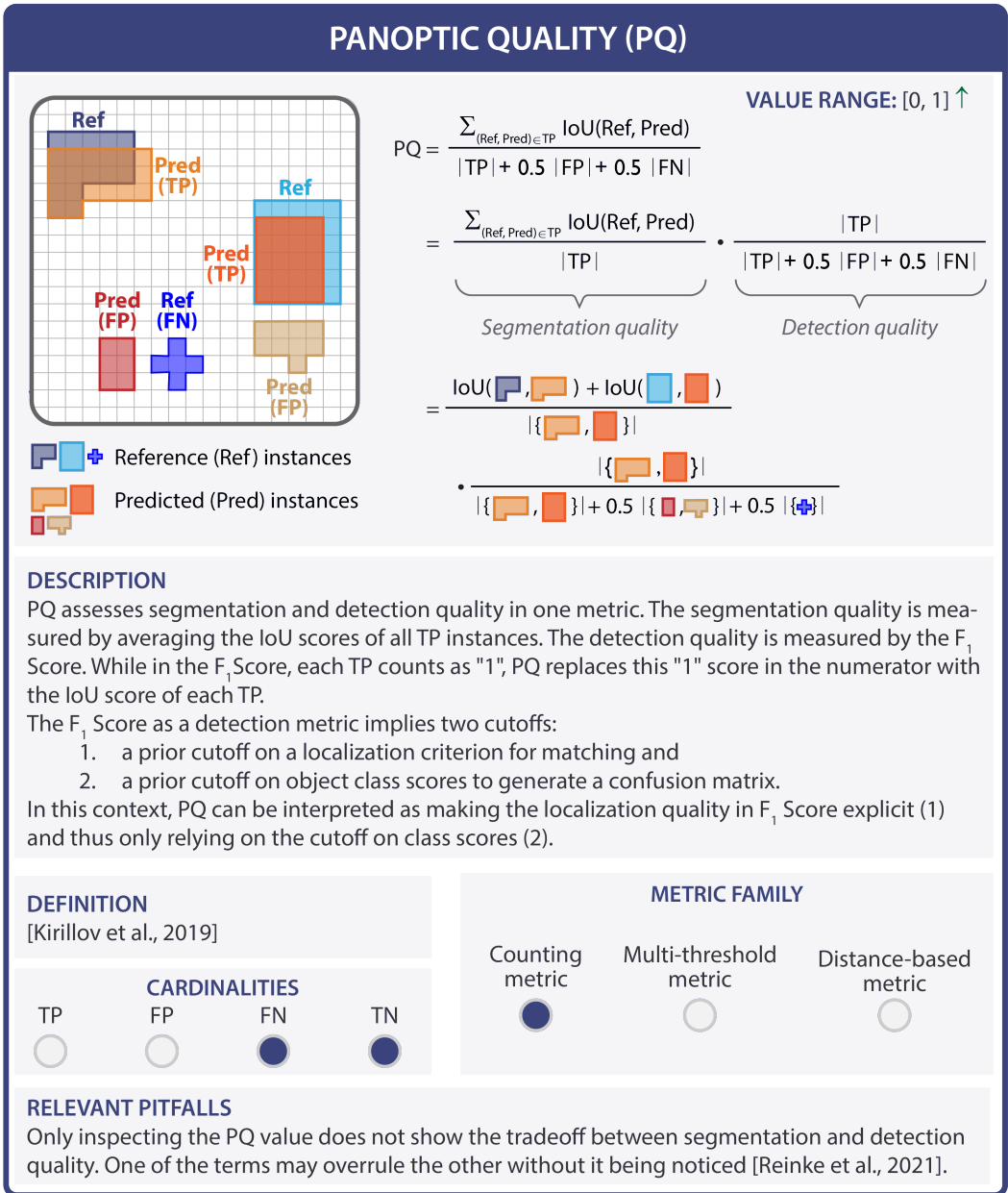


Fig. SN 3.49. Metric profile of Panoptic Quality (PQ). The upward arrow in the value range indicates that higher values are better than lower values. Abbreviations: Average Precision (AP), False Negative (FN), False Positive (FP), Free-Response Receiver Operating Characteristic (FROC), Intersection over Union (IoU), True Negative (TN), True Positive (TP). References: Kirillov et al., 2019: [36], Reinke et al., 2021: [54].

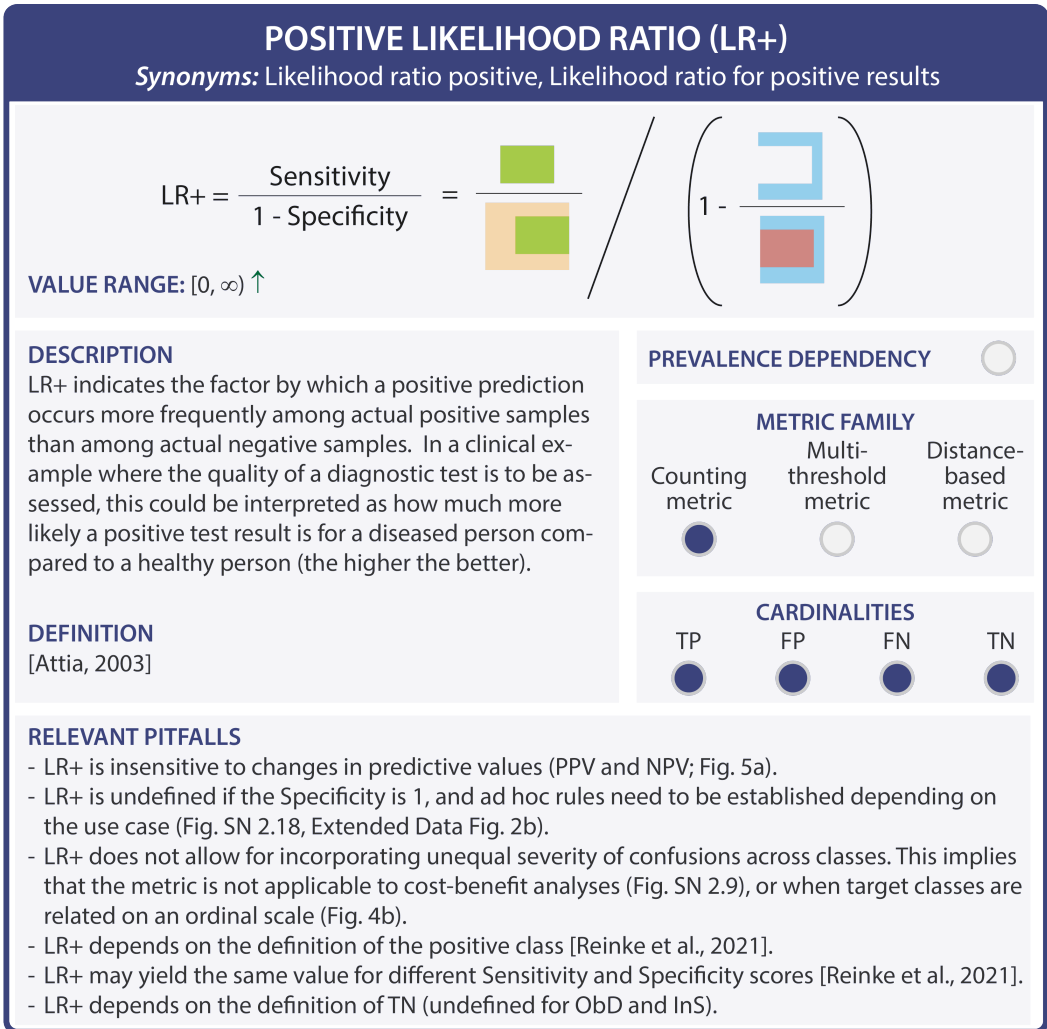


Fig. SN 3.50. Metric profile of Positive Likelihood Ratio (LR+). The upward arrow in the value range indicates that higher values are better than lower values. Abbreviations: False Negative (FN), False Positive (FP), Instance Segmentation (InS), Object Detection (ObD), Positive Predictive Value (PPV), True Negative (TN), True Positive (TP). References: Attia, 2003: [2], Reinke et al., 2021: [54]. Mentioned figures: Figs. 4b, 5a, SN 2.9, SN 2.18, Extended Data Fig. 2b.

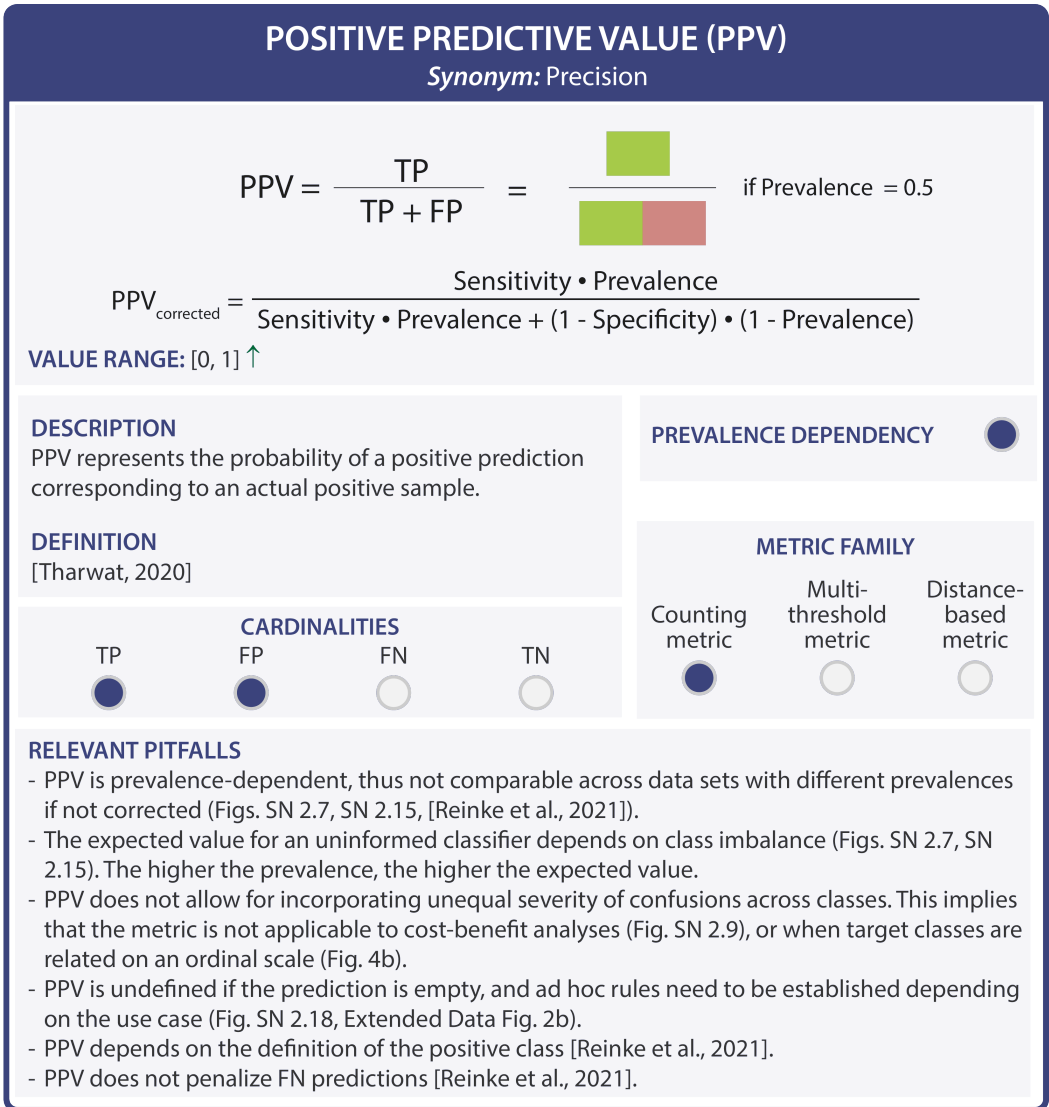


Fig. SN 3.51. Metric profile of the Positive Predictive Value (PPV). The upward arrow in the value range indicates that higher values are better than lower values. Abbreviations used in the figure: False Negative (FN), False Positive (FP), Instance Segmentation (InS), Object Detection (ObD), True Negative (TN), True Positive (TP). References used in the figure: Reinke et al., 2021: [54], Tharwat, 2020: [60]. Mentioned figures: Figs. 4b, SN 2.7, SN 2.9, SN 2.15, SN 2.18, Extended Data Fig. 2b.

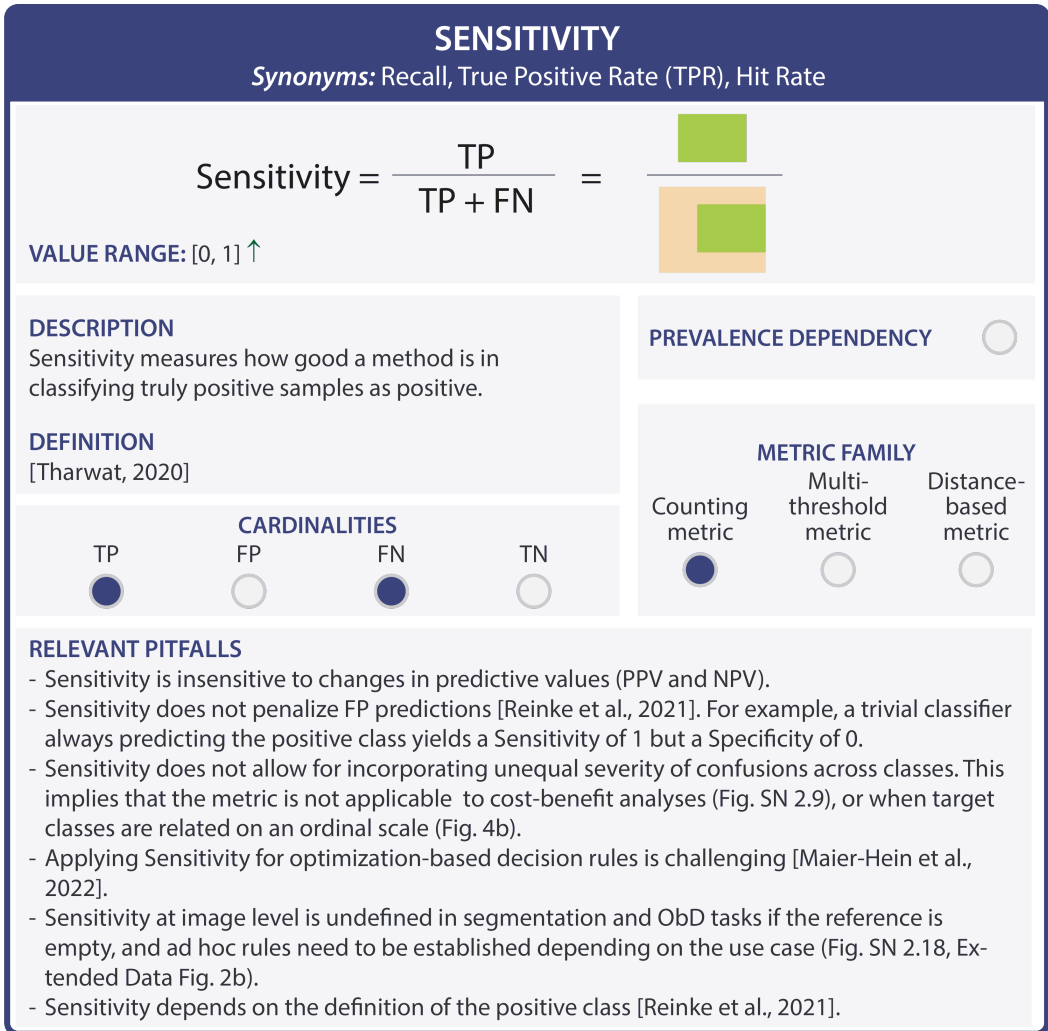


Fig. SN 3.52. Metric profile of Sensitivity. The upward arrow in the value range indicates that higher values are better than lower values. Abbreviations: False Negative (FN), False Positive (FP), Object Detection (ObD), Positive Predictive Value (PPV), True Negative (TN), True Positive (TP). References: Maier-Hein et al., 2022: [44], Reinke et al., 2021: [54], Tharwat, 2020: [60]. Mentioned figures: Figs. 4b, SN 2.9, SN 2.18, Extended Data Fig. 2b.

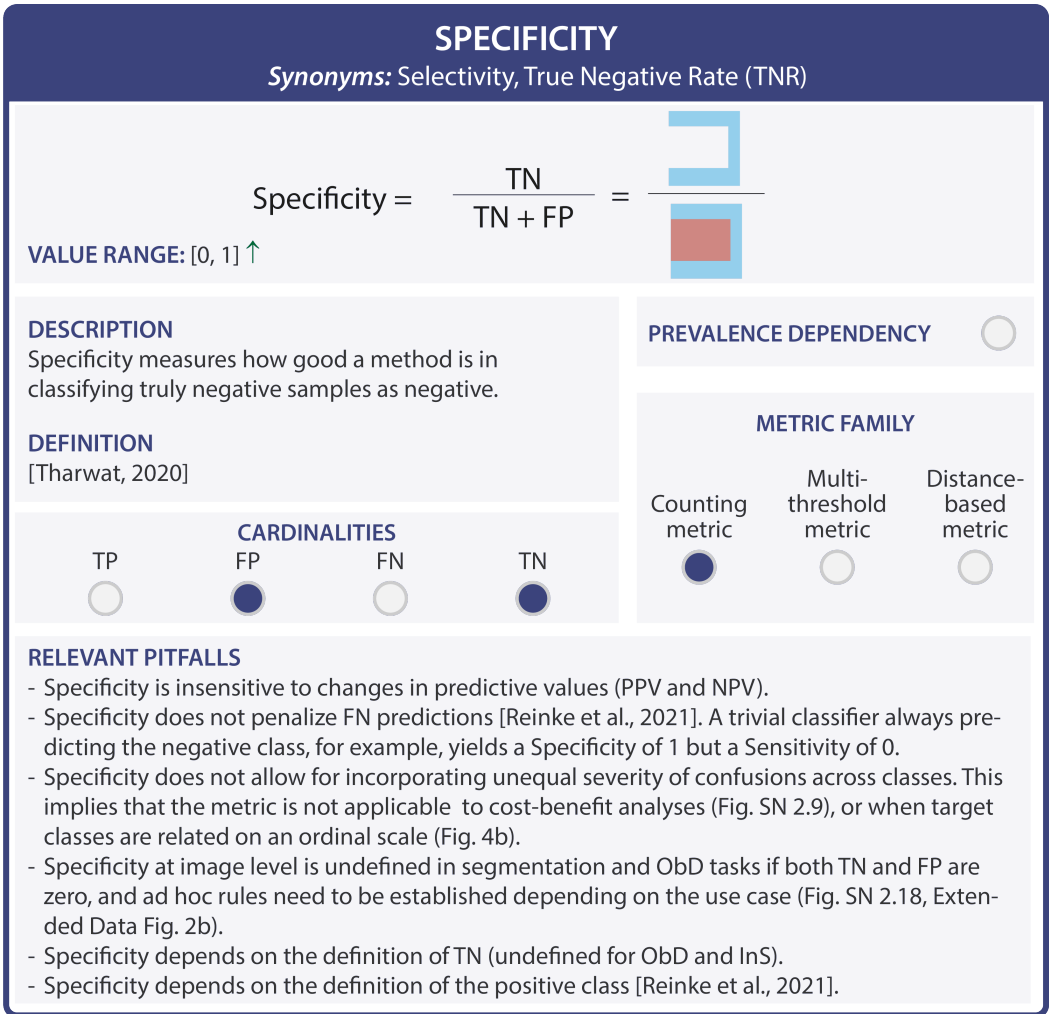


Fig. SN 3.53. Metric profile of Specificity. The upward arrow in the value range indicates that higher values are better than lower values. Abbreviations: False Negative (FN), False Positive (FP), True Negative (TN), True Positive (TP). References: Reinke et al., 2021: [54], Tharwat, 2020: [60]. Mentioned figures: Figs. 4b SN 2.9, SN 2.18, Extended Data Fig. 2b.

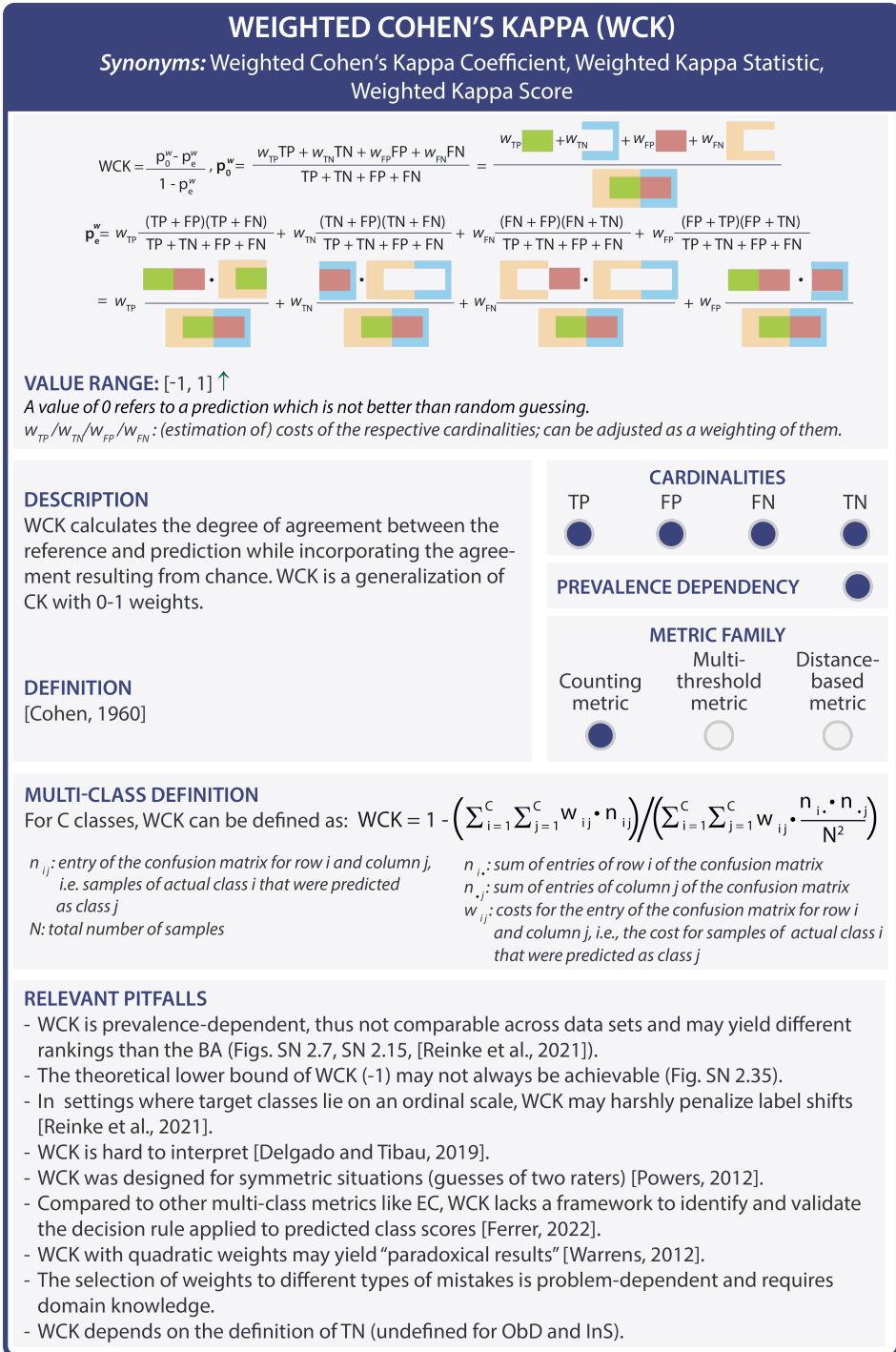


Fig. SN 3.54. Metric profile of Weighted Cohen's Kappa (WCK). The upward arrow in the value range indicates that higher values are better than lower values. Abbreviations: Balanced Accuracy (BA), Cohen's Kappa (CK), Expected Cost (EC), False Negative (FN), False Positive (FP), Instance Segmentation (InS), Object Detection (ObD), True Negative (TN), True Positive (TP). References: Cohen, 1960: [13], Delgado and Tibau, 2019: [18], Ferrer, 2022: [24], Powers, 2012: [53], Reinke et al., 2021: [54], Warrens, 2012: [67]. Mentioned figures: Figs. SN 2.7, SN 2.15, SN 2.35.

3.1.2 Multi-threshold metrics.

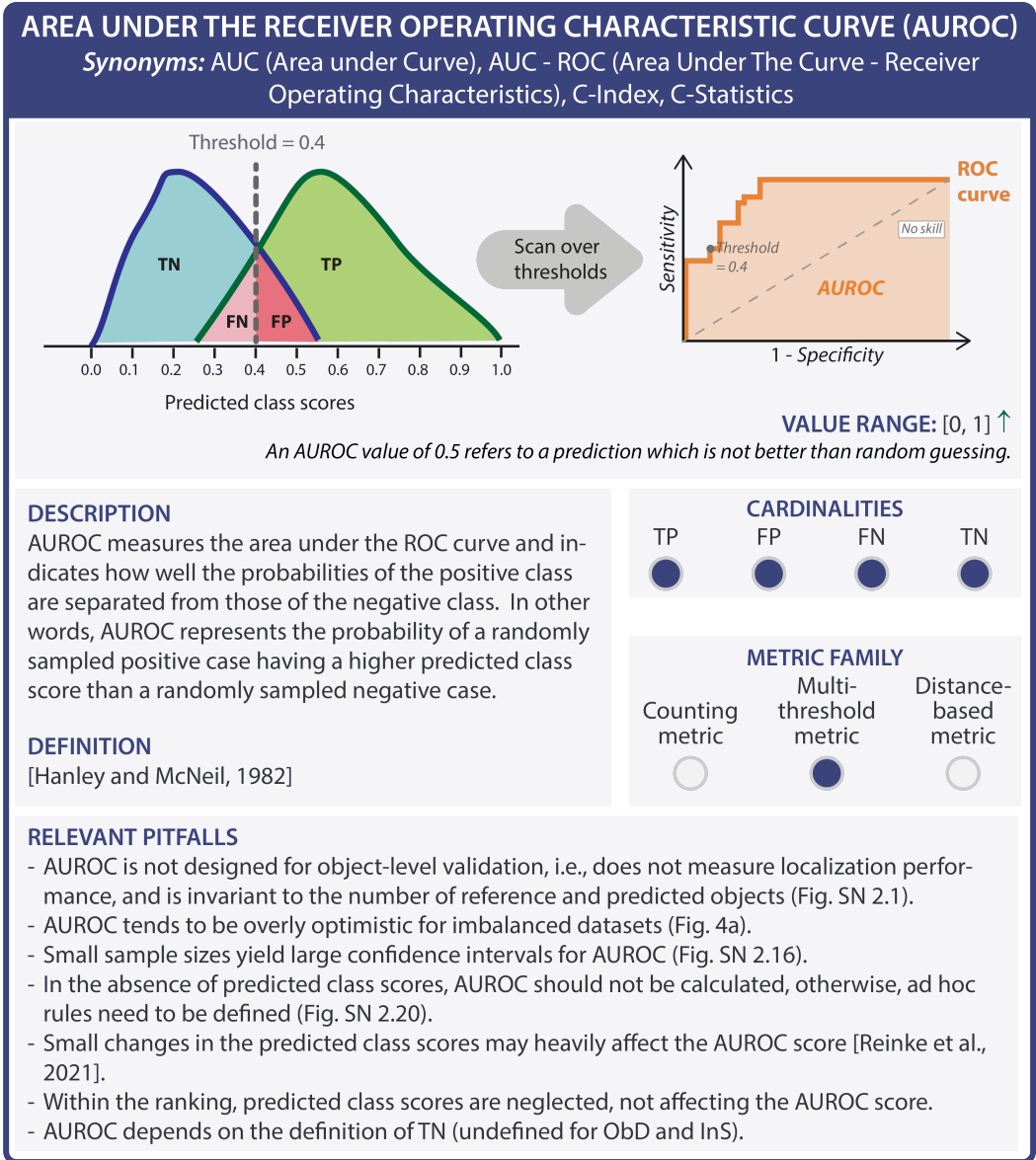


Fig. SN 3.55. Metric profile of Area under the Receiver Operating Characteristic Curve (AUROC). The upward arrow in the value range indicates that higher values are better than lower values. Abbreviations: False Negative (FN), False Positive (FP), Instance Segmentation (InS), Object Detection (ObD), Receiver Operating Characteristic (ROC), True Negative (TN), True Positive (TP). References: Hanley and McNeil, 1982: [31], Reinke et al., 2021: [54]. Mentioned figures: Figs. 5a, SN 2.1, SN 2.16, SN 2.20.

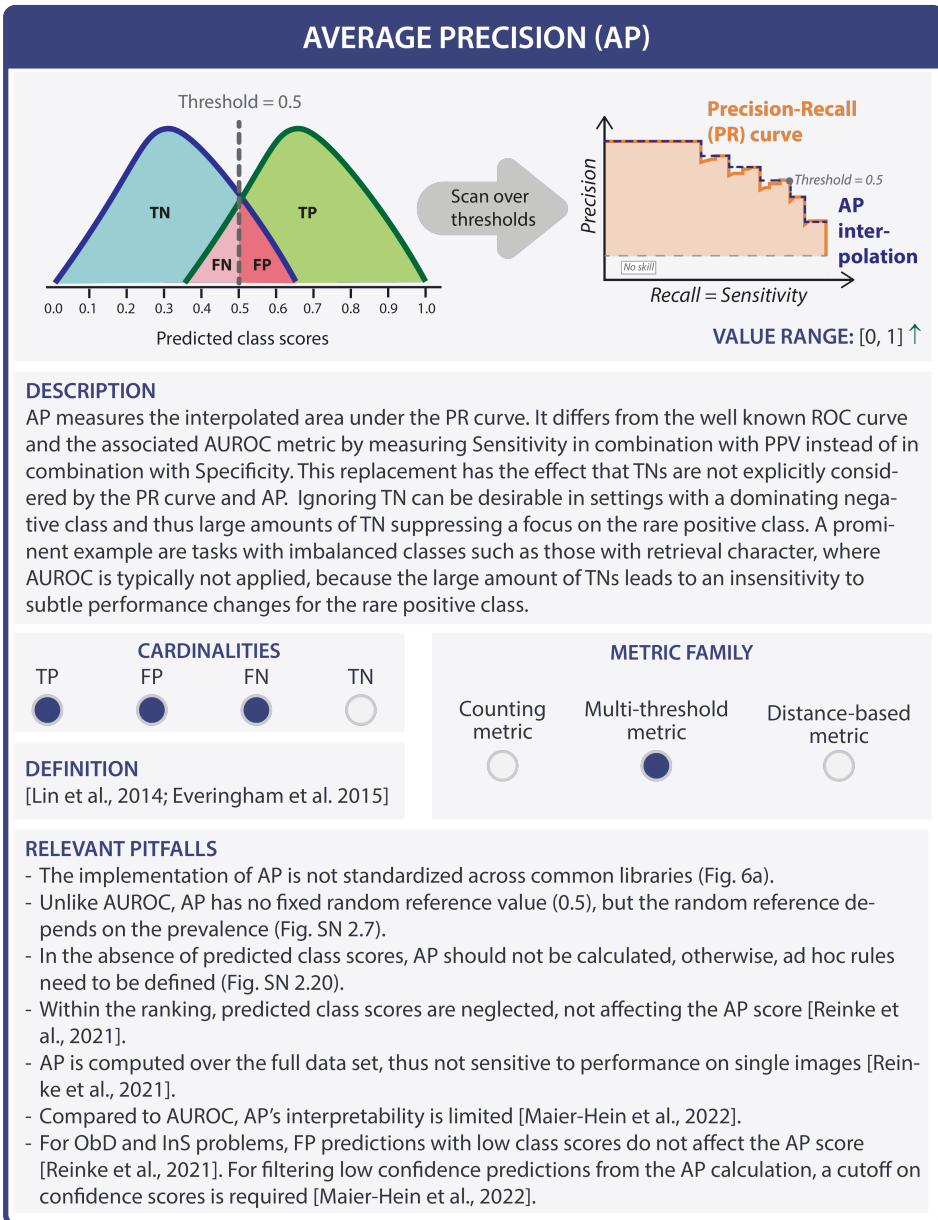


Fig. SN 3.56. Metric profile of Average Precision (AP). The upward arrow in the value range indicates that higher values are better than lower values. Abbreviations: Area under the Receiver Operating Characteristic Curve (AUROC), False Negative (FN), False Positive (FP), Instance Segmentation (InS), Object Detection (ObD), Precision-Recall (PR), True Negative (TN), True Positive (TP). References: Everingham et al., 2015: [22], Lin et al., 2014: [42], Maier-Hein et al., 2022: [44], Reinke et al., 2021: [54]. Mentioned figures: Figs. 6a, SN 2.7, SN 2.20.

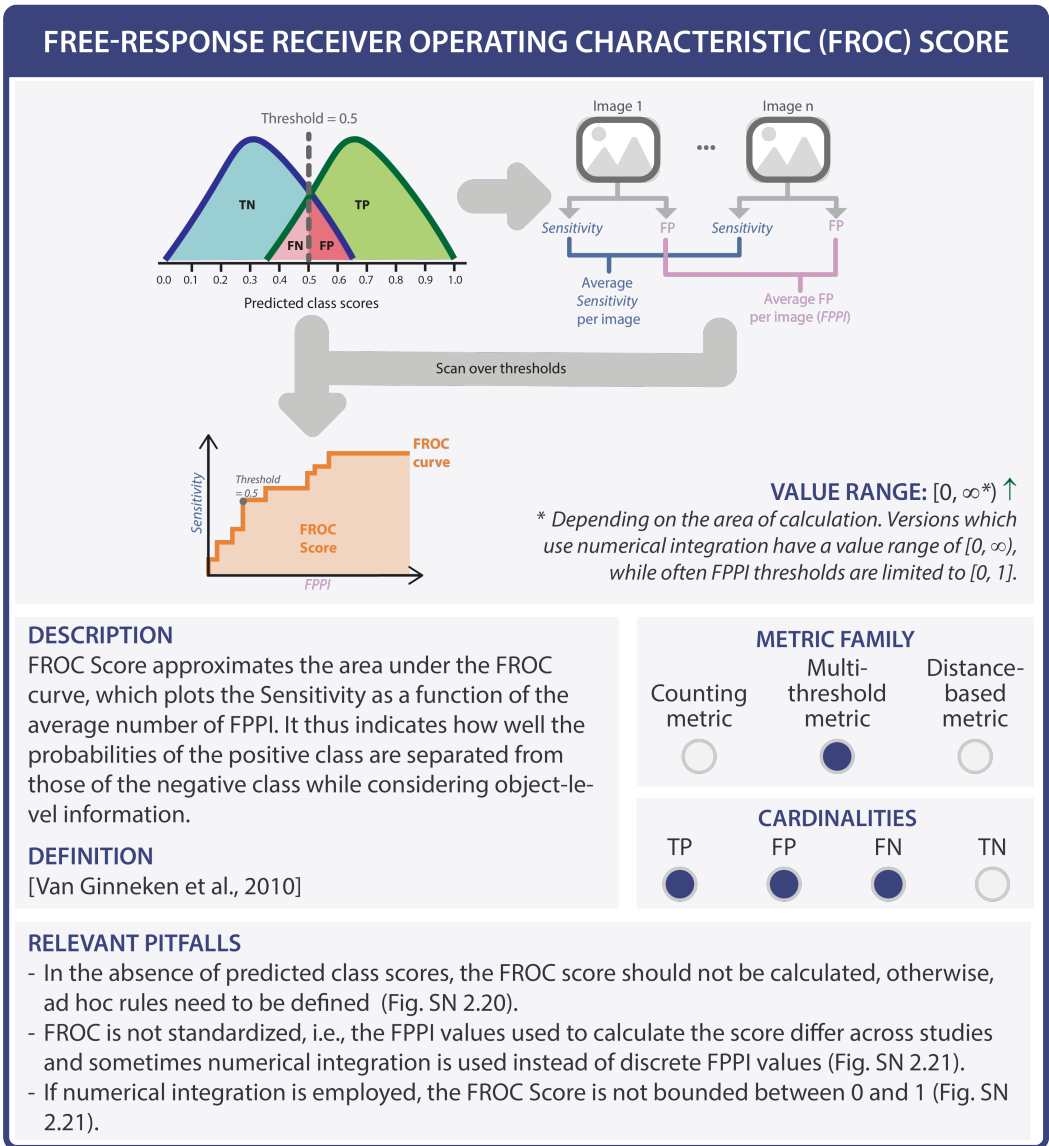


Fig. SN 3.57. Metric profile of Free-Response Receiver Operating Characteristic (FROC). The upward arrow in the value range indicates that higher values are better than lower values. Abbreviations: False Negative (FN), False Positive (FP), False Positives per Image (FPPI), True Negative (TN), True Positive (TP). References: Van Ginneken et al., 2010: [62]. Mentioned figures: Figs. SN 2.20, SN 2.21.

3.1.3 Distance-based metrics.

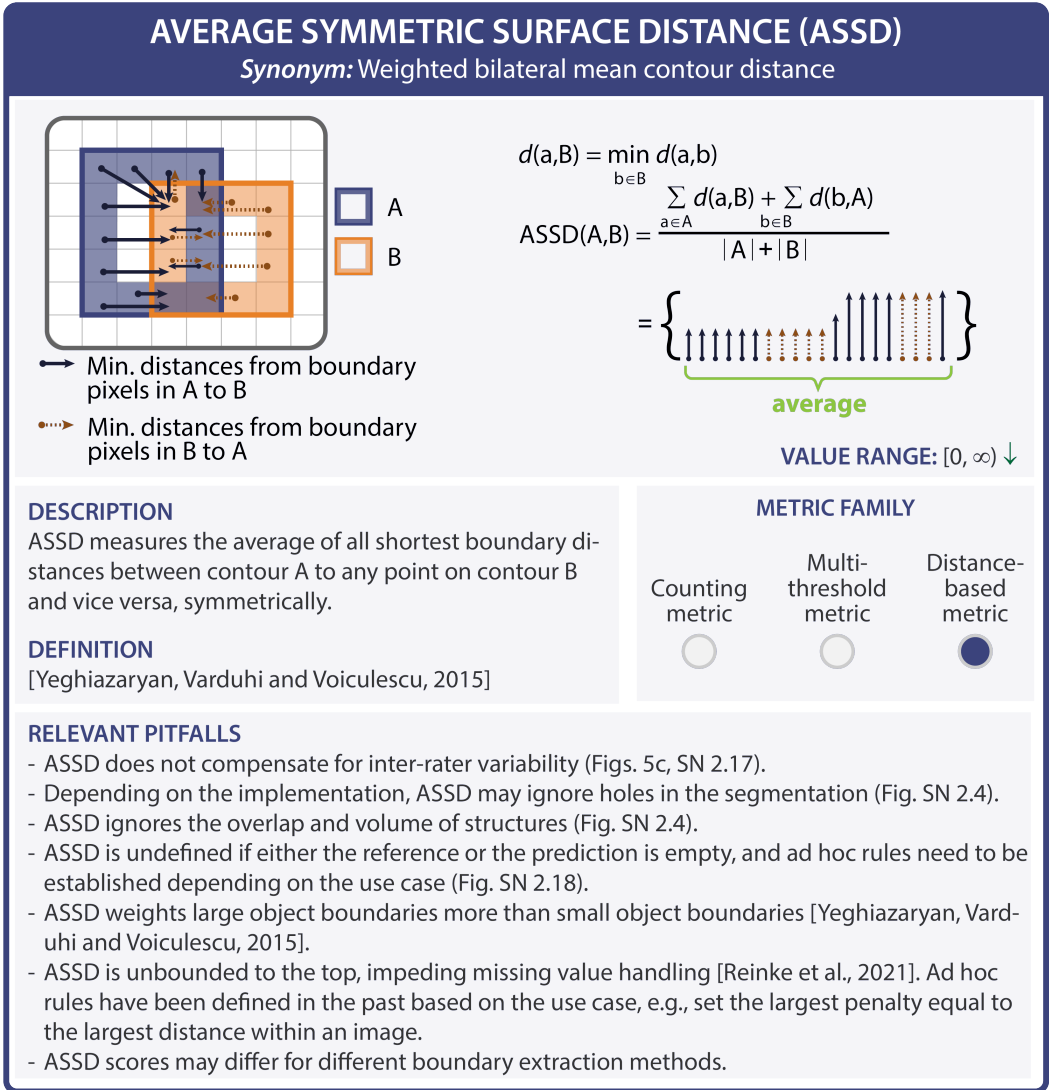


Fig. SN 3.58. Metric profile of Average Symmetric Surface Distance (ASSD). The downward arrow in the value range indicates that lower values are better than higher values. Abbreviation: Semantic Segmentation (SemS). References: Reinke et al., 2021: [54], Yeghiazaryan, Varduhi and Voiculescu, 2015: [70]. Mentioned figures: Figs. 5c, SN 2.4, SN 2.17, SN 2.18.

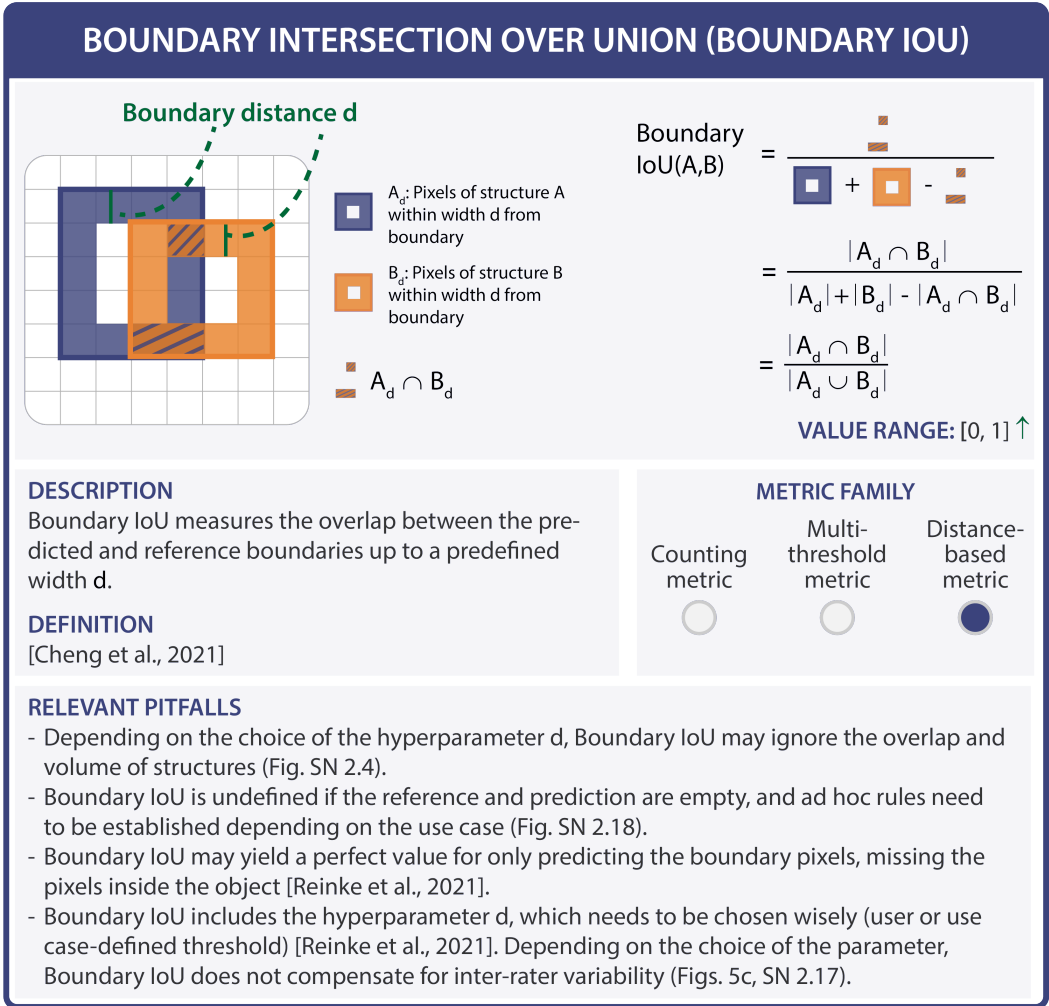


Fig. SN 3.59. Metric profile of the Boundary Intersection over Union (IoU). The upward arrow in the value range indicates that higher values are better than lower values. References: Cheng et al., 2021: [10], Reinke et al., 2021: [54]. Mentioned figures: Figs. 5c, SN 2.4, SN 2.17, SN 2.18.



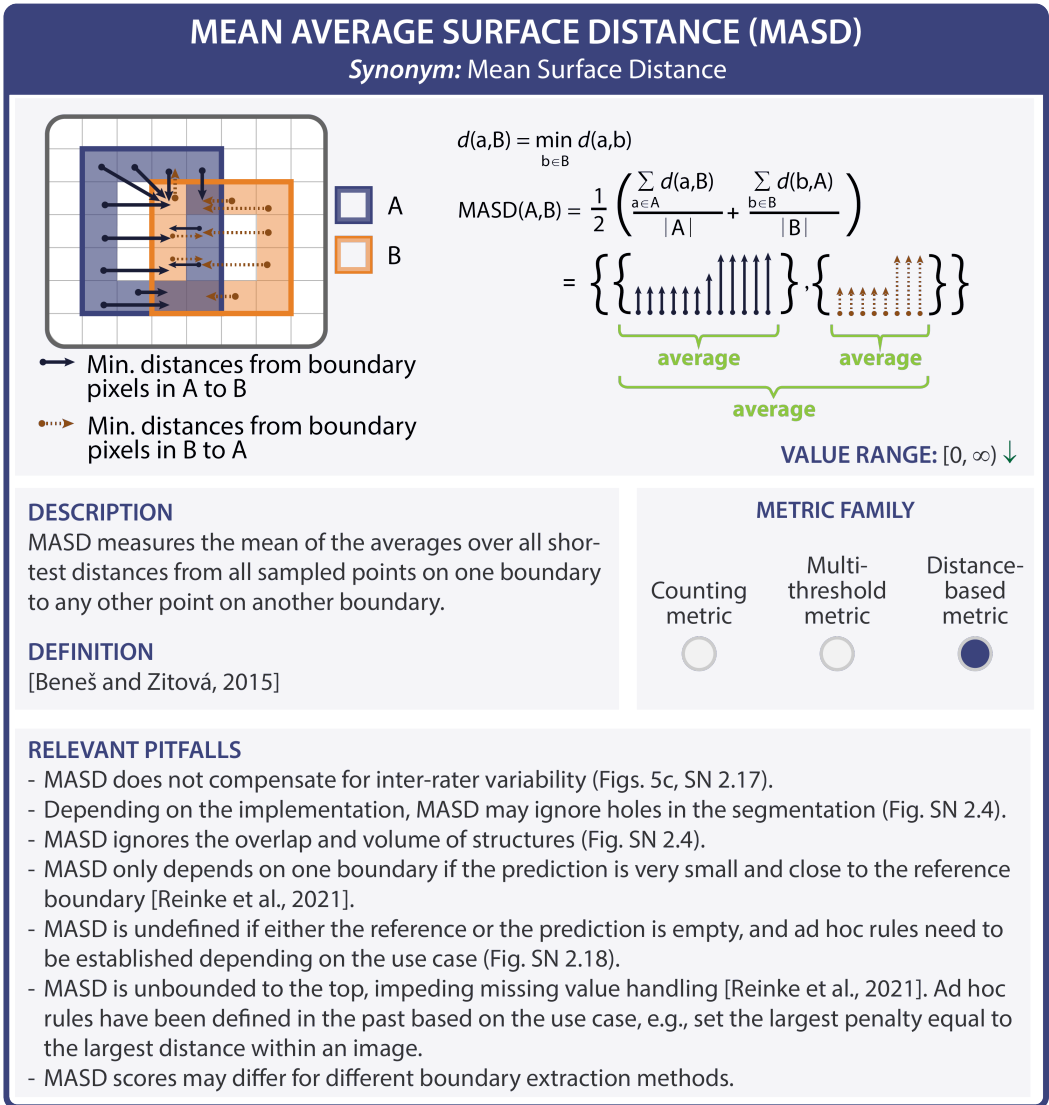


Fig. SN 3.61. Metric profile of Mean Average Surface Distance (MASD). The downward arrow in the value range indicates that lower values are better than higher values. Abbreviation: Semantic Segmentation (SemS). References: Beneš and Zitová, 2015: [6], Reinke et al., 2021: [54]. Mentioned figures: Figs. 5c, SN 2.4, SN 2.17, SN 2.18.

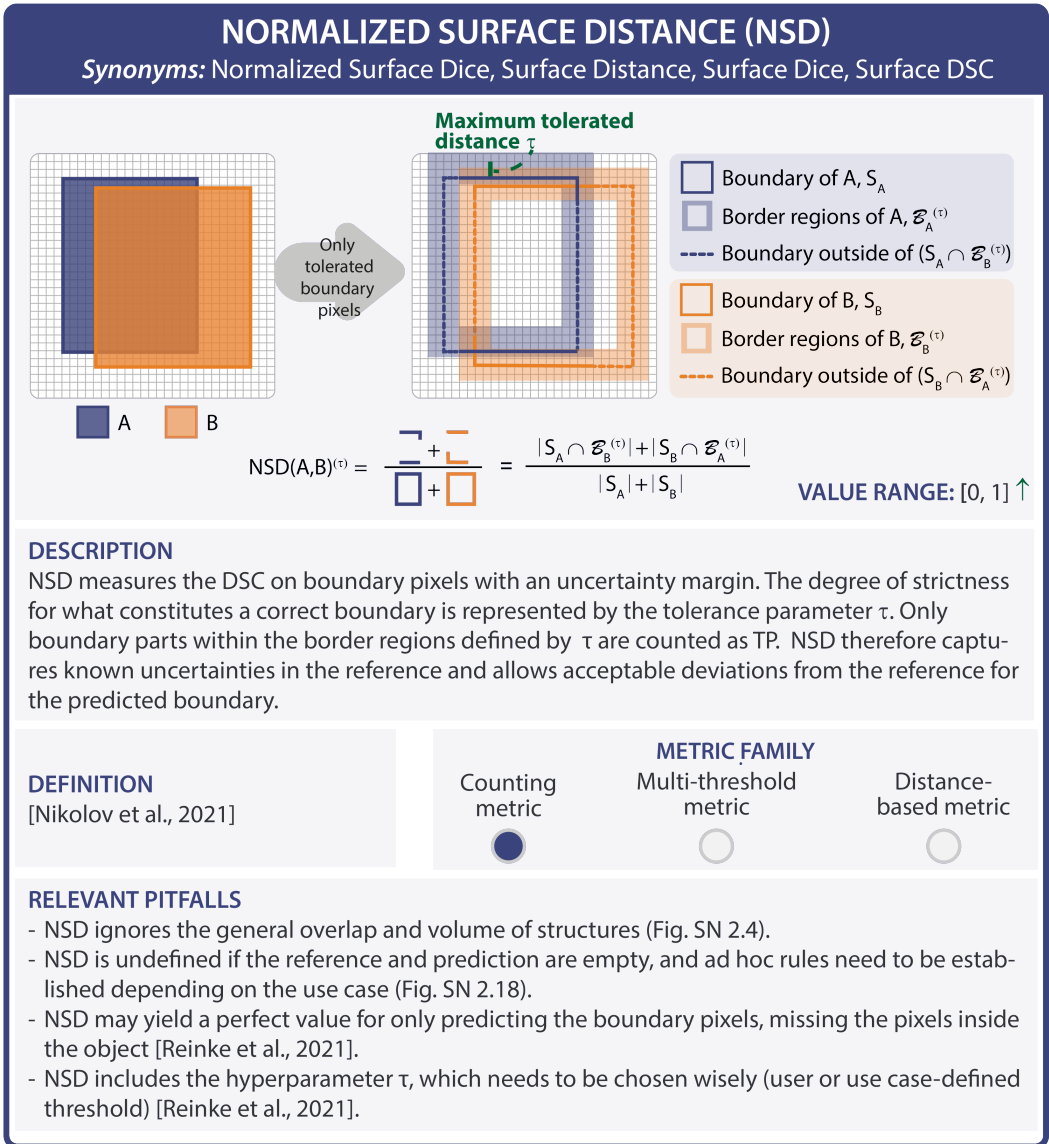


Fig. SN 3.62. Metric profile of Normalized Surface Distance (NSD). The upward arrow in the value range indicates that higher values are better than lower values. Abbreviation: Dice Similarity Coefficient (DSC). References: Nikolov et al., 2021: [50], Reinke et al., 2021: [54]. Mentioned figures: Figs. SN 2.4, SN 2.18.

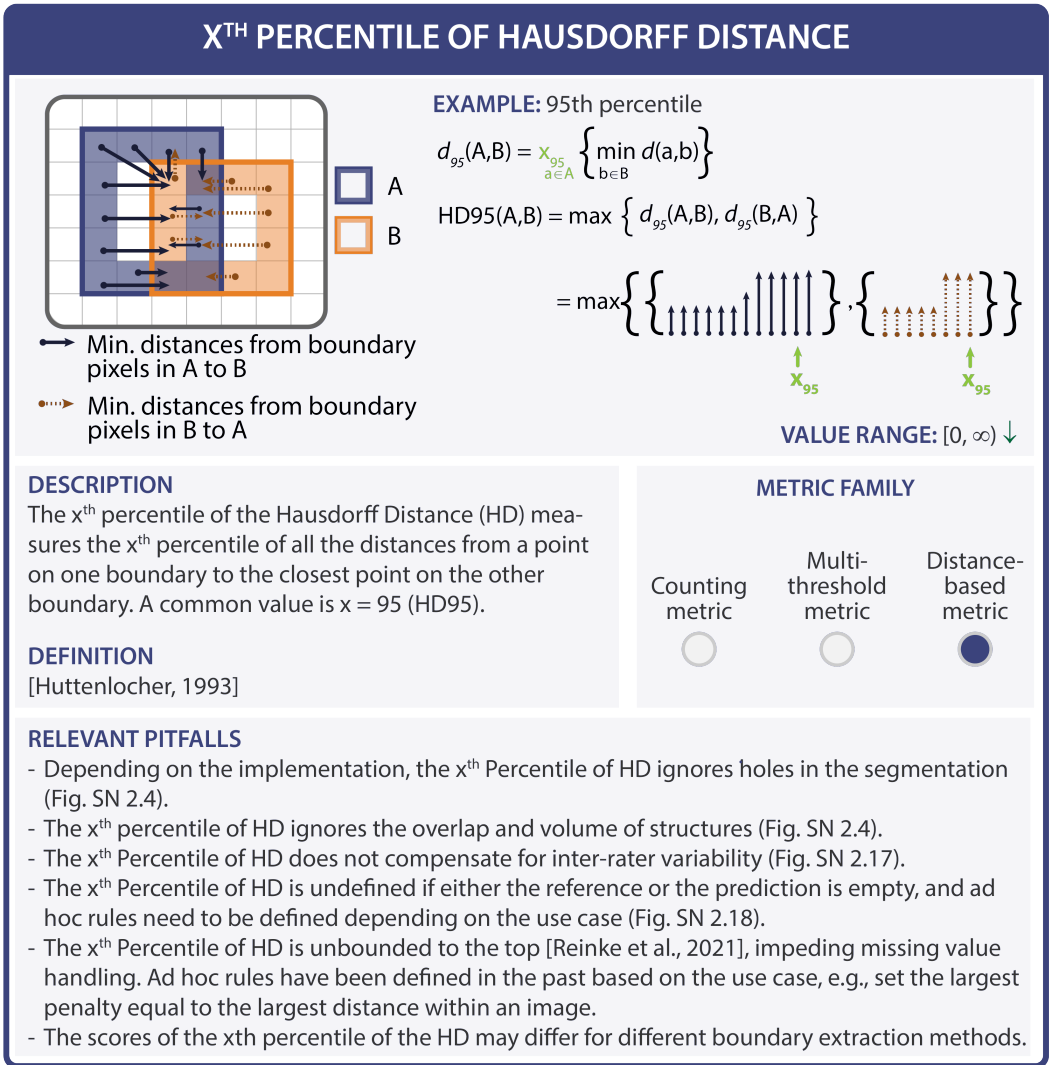


Fig. SN 3.63. Metric profile of X<sup>th</sup> Percentile of Hausdorff Distance (HD). The downward arrow in the value range indicates that lower values are better than higher values. Abbreviations: Hausdorff Distance (HD), Semantic Segmentation (SemS). References: Huttenlocher, 1993: [34], Reinke et al., 2021: [54]. Mentioned figures: Figs. SN 2.4, SN 2.17, SN 2.18.

### 3.2 Calibration metrics

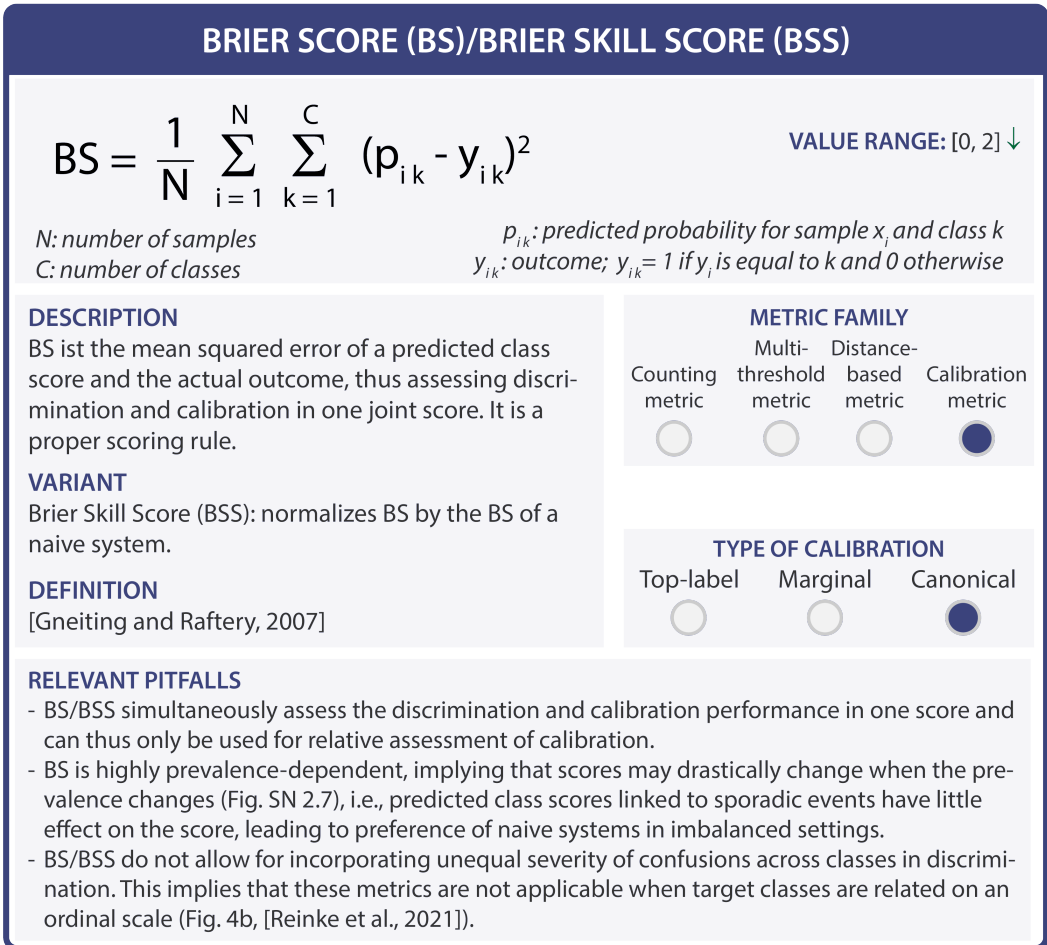


Fig. SN 3.64. Metric profile of Brier Score (BS). The downward arrow in the value range indicates that lower values are better than higher values. Abbreviation: Brier Skill Score (BSS). References: Gneiting and Raftery, 2007: [26], Reinke et al., 2021: [54]. Mentioned figure: Fig. SN 2.7.

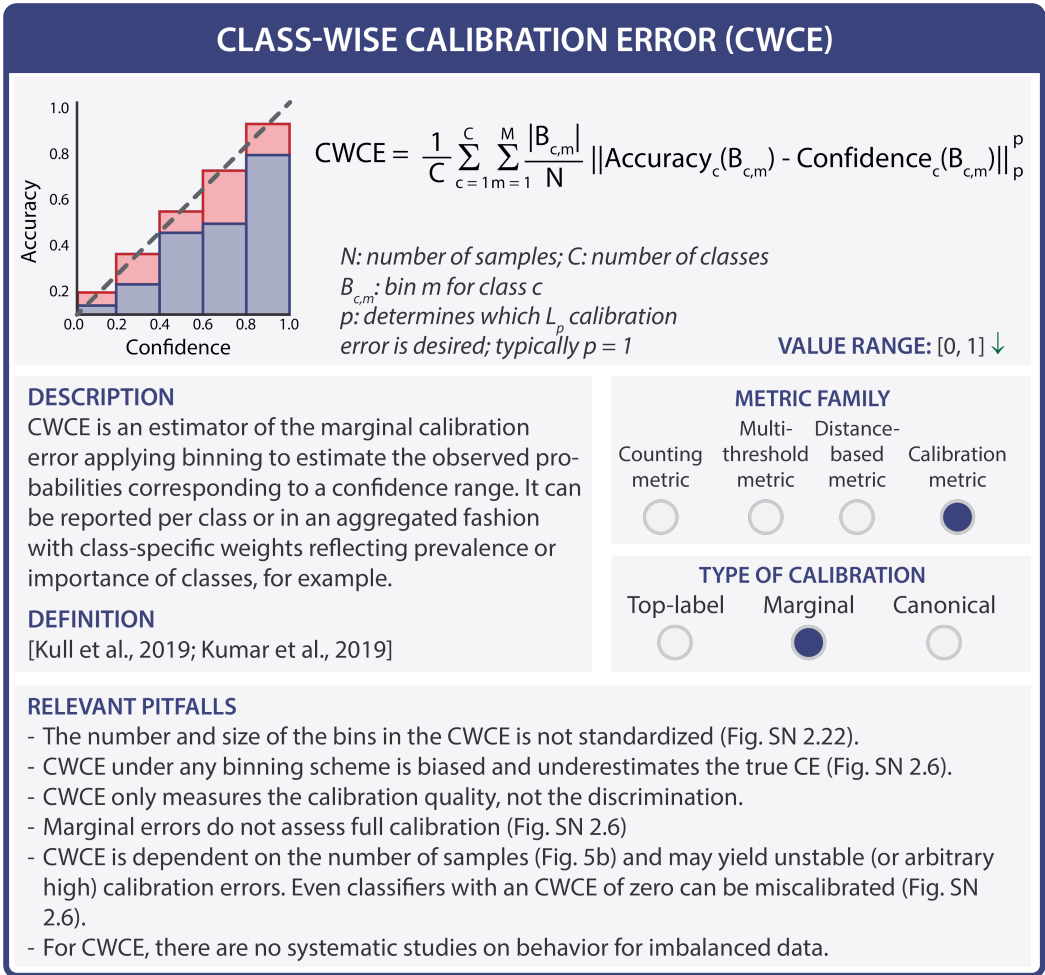


Fig. SN 3.65. Metric profile of Class-Wise Calibration Error (CWCE). The downward arrow in the value range indicates that lower values are better than higher values. References: Kumar et al., 2019: [41], Kull et al., 2019: [40]. Mentioned figures: Figs. 5b, SN 2.6, SN 2.22.

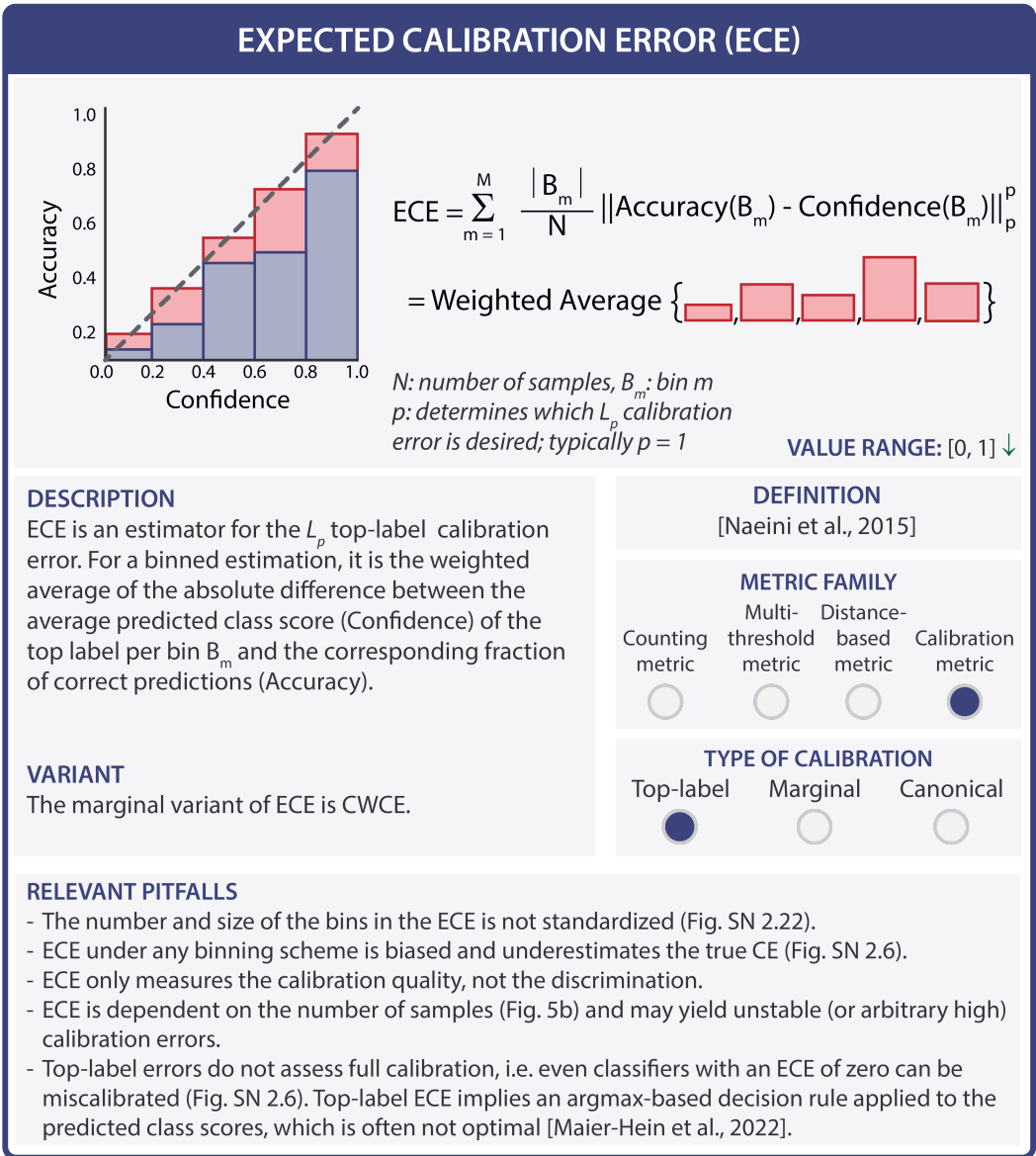


Fig. SN 3.66. Metric profile of Expected Calibration Error (ECE). The downward arrow in the value range indicates that lower values are better than higher values. References: Maier-Hein et al., 2022: [44], Naeini et al., 2015: [47], Reinke et al., 2021: [54]. Mentioned figures: Figs. 5b, SN 2.6, SN 2.22.

### EXPECTED CALIBRATION ERROR KERNEL DENSITY ESTIMATE (ECE<sup>KDE</sup>)

$$ECE^{KDE} = \frac{1}{N} \sum_{j=1}^N \left\| \frac{\sum_{i \neq j} k(f(x_j), f(x_i)) e_{y_i}}{\sum_{i \neq j} k(f(x_j), f(x_i))} - f(x_j) \right\|_p^p$$

*N*: number of samples  
*k*: kernel, e.g. Dirichlet kernel [Popordanoska et al., 2022]  
*f*(*x*): predicted probability vector, *y<sub>i</sub>*: outcome (one-hot encoded)  
*e<sub>y</sub>*: *C*-dimensional vector with *y<sub>i</sub>*-th entry being 1, else 0  
*p*: determines which *L<sub>p</sub>* calibration error is desired; typically *p* ∈ {1, 2}

**VALUE RANGE:** [0, 2] ↓

<p><b>DESCRIPTION</b>                      ECE<sup>KDE</sup> is an estimator for the canonical calibration error. It uses a kernel density estimate in contrast to the binning strategy applied by the standard ECE.</p> <p><b>DEFINITION</b>                      [Popordanoska et al., 2022]</p> <p><b>RELEVANT PITFALLS</b></p> <ul style="list-style-type: none"> <li>- ECE<sup>KDE</sup> does not scale to a large number of classes (problematic for more than 10 classes).</li> <li>- ECE<sup>KDE</sup> is a biased estimator and is particularly unreliable for small sample sizes.</li> </ul>	<p style="text-align: center;"><b>METRIC FAMILY</b></p> <table border="0" style="width: 100%; text-align: center;"> <tr> <td style="padding: 2px;">Counting metric</td> <td style="padding: 2px;">Multi- threshold metric</td> <td style="padding: 2px;">Distance- based metric</td> <td style="padding: 2px;">Calibration metric</td> </tr> <tr> <td><input type="radio"/></td> <td><input type="radio"/></td> <td><input type="radio"/></td> <td><input checked="" type="radio"/></td> </tr> </table> <p style="text-align: center;"><b>TYPE OF CALIBRATION</b></p> <table border="0" style="width: 100%; text-align: center;"> <tr> <td style="padding: 2px;">Top-label</td> <td style="padding: 2px;">Marginal</td> <td style="padding: 2px;">Canonical</td> </tr> <tr> <td><input type="radio"/></td> <td><input type="radio"/></td> <td><input checked="" type="radio"/></td> </tr> </table>	Counting metric	Multi- threshold metric	Distance- based metric	Calibration metric	<input type="radio"/>	<input type="radio"/>	<input type="radio"/>	<input checked="" type="radio"/>	Top-label	Marginal	Canonical	<input type="radio"/>	<input type="radio"/>	<input checked="" type="radio"/>
Counting metric	Multi- threshold metric	Distance- based metric	Calibration metric												
<input type="radio"/>	<input type="radio"/>	<input type="radio"/>	<input checked="" type="radio"/>												
Top-label	Marginal	Canonical													
<input type="radio"/>	<input type="radio"/>	<input checked="" type="radio"/>													

Fig. SN 3.67. Metric profile of Expected Calibration Error Kernel Density Estimate (ECE<sup>KDE</sup>). The downward arrow in the value range indicates that lower values are better than higher values. Abbreviation: Expected Calibration Error (ECE). Reference used in the figure: Popordanoska et al., 2022: [52].

## KERNEL CALIBRATION ERROR (KCE)

$$\text{KCE} = \left( \mathbb{E} \left( (e_y - f(x))^T k(f(x), f(x')) (e_y - f(x')) \right) \right)^{1/2}$$

Example estimator:  $\widehat{\text{KCE}} = \left( \binom{N}{2}^{-1} \sum_{i=1}^N \sum_{j=i+1}^N (e_{y_i} - f(x_i))^T k(f(x_i), f(x_j)) (e_{y_j} - f(x_j)) \right)^{1/2}$

*N*: number of samples; *k*: matrix-valued kernel; *f*(*x*): predicted probability vector;  
*y<sub>i</sub>*: outcome; *e<sub>y<sub>i</sub></sub>*: *C*-dimensional vector with *y<sub>i</sub>*-th entry being 1, else 0

**VALUE RANGE:** Kernel dependent; in expectation > 0 but estimator can be arbitrarily negative

### DESCRIPTION

KCE measures a canonical calibration error based on an alternative distance function, the “maximum mean discrepancy” (MMD). It is based on a matrix-valued kernel *k*.

KCE is an unbiased estimator of the calibration error measured by MMD.

### DEFINITION

[Widmann et al., 2019; Gruber and Buettner, 2022]

### RELEVANT PITFALLS

- KCE may be hard to interpret, also due to negative output values.
- KCE cannot be used as an interpretable estimate of the calibration error and should only be used for comparative calibration assessment.
- KCE depends on nontrivial configuration choices of kernels and associated hyperparameters.
- KCE is computationally expensive.

### METRIC FAMILY

Counting metric	Multi-threshold metric	Distance-based metric	Calibration metric
<input type="radio"/>	<input type="radio"/>	<input type="radio"/>	<input checked="" type="radio"/>

### TYPE OF CALIBRATION

Top-label	Marginal	Canonical
<input type="radio"/>	<input type="radio"/>	<input checked="" type="radio"/>

Fig. SN 3.68. Metric profile of Kernel Calibration Error (KCE). References: Gruber and Buettner, 2022: [28], Widmann et al., 2019: [68].

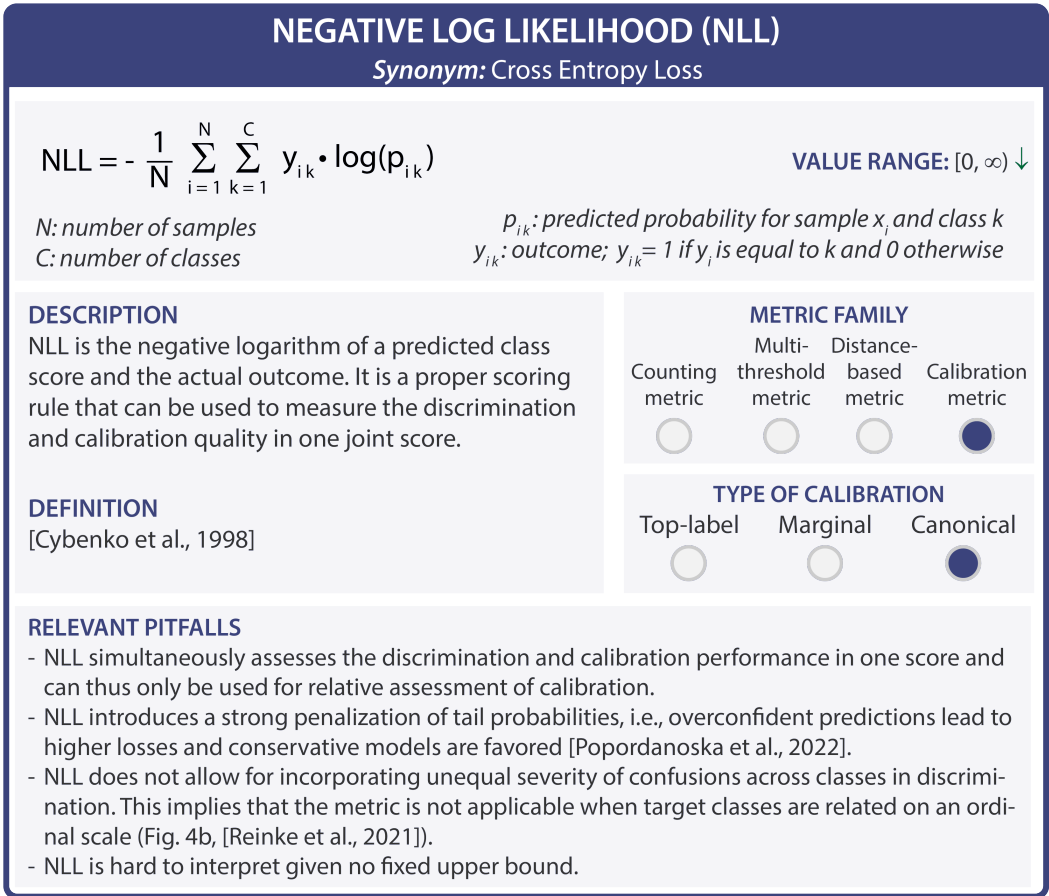


Fig. SN 3.69. Metric profile of Negative Log Likelihood (NLL). The downward arrow in the value range indicates that lower values are better than higher values. References: Cybenko et al., 1998: [14], Popordanoska et al., 2022: [52], Reinke et al., 2021: [54]. Mentioned figure: Fig. 5b.

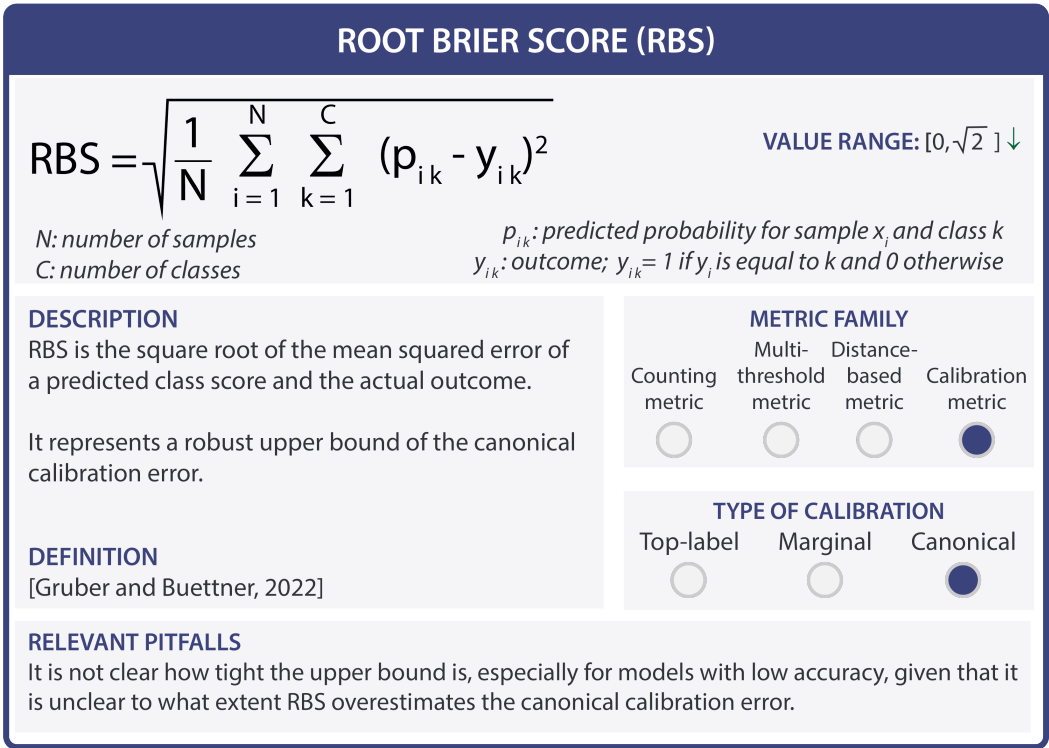


Fig. SN 3.70. Metric profile of Root Brier Score (RBS). The downward arrow in the value range indicates that lower values are better than higher values. Reference: Gruber and Buettner, 2022: [28].

3.3 Localization criteria

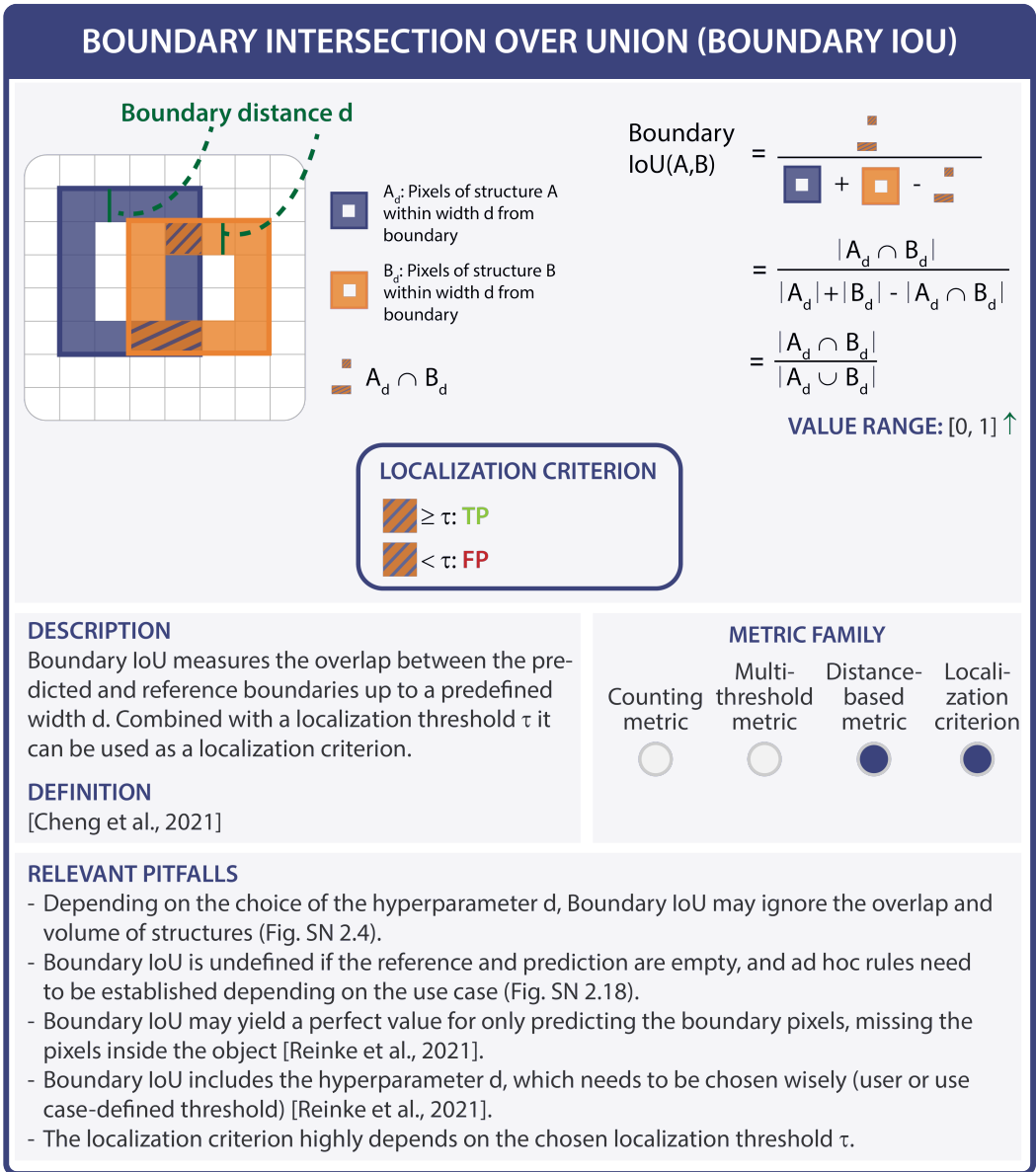


Fig. SN 3.71. Metric profile of the Boundary Intersection over Union (IoU) localization criterion. The upward arrow in the value range indicates that higher values of Boundary IoU are better than lower values. References: Cheng et al., 2021: [10], Reinke et al., 2021: [54]. Mentioned figures: Figs. SN 2.4, SN 2.18.

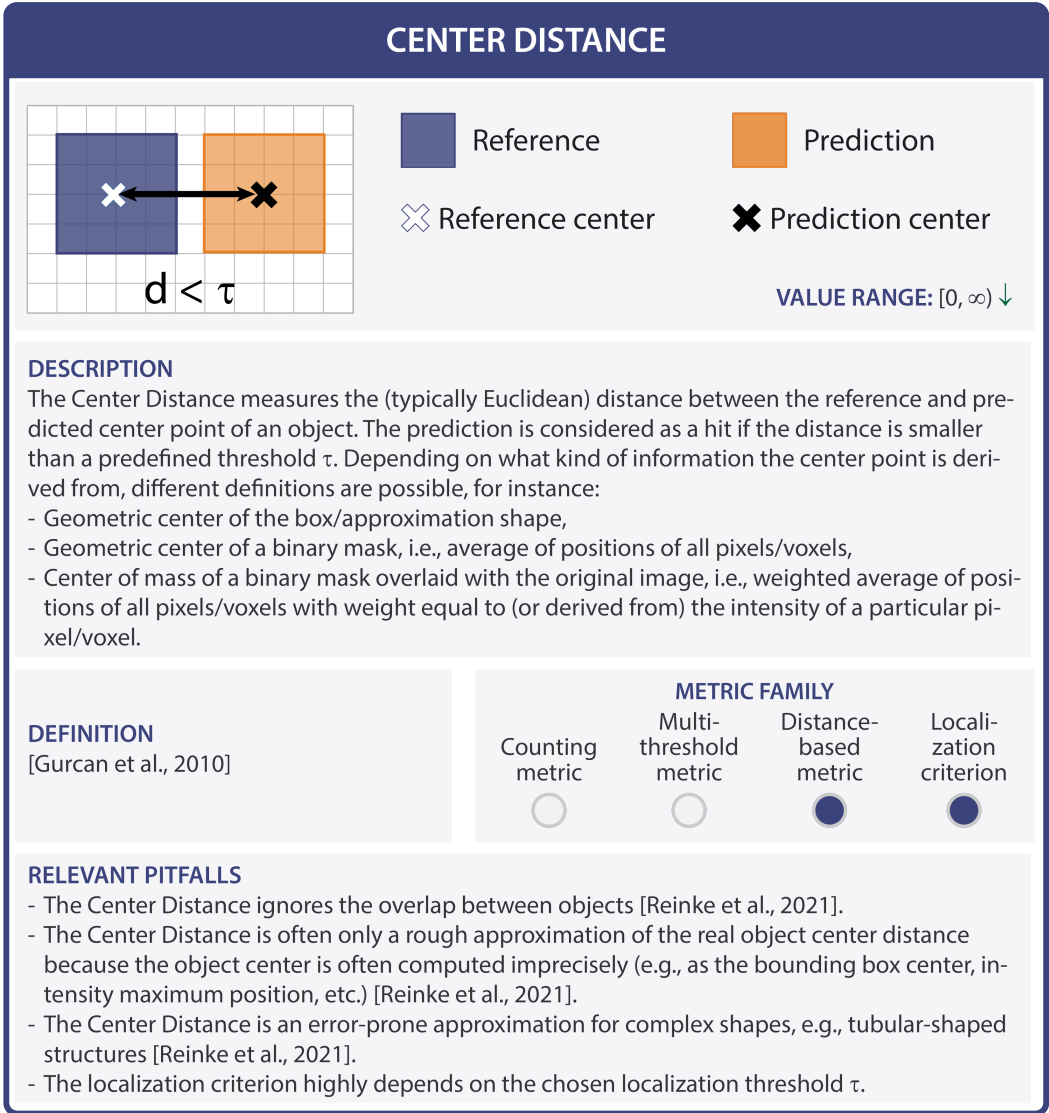


Fig. SN 3.72. Metric profile of the Center Distance localization criterion. The downward arrow in the value range indicates that lower values of the Center Distance are better than higher values. References: Gurcan et al., 2010: [30], Reinke et al., 2021: [54].

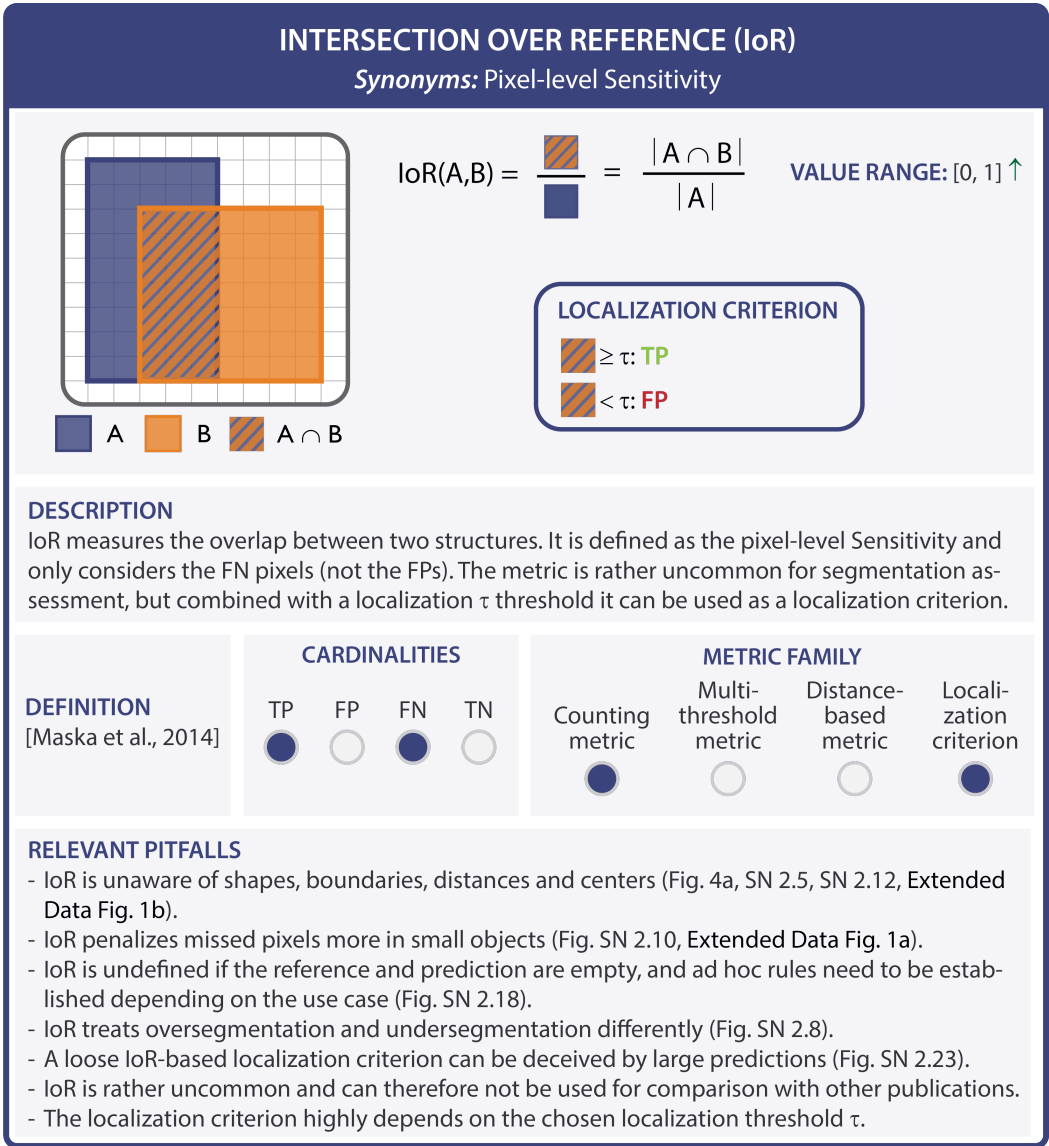
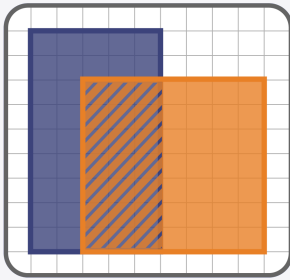


Fig. SN 3.73. Metric profile of the Intersection over Reference (IoR) localization criterion. The upward arrow in the value range indicates that higher values of IoR are better than lower values. Abbreviations: False Negative (FN), False Positive (FP), True Negative (TN), True Positive (TP). References: Maška et al., 2014: [45], Reinke et al., 2021: [54]. Mentioned figures: Figs. 4a, SN 2.5, SN 2.8, SN 2.10, SN 2.11, SN 2.12, SN 2.18, SN 2.23, Extended Data Fig. 1b.

# MASK/BOX/APPROX INTERSECTION OVER UNION (MASK/BOX/APPROX IoU)

Synonyms: Jaccard Index, Tanimoto Coefficient



■ A ■ B ■ A ∩ B

$$\begin{aligned}
 \text{IoU}(A,B) &= \frac{\text{Area of } A \cap B}{\text{Area of } A + \text{Area of } B - \text{Area of } A \cap B} \\
 &= \frac{|A \cap B|}{|A| + |B| - |A \cap B|} = \frac{|A \cap B|}{|A \cup B|} \\
 &= \frac{\text{PPV} \cdot \text{Sensitivity}}{\text{PPV} + \text{Sensitivity} - \text{PPV} \cdot \text{Sensitivity}}
 \end{aligned}$$

### LOCALIZATION CRITERION

- $\geq \tau$ : TP
- $< \tau$ : FP

### DESCRIPTION

IoU measures the overlap between two structures (see above). Combined with a localization threshold, it is a common localization criterion. It is often referred to as **Box IoU** when comparing bounding boxes, **Mask IoU** when comparing segmentation masks, or **Approx IoU** when comparing approximations of objects beyond bounding boxes.

### DEFINITION

[Jaccard, 1912]

CARDINALITIES			
TP	FP	FN	TN
<input checked="" type="radio"/>	<input checked="" type="radio"/>	<input checked="" type="radio"/>	<input type="radio"/>
METRIC FAMILY			
Counting metric	Multi-threshold metric	Distance-based metric	Localization criterion
<input checked="" type="radio"/>	<input type="radio"/>	<input type="radio"/>	<input checked="" type="radio"/>

### RELEVANT PITFALLS

- IoU is unaware of shapes, boundaries, distances and centers (Figs. 4a, SN 2.5, SN 2.12, Extended Data Fig. 1b).
- IoU penalizes missed pixels more in small objects (Figs. SN 2.10, SN 2.11, Extended Data Fig. 1a).
- Box IoU is not a good representation of complex or disconnected structures (Fig. SN 2.14).
- IoU is undefined if both the reference and prediction are empty, and ad hoc rules need to be established depending on the use case (Fig. SN 2.18).
- IoU treats oversegmentation and undersegmentation differently (Fig. SN 2.8).
- IoU does not compensate for inter-rater variability (Fig. SN 2.17).
- A loose IoU-based localization criterion can be deceived by large predictions (Fig. SN 2.23).
- IoU behaves differently in 2D and 3D settings. In 3D settings, the additional z-dimension results in a cubical increase in erroneous pixels [Reinke et al., 2021].
- An IoU-based localization criterion may highly penalize multiple predictions for the same reference object [Reinke et al., 2021].
- The localization criterion highly depends on the chosen localization threshold  $\tau$ .

Fig. SN 3.74. Metric profile of the Mask/Box/Approx Intersection over Union (IoU) localization criterion. Abbreviations: False Negative (FN), False Positive (FP), True Negative (TN), True Positive (TP). References: Jaccard, 1912: [35], Reinke et al., 2021: [54]. Mentioned figures: Figs. 4a, SN 2.5, SN 2.8, SN 2.10, SN 2.11, SN 2.12, SN 2.14, SN 2.17, SN 2.18, SN 2.23, Extended Data Fig. 1a-b.

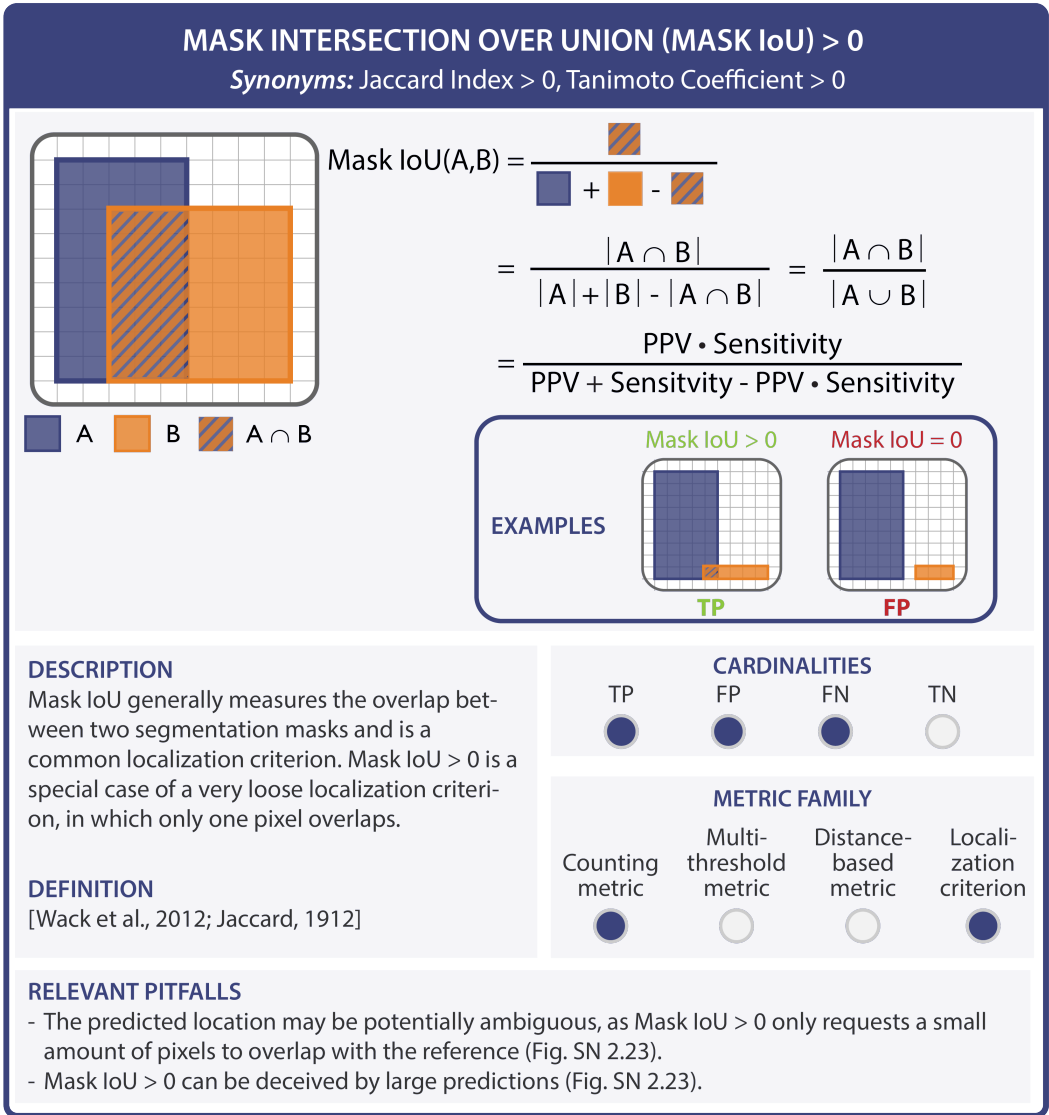


Fig. SN 3.75. Metric profile of the Mask Intersection over Union (IoU) > 0 localization criterion. Abbreviations: False Negative (FN), False Positive (FP), True Negative (TN), True Positive (TP). References: Jaccard, 1912: [35], Wack et al., 2012: [66]. Mentioned figure: Fig. SN 2.23.

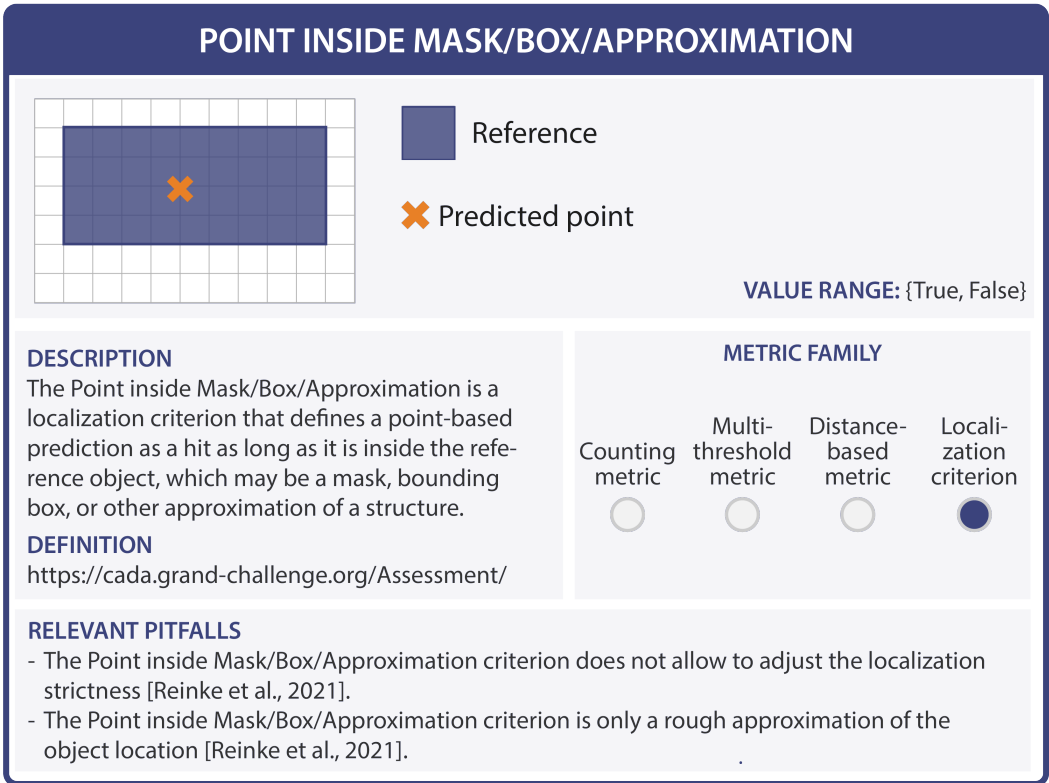
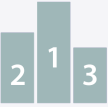


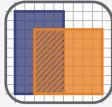
Fig. SN 3.76. Metric profile of Point inside Mask/Box/Approximation. References: <https://cada.grand-challenge.org/Assessment/>, Reinke et al., 2021: [54].

### 3.4 Assignment strategies

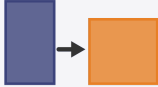
## GREEDY (BY SCORE) MATCHING



1) Rank predictions by predicted class scores; the highest score receives the first rank.



2) Compute localization criterion between all predicted and reference objects



3) Assign prediction to reference with highest localization criterion. Start with first rank.



4) Remove assigned reference object



**REPEAT**

**DESCRIPTION**

In the Greedy (by Score) Matching, all predictions in an image are ranked by their predicted class scores and iteratively (starting with the highest probability) assigned to the reference object with the highest localization criterion for this prediction. The selected reference object is subsequently removed from the process as it can not be matched to any other prediction.

**NEED FOR PREDICTED CLASS SCORES?**

**DEFINITION**  
[Everingham et al., 2015]

**RELEVANT PITFALLS**

- Assignment strategies are different ways to resolve ambiguities in model output interpretation. Importantly, the problem itself remains ambiguous, i.e., there is no correct or wrong way of interpretation thus no objective pitfalls exist.
- This assignment strategy is only applicable if predicted class scores are provided.

Fig. SN 3.77. Cheat Sheet for the Greedy (by Score) Matching. Reference used in the figure: Everingham et al., 2015: [23].

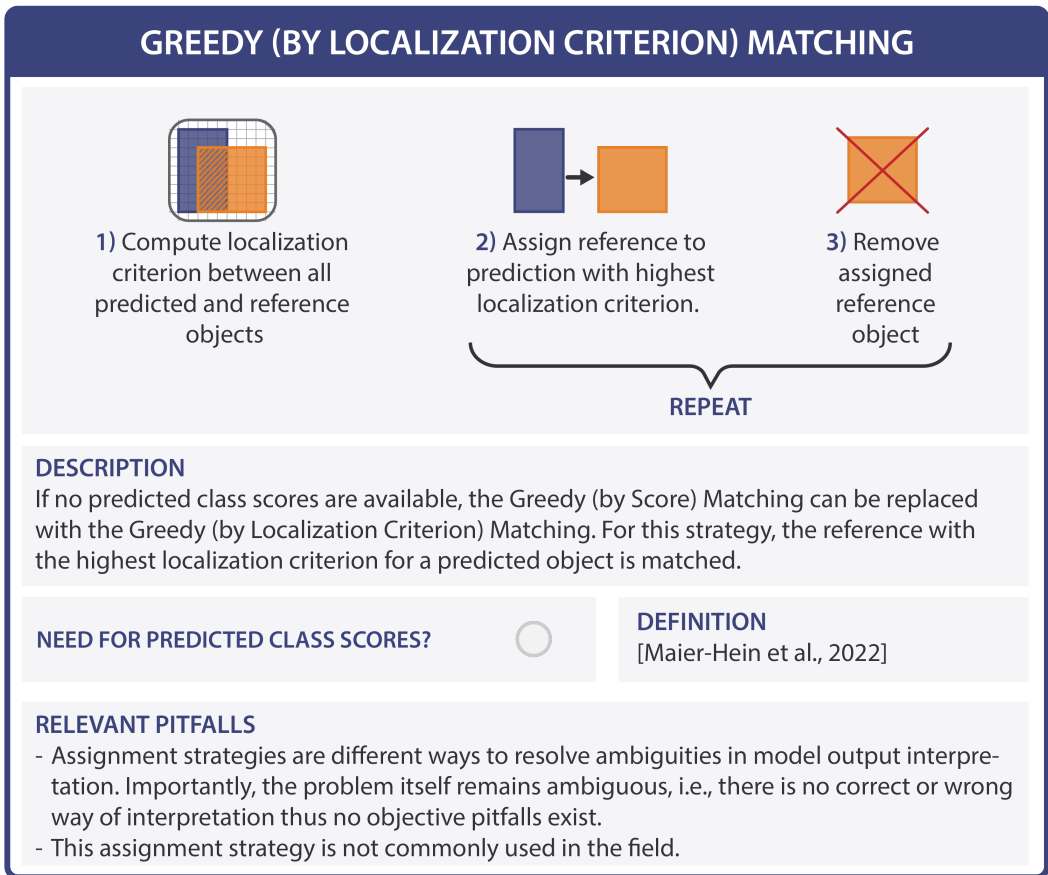
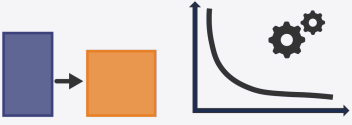


Fig. SN 3.78. Cheat Sheet for the Greedy (by Localization Criterion) Matching. Reference used in the figure: Maier-Hein et al., 2022: [44].

## OPTIMAL (HUNGARIAN) MATCHING



**1) Compute localization criterion between all predicted and reference objects**



**2) Use cost function to find the optimal assignment of predictions and references based on the localization criterion.**

**DESCRIPTION**  
The Optimal (Hungarian) Matching is associated with a cost function, usually depending on the localization criterion, which is minimized to find the optimal assignment of predictions and reference.

**NEED FOR PREDICTED CLASS SCORES?**

**DEFINITION**  
[Kuhn, 1955]

**RELEVANT PITFALLS**  
The optimization may lead to overoptimistic performance results in case of ambiguous model outputs [Maier-Hein et al., 2022].

Fig. SN 3.79. Cheat Sheet for the Optimal (Hungarian) Matching. References used in the figure: Kuhn et al., 1955: [38], Maier-Hein et al., 2022: [44].

## MATCHING VIA OVERLAP > 0.5

**PREREQUISITE:** Overlapping predictions are not possible.



1) Compute overlap-based localization criterion between all predicted and reference objects



2) If the overlap is greater than 0.5, assign prediction to the reference.



3) Remove assigned reference object

} REPEAT

---

**DESCRIPTION**

If there are no overlapping predictions, complex assignment strategies can be avoided by simply setting the localization criterion to  $\text{IoU} > 0.5$ . This strategy inherently avoids matching conflicts, because any secondary prediction would by definition have an overlap  $< 0.5$  of the same reference object.

**NEED FOR PREDICTED CLASS SCORES?**

**DEFINITION**  
[Everingham et al., 2006]

---

**RELEVANT PITFALLS**

- Matching via Overlap  $> 0.5$  is unfeasible if overlapping predictions are possible [Maier-Hein et al., 2022].
- Matching via Overlap  $> 0.5$  cannot be applied if a non-overlap based criterion is employed (e.g., Point inside Mask).

Fig. SN 3.80. Cheat Sheet for the Matching via Overlap  $> 0.5$ . References used in the figure: Everingham et al., 2006: [21], Maier-Hein et al., 2022: [44].

**SUPPL. NOTE 4 ACRONYMS**

**AI** artificial intelligence  
**AP** Average Precision  
**ASSD** Average Symmetric Surface Distance  
**AUC** Area under the Curve  
**AUROC** Area under the Receiver Operating Characteristic Curve  
**BA** Balanced Accuracy  
**BIAS** Biomedical Image Analysis ChallengeS  
**Boundary IoU** Boundary Intersection over Union  
**BS** Brier Score  
**BSS** Brier Skill Score  
**CI** Confidence Interval  
**clDice** centerline Dice Similarity Coefficient  
**COCO** Common Objects in Context  
**CK** Cohen’s Kappa  
**CWCE** Class-Wise Calibration Error  
**DSC** Dice Similarity Coefficient  
**EC** Expected Cost  
**ECE** Expected Calibration Error  
**ECE<sup>KDE</sup>** Expected Calibration Error Kernel Density Estimate  
**FN** False Negative  
**FP** False Positive  
**FPPI** False Positives per Image  
**FROC** Free-Response Receiver Operating Characteristic  
**HD** Hausdorff Distance  
**HD95** Hausdorff Distance 95th Percentile  
**InS** Instance Segmentation  
**IoU** Intersection over Union  
**IoR** Intersection over Reference  
**LR+** Positive Likelihood Ratio  
**KCE** Kernel Calibration Error  
**mAP** mean Average Precision  
**MASD** Mean Average Surface Distance  
**MCC** Matthews Correlation Coefficient  
**MCE** Maximum Calibration Error  
**MICCAI** Medical Image Computing and Computer Assisted Interventions  
**MONAI** Medical Open Network for Artificial Intelligence  
**NaN** Not a Number  
**NB** Net Benefit  
**NPV** Negative Predictive Value  
**NLL** Negative Log Likelihood  
**NSD** Normalized Surface Distance  
**PPV** Positive Predictive Value  
**ObD** Object Detection  
**PQ** Panoptic Quality  
**PR** Precision-Recall  
**RBS** Root Brier Score

**ROC** Receiver Operating Characteristic

**SemS** Semantic Segmentation

**TN** True Negative

**TNR** True Negative Rate

**TP** True Positive

**TPR** True Positive Rate

**WCK** Weighted Cohen's Kappa

## REFERENCES

- [1] Saeid Asgari Taghanaki, Kumar Abhishek, Joseph Paul Cohen, Julien Cohen-Adad, and Ghassan Hamarneh. Deep semantic segmentation of natural and medical images: a review. *Artificial Intelligence Review*, 54(1):137–178, 2021.
- [2] John Attia. Moving beyond sensitivity and specificity: using likelihood ratios to help interpret diagnostic tests. *Australian prescriber*, 26(5):111–113, 2003.
- [3] Min Bai and Raquel Urtasun. Deep watershed transform for instance segmentation. In *Proceedings of the IEEE conference on computer vision and pattern recognition*, pages 5221–5229, 2017.
- [4] D Bamira and MH Picard. Imaging: Echocardiology—assessment of cardiac structure and function. *Elsevier*, 2018.
- [5] Andriy I Bandos, Howard E Rockette, Tao Song, and David Gur. Area under the free-response roc curve (froc) and a related summary index. *Biometrics*, 65(1):247–256, 2009.
- [6] Miroslav Beneš and Barbara Zitová. Performance evaluation of image segmentation algorithms on microscopic image data. *Journal of microscopy*, 257(1):65–85, 2015.
- [7] Christopher M Bishop and Nasser M Nasrabadi. *Pattern recognition and machine learning*, volume 4. Springer, 2006.
- [8] Bernice B Brown. Delphi process: a methodology used for the elicitation of opinions of experts. Technical report, Rand Corp Santa Monica CA, 1968.
- [9] Chang Cao, Davide Chicco, and Michael M Hoffman. The mcc-f1 curve: a performance evaluation technique for binary classification. *arXiv preprint arXiv:2006.11278*, 2020.
- [10] Bowen Cheng, Ross Girshick, Piotr Dollár, Alexander C Berg, and Alexander Kirillov. Boundary iou: Improving object-centric image segmentation evaluation. In *Proceedings of the IEEE/CVF Conference on Computer Vision and Pattern Recognition*, pages 15334–15342, 2021.
- [11] Davide Chicco and Giuseppe Jurman. The advantages of the matthews correlation coefficient (mcc) over f1 score and accuracy in binary classification evaluation. *BMC genomics*, 21(1):1–13, 2020.
- [12] Nancy Chinchor. Muc-4 evaluation metrics. In *Proceedings of the 4th Conference on Message Understanding, MUC4 '92*, page 22–29, USA, 1992. Association for Computational Linguistics. ISBN 1558602739. doi: 10.3115/1072064.1072067. URL <https://doi.org/10.3115/1072064.1072067>.
- [13] Jacob Cohen. A coefficient of agreement for nominal scales. *Educational and psychological measurement*, 20(1):37–46, 1960.
- [14] George Cybenko, Dianne P O'Leary, and Jorma Rissanen. *The Mathematics of Information Coding, Extraction and Distribution*, volume 107. Springer Science & Business Media, 1998.
- [15] Jesse Davis and Mark Goadrich. The relationship between precision-recall and roc curves. In *Proceedings of the 23rd international conference on Machine learning*, pages 233–240, 2006.
- [16] Bert De Brabandere, Davy Neven, and Luc Van Gool. Semantic instance segmentation with a discriminative loss function. *arXiv preprint arXiv:1708.02551*, 2017.
- [17] Jeffrey De Fauw, Joseph R Ledsam, Bernardino Romera-Paredes, Stanislav Nikolov, Nenad Tomasev, Sam Blackwell, Harry Askham, Xavier Glorot, Brendan O'Donoghue, Daniel Visentin, et al. Clinically applicable deep learning for diagnosis and referral in retinal disease. *Nature medicine*, 24(9):1342–1350, 2018.
- [18] Rosario Delgado and Xavier-Andoni Tibau. Why cohen's kappa should be avoided as performance measure in classification. *PLoS one*, 14(9):e0222916, 2019.
- [19] Elizabeth R DeLong, David M DeLong, and Daniel L Clarke-Pearson. Comparing the areas under two or more correlated receiver operating characteristic curves: a nonparametric approach. *Biometrics*, pages 837–845, 1988.
- [20] Lee R Dice. Measures of the amount of ecologic association between species. *Ecology*, 26(3):297–302, 1945.
- [21] Mark Everingham, Andrew Zisserman, Christopher KI Williams, Luc Van Gool, Moray Allan, Christopher M Bishop, Olivier Chapelle, Navneet Dalal, Thomas Deselaers, Gyuri Dorkó, et al. The 2005 pascal visual object classes challenge. In *Machine Learning Challenges. Evaluating Predictive Uncertainty, Visual Object Classification, and Recognising Textual Entailment: First PASCAL Machine Learning Challenges Workshop, MLCW 2005, Southampton, UK, April 11-13, 2005, Revised Selected Papers*, pages 117–176. Springer, 2006.

- [22] Mark Everingham, Luc Van Gool, Christopher KI Williams, John Winn, and Andrew Zisserman. The pascal visual object classes (voc) challenge. *International journal of computer vision*, 88(2):303–338, 2010.
- [23] Mark Everingham, SM Ali Eslami, Luc Van Gool, Christopher KI Williams, John Winn, and Andrew Zisserman. The pascal visual object classes challenge: A retrospective. *International journal of computer vision*, 111(1):98–136, 2015.
- [24] Luciana Ferrer. Analysis and comparison of classification metrics. *arXiv preprint arXiv:2209.05355*, 2022.
- [25] Naiyu Gao, Yanhu Shan, Yupei Wang, Xin Zhao, Yinan Yu, Ming Yang, and Kaiqi Huang. Ssap: Single-shot instance segmentation with affinity pyramid. In *Proceedings of the IEEE/CVF International Conference on Computer Vision*, pages 642–651, 2019.
- [26] Tilmann Gneiting and Adrian E Raftery. Strictly proper scoring rules, prediction, and estimation. *Journal of the American statistical Association*, 102(477):359–378, 2007.
- [27] Margherita Grandini, Enrico Bagli, and Giorgio Visani. Metrics for multi-class classification: an overview. *arXiv preprint arXiv:2008.05756*, 2020.
- [28] Sebastian Gruber and Florian Buettner. Trustworthy deep learning via proper calibration errors: A unifying approach for quantifying the reliability of predictive uncertainty. *arXiv preprint arXiv:2203.07835*, 2022.
- [29] Chuan Guo, Geoff Pleiss, Yu Sun, and Kilian Q Weinberger. On Calibration of Modern Neural Networks. *ICML*, page 10, 2017.
- [30] Metin N Gurcan, Anant Madabhushi, and Nasir Rajpoot. Pattern recognition in histopathological images: An icpr 2010 contest. In *International Conference on Pattern Recognition*, pages 226–234. Springer, 2010.
- [31] James A Hanley and Barbara J McNeil. The meaning and use of the area under a receiver operating characteristic (roc) curve. *Radiology*, 143(1):29–36, 1982.
- [32] Trevor Hastie, Robert Tibshirani, Jerome H Friedman, and Jerome H Friedman. *The elements of statistical learning: data mining, inference, and prediction*, volume 2. Springer, 2009.
- [33] Peter Hirsch, Lisa Mais, and Dagmar Kainmueller. Patchperpix for instance segmentation. *arXiv preprint arXiv:2001.07626*, 2020.
- [34] Daniel P Huttenlocher, Gregory A. Klanderman, and William J Rucklidge. Comparing images using the hausdorff distance. *IEEE Transactions on pattern analysis and machine intelligence*, 15(9):850–863, 1993.
- [35] Paul Jaccard. The distribution of the flora in the alpine zone. 1. *New phytologist*, 11(2):37–50, 1912.
- [36] Alexander Kirillov, Kaiming He, Ross Girshick, Carsten Rother, and Piotr Dollár. Panoptic segmentation. In *Proceedings of the IEEE/CVF Conference on Computer Vision and Pattern Recognition*, pages 9404–9413, 2019.
- [37] Jonathan Krause, Varun Gulshan, Ehsan Rahimi, Peter Karth, Kasumi Widner, Greg S Corrado, Lily Peng, and Dale R Webster. Grader variability and the importance of reference standards for evaluating machine learning models for diabetic retinopathy. *Ophthalmology*, 125(8):1264–1272, 2018.
- [38] Harold W Kuhn. The hungarian method for the assignment problem. *Naval research logistics quarterly*, 2(1-2):83–97, 1955.
- [39] Victor Kulikov and Victor Lempitsky. Instance segmentation of biological images using harmonic embeddings. In *Proceedings of the IEEE/CVF Conference on Computer Vision and Pattern Recognition*, pages 3843–3851, 2020.
- [40] Meelis Kull, Miquel Perello Nieto, Markus Kängsepp, Telmo Silva Filho, Hao Song, and Peter Flach. Beyond temperature scaling: Obtaining well-calibrated multi-class probabilities with dirichlet calibration. *Advances in neural information processing systems*, 32, 2019.
- [41] Ananya Kumar, Percy S Liang, and Tengyu Ma. Verified uncertainty calibration. *Advances in Neural Information Processing Systems*, 32, 2019.
- [42] Tsung-Yi Lin, Michael Maire, Serge Belongie, James Hays, Pietro Perona, Deva Ramanan, Piotr Dollár, and C Lawrence Zitnick. Microsoft coco: Common objects in context. In *European conference on computer vision*, pages 740–755. Springer, 2014.
- [43] Lena Maier-Hein, Matthias Eisenmann, Annika Reinke, Sinan Onogur, Marko Stankovic, Patrick Scholz, Tal Arbel, Hrvoje Bogunovic, Andrew P Bradley, Aaron Carass, et al. Why rankings of biomedical image analysis competitions should be interpreted with care. *Nature communications*, 9(1):1–13, 2018. With this comprehensive analysis of biomedical image analysis competitions (challenges), the authors initiated a shift in how such challenges are designed, performed, and reported in the biomedical domain. Its concepts and guidelines have been adopted by reputed organizations such as MICCAI.
- [44] Lena Maier-Hein, Annika Reinke, Evangelia Christodoulou, Ben Glocker, Patrick Godau, Fabian Isensee, Jens Kleesiek, Michal Kozubek, Mauricio Reyes, Michael A Riegler, et al. Metrics reloaded: Pitfalls and recommendations for image analysis validation. *arXiv preprint arXiv:2206.01653*, 2022.
- [45] Martin Maška, Vladimír Ulman, David Svoboda, Pavel Matula, Petr Matula, Cristina Ederra, Ainhoa Urbiola, Tomás España, Subramanian Venkatesan, Deepak MW Balak, et al. A benchmark for comparison of cell tracking algorithms. *Bioinformatics*, 30(11):1609–1617, 2014.

- [46] Brian W Matthews. Comparison of the predicted and observed secondary structure of t4 phage lysozyme. *Biochimica et Biophysica Acta (BBA)-Protein Structure*, 405(2):442–451, 1975.
- [47] Mahdi Pakdaman Naeini, Gregory Cooper, and Milos Hauskrecht. Obtaining well calibrated probabilities using bayesian binning. In *Twenty-Ninth AAAI Conference on Artificial Intelligence*, 2015.
- [48] Ying-Hwey Nai, Bernice W Teo, Nadya L Tan, Sophie O’Doherty, Mary C Stephenson, Yee Liang Thian, Edmund Chiong, and Anthonin Reilhac. Comparison of metrics for the evaluation of medical segmentations using prostate mri dataset. *Computers in Biology and Medicine*, 134:104497, 2021.
- [49] Prashant Nasa, Ravi Jain, and Deven Juneja. Delphi methodology in healthcare research: how to decide its appropriateness. *World Journal of Methodology*, 11(4):116, 2021.
- [50] Stanislav Nikolov, Sam Blackwell, Alexei Zverovitch, Ruheena Mendes, Michelle Livne, Jeffrey De Fauw, Yojan Patel, Clemens Meyer, Harry Askham, Bernadino Romera-Paredes, et al. Clinically applicable segmentation of head and neck anatomy for radiotherapy: deep learning algorithm development and validation study. *Journal of Medical Internet Research*, 23(7):e26151, 2021.
- [51] Hung Viet Pham, Shangshu Qian, Jiannan Wang, Thibaud Lutellier, Jonathan Rosenthal, Lin Tan, Yaoliang Yu, and Nachiappan Nagappan. Problems and opportunities in training deep learning software systems: An analysis of variance. In *Proceedings of the 35th IEEE/ACM international conference on automated software engineering*, pages 771–783, 2020.
- [52] Teodora Popordanoska, Raphael Sayer, and Matthew B Blaschko. A consistent and differentiable lp canonical calibration error estimator. In *Advances in Neural Information Processing Systems*, 2022.
- [53] David Martin Ward Powers. The problem with kappa. In *Proceedings of the 13th Conference of the European Chapter of the Association for Computational Linguistics*, pages 345–355, 2012.
- [54] Annika Reinke, Matthias Eisenmann, Minu D Tizabi, Carole H Sudre, Tim Radsch, Michela Antonelli, Tal Arbel, Spyridon Bakas, M Jorge Cardoso, Veronika Cheplygina, Keyvan Farahani, Ben Glocker, Doreen Heckmann-Nötzel, Fabian Isensee, Pierre Jannin, Charles Kahn, Jens Kleesiek, Tahsin Kurc, Michal Kozubek, Bennett A Landman, Geert Litjens, Klaus Maier-Hein, Anne L Martel, Henning Müller, Jens Petersen, Mauricio Reyes, Nicola Rieke, Bram Stieltjes, Ronald M Summers, Sotirios A Tsafaris, Bram van Ginneken, Annette Kopp-Schneider, Paul Jäger, and Lena Maier-Hein. Common limitations of image processing metrics: A picture story. *arXiv preprint arXiv:2104.05642*, 2021.
- [55] Azriel Rosenfeld and John L Pfaltz. Sequential operations in digital picture processing. *Journal of the ACM (JACM)*, 13(4):471–494, 1966.
- [56] Anindo Saha, Joeran Bosma, Jasper Linmans, Matin Hosseinzadeh, and Henkjan Huisman. Anatomical and diagnostic bayesian segmentation in prostate mri – should different clinical objectives mandate different loss functions? *arXiv preprint arXiv:2110.12889*, 2021.
- [57] Suprosanna Shit, Johannes C Paetzold, Anjany Sekuboyina, Ivan Ezhov, Alexander Unger, Andrey Zhylyka, Josien PW Pluim, Ulrich Bauer, and Bjoern H Menze. cldice-a novel topology-preserving loss function for tubular structure segmentation. In *Proceedings of the IEEE/CVF Conference on Computer Vision and Pattern Recognition*, pages 16560–16569, 2021.
- [58] Abdel Aziz Taha and Allan Hanbury. Metrics for evaluating 3d medical image segmentation: analysis, selection, and tool. *BMC medical imaging*, 15(1):1–28, 2015. The paper discusses the importance of effective metrics for evaluating the accuracy of 3D medical image segmentation algorithms. The authors analyze existing metrics, propose a selection methodology, and develop a tool to aid researchers in choosing appropriate evaluation metrics based on the specific characteristics of the segmentation task.
- [59] Abdel Aziz Taha, Allan Hanbury, and Oscar A Jimenez del Toro. A formal method for selecting evaluation metrics for image segmentation. In *2014 IEEE international conference on image processing (ICIP)*, pages 932–936. IEEE, 2014.
- [60] Alaa Tharwat. Classification assessment methods. *Applied Computing and Informatics*, 2020.
- [61] Juozas Vaicenavicius, David Widmann, Carl Andersson, Fredrik Lindsten, Jacob Roll, and Thomas Schön. Evaluating model calibration in classification. In *The 22nd International Conference on Artificial Intelligence and Statistics*, pages 3459–3467. PMLR, 2019.
- [62] Bram Van Ginneken, Samuel G Armato III, Bartjan de Hoop, Saskia van Amelsvoort-van de Vorst, Thomas Duindam, Meindert Niemeijer, Keelin Murphy, Arnold Schilham, Alessandra Retico, Maria Evelina Fantacci, et al. Comparing and combining algorithms for computer-aided detection of pulmonary nodules in computed tomography scans: the anode09 study. *Medical image analysis*, 14(6):707–722, 2010.
- [63] C Van Rijsbergen. Information retrieval: theory and practice. In *Proceedings of the Joint IBM/University of Newcastle upon Tyne Seminar on Data Base Systems*, volume 79, 1979.
- [64] Andrew J Vickers and Elena B Elkin. Decision curve analysis: a novel method for evaluating prediction models. *Medical Decision Making*, 26(6):565–574, 2006.
- [65] Andrew J Vickers, Ben Van Calster, and Ewout W Steyerberg. Net benefit approaches to the evaluation of prediction models, molecular markers, and diagnostic tests. *bmj*, 352, 2016.

- [66] David S Wack, Michael G Dwyer, Niels Bergsland, Carol Di Perri, Laura Ranza, Sara Hussein, Deepa Ramasamy, Guy Poloni, and Robert Zivadinov. Improved assessment of multiple sclerosis lesion segmentation agreement via detection and outline error estimates. *BMC medical imaging*, 12(1):1–10, 2012.
- [67] Matthijs J Warrens. Some paradoxical results for the quadratically weighted kappa. *Psychometrika*, 77(2):315–323, 2012.
- [68] David Widmann, Fredrik Lindsten, and Dave Zachariah. Calibration tests in multi-class classification: A unifying framework. *Advances in Neural Information Processing Systems*, 32, 2019.
- [69] Manuel Wiesenfarth, Annika Reinke, Bennett A Landman, Matthias Eisenmann, Laura Aguilera Saiz, M Jorge Cardoso, Lena Maier-Hein, and Annette Kopp-Schneider. Methods and open-source toolkit for analyzing and visualizing challenge results. *Scientific Reports*, 11(1):1–15, 2021.
- [70] Varduhi Yeghiazaryan and Irina Voiculescu. An overview of current evaluation methods used in medical image segmentation. *Department of Computer Science, University of Oxford*, 2015.
- [71] Varduhi Yeghiazaryan and Irina D Voiculescu. Family of boundary overlap metrics for the evaluation of medical image segmentation. *Journal of Medical Imaging*, 5(1):015006, 2018.
- [72] Qiuming Zhu. On the performance of matthews correlation coefficient (mcc) for imbalanced dataset. *Pattern Recognition Letters*, 136:71–80, 2020.